AD NUMBER

AD480516

NEW LIMITATION CHANGE

TO

Approved for public release, distribution unlimited

FROM

Distribution authorized to U.S. Gov't. agencies and their contractors; Critical Technology; MAR 1966. Other requests shall be referred to Air Force Rocket Propulsion Laboratory, Attn: RPPR-STINFO, Edwards AFB, CA 93523.

AUTHORITY

AFRPL ltr, 20 Dec 1971

AFSC Report No. AFRPL-TR-66-52

PARAMETRIC STUDY

OF ROCKET GRAIN CONFIGURATIONS

BY PHOTOELASTIC ANALYSIS

by

M.E. Fourney
R.R. Parmerter

to

AIR FORCE ROCKET PROPULSION LABORATORY
Edwards, California

March 1966

Mathematical Sciences Corporation
RESEARCH • DEVELOPMENT • ANALYSIS

When U.S. Government drawings, specifications, or other data are used for any purpose other than a definitely related Government procurement operation, the Government thereby incurs no responsibility nor any obligation whatsoever, and the fact that the Government may have formulated, furnished, or in any way supplied the said drawings, specifications, or other data, is not to be regarded by implication or otherwise, or in any manner licensing the holder or any other person or corporation, or conveying any rights or permission to manufacture, use, or sell any patented invention that may in any way be related thereto.

This document is subject to special export controls and each transmittal to foreign governments or foreign nationals may be made only with prior approval of AFRPL (RPPR-STINFO), Edwards, California 93523.

AFSC Report No. AFRPL-TR-66-52
MSC Report No. 65-29-12

PARAMETRIC STUDY OF ROCKET GRAIN CONFIGURATIONS BY PHOTOELASTIC ANALYSIS

Research Contract Final Report

Contract No. AF 04(611)-10529

to

AIR FORCE ROCKET PROPULSION LABORATORY
Edwards, California

Prepared by:

M. E. Fourney

R. R. Parmerter

Approved by:

M. E. Fourney
Director of Engineering

MATHEMATICAL SCIENCES CORPORATION
Seattle Office
1107 Northeast 45th Street
Seattle, Washington

FOREWORD

This report presents the results of parametric studies on several families of rocket grain configurations obtained by photoelastic analysis. These results are presented graphically in the form of a stress factor H as a function of the various parameters. In addition, empirical relationships have been derived for most of the studies conducted which represent the observed dependency. A section on the application of the test results to more general engineering problems is presented. In this section a comparison is made between a recommended method of application and a limited number of numerical solutions obtained via computer analysis.

The authors wish to acknowledge the able assistance in the conduct of the experimental portion of this work of A. P. Waggoner and W. L. Fourney.

This technical report has been reviewed and is approved.

R. C. Fanning, Project Engineer

ABSTRACT

This report presents the results of parametric studies on several families of rocket grain configurations obtained by photoelastic analysis. In an earlier paper the authors described a parametric investigation of a family of grains which were defined by three parameters: N the number of star points, a/b the port fraction, and a/ρ the fillet radius factor. The results of that study led to the following empirical formula for the stress concentration factor,

$$H = \sqrt{\frac{1 + a/b}{1 - a/b}} \; N^{-1/3} \left\{ 1 + 2\sqrt{a/\rho} \right\}$$

In the present investigation the study has been extended to include families requiring four parameters to complete their description. Four additional families have been investigated to determine the effect of a) slot width, b) positive wedge angles of the star slot, c) negative wedge angles of the star slot, and d) eccentricity of elliptically shaped star tips. In each of the studies it is shown that the $N^{-1/3}$ rule holds approximately, and empirical formulas similar to the one given above have been derived in some cases.

A section on the application of the test results to more general engineering problems is presented. In this section a comparison is made between a recommended method of application and a limited number of numerical solutions obtained via computer analysis. Under the worst set of conditions available, the stress calculations agreed within 10% and the strain within 15%.

As a result of the large number of parameters used in this study, it is practical to obtain the maximum stress for most grain configurations using the data presented.

TABLE OF CONTENTS

LIST OF SYMBOLS

A	Calculated slope of pressure versus fringe order curve
B	Calculated intercept of pressure versus fringe order curve
D	Diameter of calibration disk
E	Young's modulus
E_c	Young's modulus of case
F	Load
H	Stress factor
K	Stress-optic coefficient
N	Number of star points
S	Standard deviation
T	Temperature
$\vec{T}$	Surface traction
a	Outer radius minus web thickness
b	Outer radius
d	Slot width
$\vec{m}$	Outward normal unit vector of internal surface
m_i	i-th component of $\vec{m}$
n	Fringe order number
$\vec{n}$	Outward normal unit vector of external surface
n_i	i-th component of $\vec{n}$
p(t)	Pressure as a function of time
p_i	Inner pressure
p_o	Outer pressure

LIST OF SYMBOLS (Continued)

p'	Equivalent outer pressure for case-bonded grains
r	Cylindrical coordinate
t	Model thickness
t_c	Case thickness
x	Cartesian coordinate
y	Cartesian coordinate
Δ	Pressure factor
ΔT	Temperature difference measured from strain-free state
∇^2	Laplacian operator
α	Positive wedge angle
α_c	Coefficient of thermal expansion of case
α_T	Coefficient of thermal expansion of grain
β	Negative wedge angle
γ_{ij}	Engineering shear strain
δ	$0.5 - \nu$
ϵ	Ratio of minor to major axis of elliptical slot tip
ϵ_T	Tangential component of strain
ϵ_{ij}	Strain component
θ	Cylindrical coordinate
ν	Poisson's ratio
ν_c	Poisson's ratio of case
ρ	Fillet radius
ρ'	Semimajor axis of elliptical slot tip

σ_1, σ_2	Principal stresses
σ_M	Maximum difference in principal stresses
σ_n	Principal stress normal to boundary
σ_T	Principal stress tangent to boundary
σ_{ij}	Stress component

I.

INTRODUCTION

In the design of solid propellant rocket engines, the use of internal slot configurations has complicated the analysis of stress and strain. Additional complications enter into the problem because of the use of viscoelastic materials, elastic cases, and tapered shapes and because of end effects and finite deformations. Ignoring these complications for a moment, we might consider the problem of an infinitely long, star-perforated cylindrical body of linearly elastic material subjected to infinitesimal deformations. Even the solution of this highly simplified problem defies exact analytical analysis! However, it may be solved by approximate methods of analysis or by using the techniques of photoelasticity. If the solution to this problem has some application in the solution of the even more difficult finite length, case-bonded, viscoelastic problem, then it serves a worthwhile purpose. It will be shown that this is indeed the case.

In view of this, several photoelastic investigations of stresses in solid propellant rocket grains have been conducted.[1,2,3]* This report presents the results of a series of parametric tests on four families of grain configurations. The geometry of each family is completely characterized by four parameters.

The present results are compared to previous work by the authors;[3] the agreement is excellent. An error analysis of the data has been conducted; the method of analysis and the results are outlined. The analysis indicates that the data which is presented is accurate within $\pm$ 5% over the range of interest.

---

*Numbers enclosed in parentheses refer to References listed on Page 48.

II.

GENERAL THEORY

The solution to the problem of an infinitely long, star-perforated cylindrical body (Figure 1-a) is (by symmetry) independent of the axial coordinate (which is taken to be the z coordinate), provided the loading on the cylindrical surfaces is independent of z and the z component of all loads is zero. The problem is classified as a problem in plane strain. If the material is homogeneous, isotropic, and linearly elastic and if the body forces are zero, then the following equations can be shown to govern the problem.[4]

Field equations for the stress components σ_{xx}, σ_{yy}, σ_{xy}

$$\frac{\partial \sigma_{xx}}{\partial x} + \frac{\partial \sigma_{xy}}{\partial y} = 0$$

$$\frac{\partial \sigma_{xy}}{\partial x} + \frac{\partial \sigma_{yy}}{\partial y} = 0 \qquad (1)$$

$$\nabla^2(\sigma_{xx} + \sigma_{yy}) = 0$$

Constitutive equations relating strain to stress

$$\epsilon_{xx} = \frac{1+\nu}{E}\left\{(1-\nu)\sigma_{xx} - \nu\sigma_{yy}\right\}$$

$$\epsilon_{yy} = \frac{1+\nu}{E}\left\{(1-\nu)\sigma_{yy} - \nu\sigma_{xx}\right\} \qquad (2)$$

$$\epsilon_{xy} = \frac{1+\nu}{E}\sigma_{xy} \equiv \frac{\gamma_{xy}}{2}$$

Auxiliary equations for calculating the remaining stress and strain components

$$\epsilon_{zz} = \epsilon_{xz} = \epsilon_{yz} = \sigma_{xz} = \sigma_{yz} = 0$$

$$\sigma_{zz} = \nu(\sigma_{xx} + \sigma_{yy}) \tag{3}$$

Now consider a thin slice cut from this cylinder and subjected to the same load per unit area on the cylindrical surfaces (see Figure 1-b). The upper and lower surfaces are assumed to be free of tractions. This problem is classified as a problem in plane stress, and its solution is governed by the following set of equations.[4]

Field equations for the stress components σ_{xx}, σ_{yy}, σ_{xy}

$$\frac{\partial \sigma_{xx}}{\partial x} + \frac{\partial \sigma_{xy}}{\partial y} = 0$$

$$\frac{\partial \sigma_{xy}}{\partial x} + \frac{\partial \sigma_{yy}}{\partial y} = 0 \tag{4}$$

$$\nabla^2(\sigma_{xx} + \sigma_{yy}) = 0$$

Constitutive equations relating stress to strain

$$\epsilon_{xx} = \frac{1}{E}(\sigma_{xx} - \nu\sigma_{yy})$$

$$\epsilon_{yy} = \frac{1}{E}(\sigma_{yy} - \nu\sigma_{xx}) \qquad (5)$$

$$\epsilon_{xy} = \frac{1+\nu}{E}\sigma_{xy} \quad \frac{\gamma_{xy}}{2}$$

Auxiliary equations for calculating the remaining stress and strain components

$$\sigma_{zz} = \sigma_{xz} = \sigma_{yz} = \epsilon_{xz} = \epsilon_{yz} = 0$$

$$\epsilon_{zz} = -\frac{\nu}{E}(\sigma_{xx} + \sigma_{yy}) \qquad (6)$$

In each problem, the field equations are to be solved subject to certain boundary conditions. The stress components σ_{xx}, σ_{yy}, σ_{xy} obtained from the solution are then substituted into the remaining equations to find the complete stress-strain field. Notice that the field equations of plane stress and plane strain, with zero body force, are identical. Thus, if the stress boundary conditions for a problem in plane strain are identical to the stress boundary conditions for a problem in plane stress, the two solutions for σ_{xx}, σ_{yy}, σ_{xy} must be the same and will be independent of material properties as long as E and ν do not enter the boundary conditions. This observation is the basis for the application of photoelastic analysis to the rocket grain (plane strain) problem.

Let us consider the specific case of a long circular cylinder with a star-shaped cylindrical perforation (Figure 1-a). If there

are no body forces and if the surface tractions are a uniformly distributed pressure p_o on the external cylindrical surface and a uniformly distributed pressure p_i on the internal cylindrical surface, then the boundary conditions are:

External Surface:

Outward Normal $\vec{n}$

Surface Traction $\vec{T} = -p_o\vec{n}$

Boundary Conditions

$$\sigma_{xx}n_x + \sigma_{xy}n_y = -p_o n_y$$

$$\sigma_{xy}n_x + \sigma_{yy}n_y = -p_o n_y \qquad (7)$$

Internal Surface:

Outward Normal $\vec{m}$

Surface Traction $\vec{T} = -p_i\vec{m}$

Boundary Conditions

$$\sigma_{xx}m_x + \sigma_{xy}m_y = -p_i m_x$$

$$\sigma_{xy}m_x + \sigma_{yy}m_y = -p_i m_y \qquad (8)$$

These boundary conditions are independent of E and ν. Therefore, a geometrically similar thin disk of any linearly elastic material, loaded with the same internal and external pressure, will be subjected to the same stress components σ_{xx}, σ_{yy}, σ_{xy}. Hence the stress field in the disk may be obtained by the methods of photoelasticity.

The photoelastic test is performed in the following manner. A thin disk model of the appropriate shape is prepared from a material that exhibits birefringence when subjected to strain. This model could then be loaded with internal pressure p_i' and external pressure p_o' and viewed in a circular polariscope. The isochromatic fringe pattern which would be observed is directly related to the difference in principal stress, $\sigma_1 - \sigma_2$, at each point in the model.

In practice, it is difficult to apply a uniform pressure p_i' to the geometrically complicated inner boundary. It is much more convenient to apply only p_o' to the simple circular outer boundary. Fortunately the solution for internal and external pressure can be easily deduced from observations made on a model with external pressure only. This result follows from the well known principle of superposition for the linear theory of elasticity.

Consider two loading conditions applied to the disk. Loading A consists of equal internal and external pressure p_i'. Loading B consists of external pressure $p_o' - p_i'$ and zero internal pressure. It is clear that the superposition of the solutions to these two problems is the solution for the problem with internal pressure p_i' and external pressure p_o'. Problem B is convenient for photoelastic analysis. Problem A is a case of two-dimensional hydrostatic loading and has the solution

$$\sigma_{xx} = \sigma_{yy} = -p_i'$$

$$\sigma_{xy} = 0 \qquad (9)$$

All directions in the x,y plane are principal directions. Thus

$$\sigma_1 = \sigma_2 = -p_i' \qquad (9\text{-a})$$

Since the equations which govern problem B are linear, it is clear that the magnitude of any stress component at any point in the disk is linearly proportional to the magnitude of the external pressure. If we let $p_o = p_o' - p_i'$ and if we designate the magnitude of the maximum stress which occurs in the solution to B for a given value of p_o by σ_M, then σ_M/p_o will be a constant for all values of p_o. The determination of the value of this constant, as a function of various parameters describing the star geometry, is the primary objective of this study.

In star configurations loaded with external pressure p_o, the maximum stress is found to occur on the inner boundary at the star tip. Since the inner boundary is free from tractions, the principal directions along the boundary are the directions perpendicular to and tangent to the boundary. The principal stress acting on the surface with a normal perpendicular to the boundary is zero. The principal stress acting on a surface with a normal parallel to the boundary, at the point on the boundary where the maximum fringe order (difference in principal stress) occurs is σ_M. Since one principal stress is zero, it follows that the magnitude of the difference of principal stress $|\sigma_1 - \sigma_2| = |\sigma_M|$. The difference in principal stress is directly related to the fringe order n observed at the point by the stress optic law

$$\sigma_1 - \sigma_2 = \frac{Kn}{t} \qquad (10)$$

where K is the fringe constant and t is the model thickness; hence, σ_M can be directly determined from observation of the fringe order n.

III.

TESTING PROCEDURES

A test jig has been designed which allows a uniform pressure p_o to be applied to the external periphery of the model. In practice this pressure is supplied by a regulator from a high pressure nitrogen bottle and may be varied between 0 and 500 psi. The ratio σ_M/p_o can be obtained from observations at one pressure. However, random error will be reduced if a series of observations are made at various pressures. The resulting curve of σ_M versus p_o should be a straight line, and its slope is the desired ratio σ_M/p_o .

The direct observable in these experiments is the fringe order n , which has been shown to be proportional to σ_M . The experimental procedure therefore is to measure the pressure p_1 which is required to cause a first order fringe at the concentration point, the pressure p_2 required to cause a second order fringe, etc., up to some maximum fringe order dictated by the pressure limitations of the system or by the limits of elasticity of the model. For the present series of tests the pressure limit was usually reached between the sixth and eighth fringe order. Thus six to eight data points were available on the p_o versus n curve, and a precise slope could be easily determined. Moreover, either four or eight equal stress concentrations appear in the model (The number depends upon geometry. See Figures 2 and 3.) so that this procedure can be repeated four or eight times, and a weighted average of the slopes is then used to determine the best value of σ_M/p_o for the particular geometry being tested. A least squares

data reduction method has been used. It is described later in the report. A typical set of curves of pressure versus fringe order is shown in Figure 4.

In order to convert the direct experimental result n/p_o (fringe order/pressure) into the desired quantity σ_M/p_o, it is necessary to know the fringe constant K in the stress optic law, equation (10).

The fringe constant has been determined for each sheet of material (CR-39) used in these tests. The value was derived from several tests in which the fringe order versus the load F was observed in a specimen for which $\sigma_1 - \sigma_2$ versus load was known from analytical considerations. The particular test which was used was the diametral compression of a solid disk (Figure 5). The stress solution of this problem is[4]

$$\sigma_1 - \sigma_2 = \frac{8F}{\pi tD} \tag{11}$$

A typical curve of fringe order versus F is shown in Figure 5. As an example of the consistency of the tests, ten specimens were tested from Sheet #1, and the range of K observed was 93.4 ± 1.0 psi-in/fringe.

Two additional tests were used to check the overall validity of the test procedure. In one test, 10 thick-walled cylinders were loaded with external pressure in the pressure jig. Since the stress solution is known in this case from theory, the correlation between test results and theory can be observed. The test results are shown in Figure 6. Unfortunately, the test is not too sensitive since the stress levels for a given amount of external pressure are low, so that within the 500 psi test limits only 3 or 4 fringes can be observed. In addition,

the stress gradients are low so that the fringes are not sharply defined. Nevertheless, the agreement between theory and experiment is good and, because of the limitations inherent in the test, this discrepancy probably indicates the maximum overall deviation to be expected between the true values of H and the experimental values in this type of testing.

To check consistency with previous experimental work, a number of simple slot configurations were tested (Figure 7-a). The result of the present tests is compared to previous test results in Figure 8. Parametric studies of this configuration have been published in Reference 3. Excellent agreement was found between the two sets of data.

IV.

DATA REDUCTION

Typical data from a test on one specific geometry consists of the pressures corresponding to the first 6 to 8 fringe orders for each of the locations where the maximum stress occurs. The objective of the data reduction process is to extract from this set of 50 or 60 values of pressure the best value for the ratio $-\sigma_M/p_o$.

As a first step, the best value of σ_M/p_o is determined for each of the locations where maximum stress occurs. σ_M/p_o is related via the fringe constant to the slope of the best straight line through the data presented in a pressure versus fringe order plot. If all of the data is given equal weight, the slope of the best straight line through the data can be found by a least mean squares process.[5] If the data is thought of as a set of M pairs of numbers (x_i, y_i) , then the best slope can be shown to be

$$A = \frac{M\sum_{i=1}^{M} x_i y_i - \left(\sum_{i=1}^{M} x_i\right)\left(\sum_{i=1}^{M} y_i\right)}{M\sum_{i=1}^{M} x_i^2 - \left(\sum_{i=1}^{M} x_i\right)^2} \tag{12}$$

where $y = AX + B$. The standard deviation of A can be shown to be

$$S = \sqrt{\left\{\frac{\sum_{i=1}^{M} (AX + B - y_i)^2}{M - 2}\right\} \cdot \left\{\frac{M}{M\sum_{i=1}^{M} x_i^2 - \left(\sum_{i=1}^{M} x_i\right)^2}\right\}} \tag{13}$$

In this way, L values of best slope A_i, with corresponding standard deviations S_j, are calculated. The best value of A is then taken to be a weighted average of these L values.

$$\bar{A} = \text{best estimate of } A = \frac{\sum_{j=1}^{L} A_j/S_j^2}{\sum_{j=1}^{L} 1/S_j^2} \tag{14}$$

The standard deviation of $\bar{A}$ is calculated from

$$S_{\bar{A}} = \sqrt{\frac{\sum_{j=1}^{L} (\bar{A} - A_j)^2}{S_i^2} \Bigg/ (L - 1) \sum_{j=1}^{L} 1/S_j^2} \tag{15}$$

V.

DATA REDUCTION EXAMPLE

The following raw data was obtained from Test #29.

Table I

n Fringe Order \ External Pressure p_o	Location of Stress Concentration							
	#1	#2	#3	#4	#5	#6	#7	#8
1	62	58	61	55	64	62	66	65
2	115	105	113	111	113	113	115	122
3	179	169	171	172	177	173	179	187
4	231	225	227	234	228	229	230	244
5	293	284	284	295	293	284	288	305
6	357	347	348	360	357	350	352	373
Best Slope A	6.44	6.52	6.63	6.21	6.45	6.61	6.62	6.18
Std. Deviation S	0.10	0.12	0.09	0.07	0.14	0.10	0.12	0.07

The best slope A is calculated for each point of stress concentration using equation (12). For example, for stress concentration #1, $M = 6$, $t = 0.246$, $A = 6.44$, and $S = 0.10$. The value of A for each of the eight points of stress concentration is shown in the above table, with corresponding values of S. Equation (14) is now used to find $\bar{A}$, the best value of A, with $L = 8$.

$$\bar{A} = 6.40$$

Equation (15) gives the standard deviation of $\bar{A}$.

$$S_{\bar{A}} = 0.07$$

Thus, for the geometry of Test #29, the bracket $H = 6.40 \pm 0.07$ contains the correct value of H with a probability of 67%. The bracket $H = 6.40 \pm 0.14$ contains the correct value of H with a probability of 95%.

VI.

TEST RESULTS

The tests conducted during this program have established the stress variations which arise when the simple slot configuration shown in Figure 7-a is modified by either changing the shape of the tip or the slope of the slot walls. An extensive series of tests of the simple slot configuration has been previously reported.[3] For completeness, the results are shown in Figures 9 through 14. The simple slot configuration is characterized by three parameters: a/b , a/ρ , and N . The variation of H as a function of a/ρ , with N and a/b fixed is shown in Figures 9 through 13. A typical photoelastic fringe pattern is shown in Figure 2. One of the more interesting results of this study was that the variation of H as a function of N , with a/ρ and a/b fixed, was of the form $H \sim N^{-1/3}$ over the range tested, except near the limit points $a/\rho \rightarrow 1$. (It is clear that for all values of N and ρ , when $a = \rho$, the simple slot configuration becomes a circular port.) This behavior is shown in crossplots (Figure 14). The following empirical formula was derived for H

$$H = \sqrt{\left(\frac{a+b}{b-a}\right)}\, N^{-1/3} \left[1 + 2\sqrt{\frac{a}{\rho}}\right] \qquad (16)$$

and as shown in Figures 9 through 14 fits the data within 5% for $a/\rho > 4$.

In the present series of tests the simple slot configuration was modified by

a) Widening the slot tips--see Figure 15.

b) Replacing the parallel slot walls with nonparallel walls--both positive and negative angle--see Figures 16 and 17.

c) Replacing the semicircular star tip with a semiellipse--see Figure 18.

The following sections of the report give further details on the configurations tested and the values of H observed.

VII.

SLOT WIDTH FACTOR TESTS

A series of tests was run to determine the effect of slot width on maximum stress. The geometry is shown in Figure 15. It is completely defined by the four parameters: N the number of star points, a/b the port fraction, a/ρ fillet radius factor, and $d/2\rho$ the slot width factor. The majority of the tests were of configurations with $N = 4$. In addition, 6 tests were made of configurations with $N \neq 4$. The results of the tests with $N = 4$ are presented in Figures 19 through 22 by holding $d/2\rho$ constant at integral values from 2 to 5 inclusively and plotting H versus a/ρ for constant values of a/b .

The slot width factor is varied between the limit point, where $d/2\rho = 1$, which represents a simple slotted grain (See Figure 8), and the limit point where d is allowed to increase to the value $d = 2a$. These limiting geometries are shown in Figure 7. Both of these limit points were established by means of photoelastic tests. The limit point corresponding to $d/2\rho = 1$ is identical to the configuration treated in Reference 3; however, 17 additional tests were conducted to confirm the correlation between these two series of tests. The other limit point was established by photoelastic tests on the geometry shown in Figure 7-b. In this case the internal geometry is a square with a finite radius of curvature at each corner. Due to the close proximity of the outer boundary, an analytical solution is not available. In lieu of this a parametric study was made. Two

parameters were necessary to describe the square: a/b the port fraction and a/ρ the fillet radius factor. The results of this study are shown in Figure 23. The limit points required for this series may then be determined from this curve. A typical photoelastic picture of this limit configuration is shown in Figure 24.

The actual curves used to present the data are obtained by holding $d/2\rho$ fixed and plotting the factor H as a function of a/ρ for several values of a/b. Each member in the resulting family of curves is located by 3 to 4 test points. In general the correlation of these tests in establishing a single curve is excellent. It will be noted that the limit points are indicated by a vertical crosshatched line and are a function of $d/2\rho$ only. For large values of a/b the limiting geometry cannot be realized, as the limiting square is larger than the outer circular boundary.

In general the curves are quite smooth except near the limit point where a rapid increase in the factor H is indicated. Also it will be noted that the factor H is significantly reduced for values of $d/2\rho > 1$ (with the exception of points in the neighborhood of the limit points). Also, as indicated in Figure 25, a minimum value of H is obtained for fixed values of the other remaining parameters. The value of $d/2\rho$ where this minimum occurs is not constant but is a function of the other parameters.

In the simple slot tests for values of N from $N = 3$ to $N = 8$, the empirical rule $H \approx N^{-1/3}$ was observed (See Figure 14). If the same rule were to hold for $d/2\rho \neq 1$, then the results of the

current series of tests could be immediately extended for $N \neq 4$. To test this hypothesis a series of six tests for $N = 2, 3, 4, 5, 6,$ and 7 was conducted with the remaining three parameters held constant at $d/2\rho = 3$, $a/b = 60\%$, $a/\rho = 13$. The results of the tests showing the variation with N are shown in Figure 26. The dotted line indicates the curve which would be anticipated if an $N^{-1/3}$ rule governed the behavior. This curve represents the data particularly well in view of the rather peculiar shape of the curve. The curve shown has been drawn to give the best fit to all the data, rather than to tie to the $N = 4$ results. The largest disagreement of the two curves shown is 6%.

It would be advisable to make additional tests to obtain cross-plots similar to Figure 26 for other fixed values of $d/2\rho$, a/b , and a/ρ to determine the limits of applicability of an $N^{-1/3}$ rule. This work however was not within the scope of this investigation.

VIII.

POSITIVE WEDGE ANGLE TESTS

A series of tests was conducted to determine the effect of a positive wedge angle on the stress factor H. The geometry used in this series is defined in Figure 16. It is completely specified by four parameters: N the number of star points, a/b the port fraction, a/ρ the fillet radius factor, and α the wedge angle. A total of 63 tests were conducted for $N = 4$; $a/b = 40\%$, 50%, 60%, 70%, and 80%; $\alpha = 10^{\circ}$, 20°, 30°, and 40°; and an appropriate range of a/ρ. In addition five tests were conducted for values of N other than 4 to determine the effect of N.

The results for $N = 4$ are shown in Figures 27 through 30. In each of these figures α and N have been held constant and H is plotted as a function of a/ρ for various values of a/b. Each curve is defined by three test points and a limit point at $a/\rho = 1$. At this limit point the geometry reduces to a circular port for which the value of the stress may be easily calculated. A typical isochromatic fringe pattern for this geometry is shown in Figure 31.

If these curves are compared to the simple slot tests of Figure 8, which corresponds to this geometry with $\alpha = 0$, it is observed that even moderate positive wedge angles lead to significant reductions in stress. This is clearly seen in the crossplots presented in Figures 32 and 33, where H is plotted versus α for various values of a/b with a/ρ held constant.

The results of the tests showing the variation of H with N are shown in Figure 34. Again the stress factor H decreases as N increases, and the $N^{-1/3}$ rule (dotted curve) is in reasonable agreement with the data.

IX.

NEGATIVE WEDGE ANGLE TESTS

A series of tests was conducted to determine the effect of a negative wedge angle on the stress factor H . The geometry used in this series is shown in Figure 17. The definition of this geometry requires four parameters. They are: N the number of star points, a/b the port fraction , a/ρ the fillet radius factor, and β the wedge angle. The wedge angle has been denoted by β , a positive number, for convenience. It will be noted that this corresponds to an extension of the series reported in the previous section for negative values of α .

Tests were conducted for N = 4 , a/b = 40%, 50%, 60%, 70%, and 80% , $\beta = 10^{\circ}$, 20°, and 40° , and an appropriate range of a/ρ . An additional series of tests was conducted for values of N from 2 to 8.

A typical isochromatic fringe pattern is shown in Figure 35. The results for N = 4 are shown in Figures 36 through 39. In each of these figures, β and N have been held constant and H is plotted as a function of a/ρ for various values of a/b . Each curve is defined by three test points and a limit point at $a/\rho = 1$. At this limit point the geometry reduces to a circular port for which the value of the stress may be easily calculated. The curve for $\beta = 0$ again corresponds to a simple slot configuration (See Figure 8). The curve for $\beta = 30^{\circ}$ has been obtained by interpolation.

The results of the tests showing the variation of H as a function of N are shown in Figure 40. It will be noted that the stress decreases as N increases and that the $N^{-1/3}$ rule (dotted line) closely represents the data. This is particularly true for values of N greater than 3. In the limit when N = 2 , the disagreement is only 6.7%. However it must be emphasized that this validates this rule only within the range tested.

Cross plots of the data are presented in Figures 41 through 43. In these plots N and a/ρ are held constant and H is plotted as a function of β for various values of a/b . The limit point for $\beta = 0^\circ$ corresponds to a simple slot configuration; the other extreme, $\beta = 90^\circ$, corresponds to a square with finite radius of curvature at the corners. Both of these configurations have been investigated. It is seen from these plots that the variation of H as a function of β is relatively small for angles up to 50°. Particularly notice that for smaller port fractions the value of H is essentially constant for $\beta < 45^\circ$. For this reason the curve for $\beta = 30^\circ$ was obtained by interpolation of this data.

X.

ELLIPTICAL SLOT TIP TESTS

The nature of the stress concentration at a star tip is determined by the star tip geometry. In the case where the slot is terminated in a semicircular tip, one point of stress concentration occurs, and it is located on the centerline of the slot (Figure 2). On the other hand, when the slot is terminated with a tip similar to those used for the slot width effect tests, two points of stress concentration occur (Figure 3). With these observations in mind, consider the nature of the stress concentration where the slot is terminated by a semiellipse (Figure 18). If we define ϵ to be the ratio of the minor axis of the ellipse to the major axis of the ellipse, then as $\epsilon \longrightarrow 1$ the star tip approaches a semicircle (Figure 44), and a single point of stress concentration would be expected. On the other hand, when ϵ is small ($\epsilon \longrightarrow 0$), the star tip resembles the type used in the slot width effect tests, and two points of concentration would be expected. It is clear that at some intermediate value of ϵ the transition from one point of concentration to two points of concentration must occur, and for this transition geometry the stress must be quite uniformly distributed around the tip. Intuitively one feels that this more uniform stress distribution, relatively free from concentration points, will be a minimum stress configuration.

To test this hypothesis, a series of tests was conducted with elliptical star tip geometries, with values of ϵ = 1, 0.8, 0.6, 0.4, and 0.35. In all cases it was found that as ϵ is varied while all

other parameters of the geometry are held constant, a configuration of minimum stress occurs for a value of ϵ in the range $0.35 < \epsilon < 0.70$. As anticipated, this minimum stress configuration is found at the value of ϵ where the transition from one concentration point to two concentration points is occurring.

The geometry of a star grain with elliptical star tips can be specified by four dimensionless parameters, a/b, N, a/ρ', and ϵ. The majority of the tests were conducted for $N = 4$. Typical fringe patterns are shown in Figure 45. Curves of H (stress factor) versus a/ρ', for various values of a/b and ϵ, are shown in Figures 46, 47, 48, and 49. Crossplots of H versus ϵ for fixed a/b and a/ρ' are shown in Figures 50 and 51. The shaded area indicates the value of ϵ at which a minimum H occurs.

In addition to the tests for $N = 4$, several tests were conducted for other values of N. The relationship between H and N for fixed a/ρ', a/b, and ϵ is shown in Figures 52 and 53. The dotted line indicates the variation of H if the empirical rule $H \sim N^{-1/3}$ were valid. The close agreement between the dotted curve and the experimental values indicates that once again, within the range tested, the $N^{-1/3}$ rule adequately expresses the dependence of H on N. This indicates that the extensive results obtained for $N = 4$ can be directly extended to $N \neq 4$.

A series of fringe pattern pictures is shown in Figure 45 to illustrate how the transition from one point of stress concentration to two points of concentration occurs as ϵ is varied. The pictures

were taken with a load of 350 psi, and in each configuration $N = 4$, $a/\rho' = 6.5$, and $a/b = 60\%$. Note in particular the uniform stress along the star tip in Figure 45-c where ϵ is close to the transition value as compared to Figure 45-a or 45-d.

XI.

APPLICATIONS

Internal Pressure

Maximum Stress Calculations. In the introductory section it is shown that the test result can be applied to the case of internal pressure p_i' and external pressure p_o' by superimposing a hydrostatic stress state $\sigma_{xx} = \sigma_{yy} = \sigma_1 = \sigma_2 = -p_i'$. Thus, for this case, $p_o = p_o' - p_i'$ and

$$\sigma_T = H(p_i' - p_o') - p_i' \tag{17}$$

The factor H is obtained from the parametric curves and is equal to $-\sigma_M/p_o$.

If the grain is case-bonded, then to a good degree of approximation[6] the case can be replaced by an equivalent uniform external pressure p' where

$$p' = \frac{p_i'}{\left\{\left[1 + (1 - 2\nu)\left(\frac{b}{a}\right)^2\right] + \left[\left(\frac{b}{a}\right)^2 - 1\right]\left[\frac{1 + \nu_c}{1 + \nu}\right]\frac{Eb}{E_c t_c}\right\}\frac{1}{2(1-\nu)}} \tag{18}$$

In this equation t_c is the thickness of the case and E_c and ν_c describe the elastic properties of the case. The equation has been derived for a thickwalled cylinder grain. The validity of this equation becomes questionable for a star grain when the web becomes thin. It is clear that if the web is thin the external pressure

exerted by the case will not be uniform, and shear transfer between case and grain may become appreciable.

When this equation is used to find p' for a star grain, a value for a/b must be chosen which properly represents the star grain as an "equivalent thickwalled cylinder" (equivalent in the sense that p' calculated using the chosen value of a/b is equal to the average value of normal stress which the case exerts on the actual star grain). The determination of an "equivalent thickwalled cylinder" is a key step in the application of photoelastic test data to case-bonded star grains. Engineering intuition dictates that the equivalent cylinder lies between an equal web fraction cylinder and an equal area cylinder. The problem of choosing an equivalent cylinder will be pursued in detail in a later section.

As a practical note for calculation purposes, it will be found that when typical numerical values are substituted into equation (18) the denominator will be approximately equal to 1, indicating that $p' \approx p_i$. Since the stress calculation (equation 17) depends upon the factor $(p_i - p')$, p' must be accurately determined. Computational labor is minimized if the denominator is put into the form $1 + \Delta$. Then,

$$p' = \frac{p_i}{1 + \Delta} = p_i \left\{ 1 - \Delta + \Delta^2 + 0(\Delta^3) \right\} \qquad (19)$$

and an adequate expression for p' will be obtained in most practical cases by retaining the first three terms in the expansion; i.e.,

$\Delta^3 \ll \Delta$. The value of Δ is easily calculated from the expression

$$\Delta = \frac{\left[\left(\frac{b}{a}\right)^2 - 1\right]}{2(1 - \nu)} \left\{ 1 - 2\nu + \left(\frac{1 + \nu_c^2}{1 + \nu}\right) \frac{Eb}{E_c t_c} \right\} \qquad (20)$$

In those problems where $\nu \approx 0.5$ and $E_c t_c \gg Eb$, this approach will be found to significantly reduce the computational labor. The maximum stress (equation 17) becomes

$$\sigma_T = \left[H(\Delta - \Delta^2) - 1 \right] p_i + O(Hp_i \Delta^3) \qquad (21)$$

Maximum Strain Calculations. The calculation of maximum strain follows from equations (2). For the particular case of external pressure p_o' and internal pressure p_i' , which includes case-bonded grains as indicated in the previous section, the maximum strain occurs at the point of maximum stress and is given by

$$\epsilon_T = \frac{1 + \nu}{E} \left\{ \left[(1 - \nu)H + 2\nu - 1 \right] p_i' + (\nu - 1) H p_o' \right\} \qquad (22)$$

In terms of Δ for a case-bonded grain, this equation becomes

$$\frac{\epsilon_T}{p_i} = \frac{1 + \nu}{E} \left\{ (1 - \nu)(\Delta - \Delta^2)H - (1 - 2\nu) \right\} + O\left(\frac{H}{E} \Delta^3\right) \qquad (23)$$

If $\nu \approx 0.5$, then ϵ_T depends strongly upon H , Δ , and ν . The dependence upon ν is more clearly expressed by letting

$\nu = 0.5 - \delta$, $\delta << 1$. Then equation (23) becomes

$$\frac{\epsilon_T}{p_i} = \frac{1+\nu}{E}\left\{\left[\tfrac{1}{2}(\Delta - \Delta^2) + \delta\Delta\right] H - 2\delta\right\} + O\left(\frac{H}{E}\Delta^3\right) + O\left(\frac{H}{E}\Delta^2\delta\right) \quad (24)$$

It is clear from this expression that under these conditions ($\nu \approx 0.5$), accurate strain calculations require very accurate values of ν and interface pressure p' . It is also clear that errors in interface pressure are greatly magnified when H is large.

The extension of these calculations to the case of a linear viscoelastic material is straightforward as long as the boundary conditions are of the proportional loading type. The elastic constants E and ν are replaced by appropriate differential operators and integrations carried out where required. In particular, it should be noted that equation (18) becomes a differential equation for $p'(t)$, and the time dependence of $p'(t)$ will in general not be the same as $p_i'(t)$. Thus, for a viscoelastic grain in an elastic case, the assumption of proportional loading may not be valid. Treating the problem as one with proportional loading introduces further approximation into the solution.

Thermal Shrinkage

If a case-bonded solid propellant rocket grain is strain free at some reference temperature, say $T = 0$, and if its temperature is changed, strain will be induced due to two causes. First, strain will

be induced due to the thermal expansion of the body. If the body is unrestrained and the temperature is uniform from point to point in the body, then the body will remain stress free although a nonzero strain field exists. If however the body is restrained in some manner, these restraints will produce a stress field which then gives rise to additional strains through the normal Hookean constitutive equations. This is expressed in the following equations.

$$\epsilon_{rr} = \frac{1}{E}\left[\sigma_{rr} - \nu(\sigma_{\theta\theta} + \sigma_{zz})\right] + \alpha_T \Delta T$$

$$\epsilon_{\theta\theta} = \frac{1}{E}\left[\sigma_{\theta\theta} - \nu(\sigma_{zz} + \sigma_{rr})\right] + \alpha_T \Delta T$$

$$\epsilon_{zz} = \frac{1}{E}\left[\sigma_{zz} - \nu(\sigma_{rr} + \sigma_{\theta\theta})\right] + \alpha_T \Delta T \qquad (25)$$

$$\gamma_{r\theta} = \frac{1}{G}\tau_{r\theta}, \quad \gamma_{\theta z} = \frac{1}{G}\tau_{\theta z}, \quad \gamma_{rz} = \frac{1}{G}\tau_{rz}$$

In each of these expressions for normal strain, we see the strain arises from two sources, ΔT the temperature change and the induced stresses. In these equations ΔT is the temperature change and α_T is the coefficient of thermal expansion. Note that the thermal portion of the stress field affects only the normal stress-strain relations, as thermal expansion causes no shearing strains.

Now consider the thermal stress problem in a long circular cylindrical rocket grain with constant temperature change ΔT , a thin elastic case, and a concentric circular internal port. The assumption

is made that the ends of grain are restrained in such a manner that the problem reduces to one of plane strain; i.e., $\epsilon_{zz} = 0$. The equations for the stresses and strains in the propellant are:

$$\sigma_{rr} = - \frac{p'}{(1 - a^2/b^2)} \left[1 - a^2/r^2 \right]$$

$$\sigma_{\theta\theta} = - \frac{p'}{(1 - a^2/b^2)} \left[1 + a^2/r^2 \right]$$

$$\sigma_{zz} = - \frac{2\nu p'}{(1 - a^2/b^2)} - E\alpha_T \Delta T$$

$$\epsilon_{rr} = - \frac{(1 + \nu)p'}{E(1 - a^2/b^2)} \left[(1 - 2\nu) - a^2/r^2 \right] + (1 + \nu)\alpha_T \Delta T \qquad (26)$$

$$\epsilon_{\theta\theta} = - \frac{(1 + \nu)p'}{E(1 - a^2/b^2)} \left[(1 - 2\nu) + a^2/r^2 \right] + (1 + \nu)\alpha_T \Delta T$$

$$p' = \frac{\left[1 - \left(\frac{a}{b}\right)^2 \right] \left[\frac{E}{1 + \nu} \right] \left[(1 + \nu)\alpha_T - (1 + \nu_c)\alpha_c \right] \Delta T}{\left(\frac{a}{b}\right)^2 + 1 - 2\nu + \left[1 - \left(\frac{a}{b}\right)^2 \right] \left[\frac{1 - \nu_c^2}{1 + \nu} \right] \frac{Eb}{E_c t_c}}$$

It should be noted that in the above set of equations the stresses σ_{rr} and $\sigma_{\theta\theta}$ result from the term involving the interface pressure p' only. That is, the two-dimensional stress field is completely equivalent to a pressure problem with the value of the external pressure being given by p' of the above set of equations.

It should be noted that the above expression for p' does not agree with the expressions given in Reference 6 and Reference 9.

This p' has been based on the assumption $\epsilon_{zz} = 0$ where ϵ_{zz} is the <u>total</u> z strain; i.e., mechanical strain plus thermal strain. The referenced reports give a value for p' based on holding only the mechanical part of ϵ_{zz} zero.

When the internal boundary is not a circular port, it is not possible to write expressions for the stress field similar to the pressure problem. The assumption is made that the effect of the case may be replaced by a <u>uniform</u> pressure given by p' of equation (26). Here again an equivalent circular port grain must be selected to calculate p'. In this case the equal web fraction would yield a lower bound on the stress while the equal area equivalence would yield an upper bound.

Strain calculations are most readily made by first calculating the complete stress state using equation (17) to calculate the maximum tangential stress, the internal boundary condition to calculate the normal stress, and the condition of plane strain for the axial stress $\left[\text{i.e., } \epsilon_{zz} = 0 \text{ , which implies } \sigma_{zz} = \nu(\sigma_T + \sigma_n) - E\alpha_T\Delta T\right]$. Once the stresses are known, the strains may be determined directly from equation (25). It should be noted that the expression given for maximum strain in equation (22) is incomplete when thermal strains are considered.

Calculation of an Equivalent Cylinder

Recently the results of a limited number of computer solutions of case-bonded and free star grains, loaded by pressure and thermal

loads, have been published by Becker and Brisbane.[7] Comparing these results with the ones obtained using photoelastic data and the techniques outlined in this report, one finds remarkable agreement for the free grain for both stress and strain. For case-bonded grains, the maximum stress calculations show good agreement when p' is based on an equal web fraction equivalent. However, as indicated in a previous section, considerable error can occur in the strain calculations, especially for large values of H and $\nu \approx 0.5$ since the strain calculation is particularly sensitive to errors in p'. In the examples of Becker and Brisbane, $\nu = 0.4987$ and $11 \leq H \leq 18.2$. In more typical configurations $4 < H < 10$, so that these examples probably indicate an upper bound to the expected error.

Using the examples of Becker and Brisbane and the example from the Numerical Example Section of this report, tentative rules for finding a better "equivalent cylinder" can be derived. The examples show that the correct equivalent is much closer to equal web fraction than to equal area, indicating that the portion of the star grain material inside an equal web fraction cylinder is not effectively utilized in providing hoop stiffness. The area of this ineffective material is proportional to $\left[(a/b)_W^2 - (a/b)_A^2\right]$ where $(a/b)_W$ refers to an equal web fraction equivalent and $(a/b)_A$ refers to an equal area equivalent. By considering this area to be 20% effective in increasing hoop stiffness, considerable improvement in the accuracy of strain calculations is obtained. In other words, for purposes of calculating the interface pressure p', an equivalent cylinder

$(a/b)_E$ is calculated as follows:

$$(a/b)_E = \sqrt{(a/b)_W^2 - 0.20 \left\{(a/b)_W^2 - (a/b)_A^2\right\}} \qquad (27)$$

The stresses and strains calculated using $(a/b)_W$, $(a/b)_A$, and $(a/b)_E$ are tabulated in Table II along with the corresponding computer solutions. In these examples, when $(a/b)_E$ is used to calculate p' , the maximum error in stress is less than 10% and the maximum error in strain is less than 15%. Additional comparison problems would be useful to verify the validity of the method. However, based on the information at hand, it would appear that the use of $(a/b)_E$ offers considerable improvement over $(a/b)_W$ or $(a/b)_A$.

Numerical Example

Internal Pressure. A numerical example will be presented to illustrate the dependency of the maximum stress (or strain) on the choice of the "equivalent" circular port grain. Assume that the cross section of the grain is of the simple slot family shown in Figure 7-a with the following values of parameters:

$$N = 4 \qquad d/2\rho = 1$$

$$a/b = 66.7\% \qquad a/\rho = 8$$

Hence from Figure 8 the value of the stress factor is determined to be $H = 9.6$.

TABLE II

Case-Bonded Grains with Internal Pressure

Geometry	Case	Relative Stiffness $Eb/E_c t_c$	Equal Web Fraction			Equal Area			Equivalent Port Fractions			Computer		% Error	
			$(a/b)_W$	σ_T/p_i	ϵ_T/p_i	$(a/b)_A$	σ_T/p_i	ϵ_T/p_i	$(a/b)_E$	σ_T/p_i	ϵ_T/p_i	σ_T/p_i	ϵ_T/p_i	Stress	Strain
#1	Steel	6.67×10^{-3}	0.888	-0.934	1.77×10^{-5}/psi	0.312	+0.168	2.91×10^{-6}/psi	0.729	-0.882	2.83×10^{-5}/psi	-0.872	3.07×10^{-5}/psi	1.1	7.8
#2	Steel	3.42×10^{-3}	0.900	-0.883	2.61×10^{-5}/psi	0.237	+0.269	3.16×10^{-6}/psi	0.636	-0.836	3.97×10^{-5}/psi	-0.829	4.61×10^{-5}/psi	0.8	13.9
#3	Steel	2.00×10^{-3}	0.800	-0.826	4.22×10^{-5}/psi	0.234	+0.449	3.61×10^{-6}/psi	0.567	-0.772	5.58×10^{-5}/psi	-0.757	5.95×10^{-5}/psi	2.0	6.2
#4	Steel	6.67×10^{-3}	0.800	-0.940	1.37×10^{-5}/psi	0.493	+0.676	8.02×10^{-5}/psi	0.749	-0.917	1.96×10^{-5}/psi	-0.918	1.92×10^{-5}/psi	0.1	2.1
#4	Fiberglass	66.7×10^{-3}	0.800	-0.599	9.9×10^{-5}/psi	0.493	+0.924	4.81×10^{-6}/psi	0.749	-0.448	1.37×10^{-4}/psi	-0.467	1.31×10^{-4}/psi	4.1	4.6
NBC-868 Problem	Steel	1.67×10^{-3}	0.667	-0.757	1.54×10^{-4}/psi	0.366	+0.122	8.28×10^{-6}/psi	0.618	-0.688	2.08×10^{-4}/psi	-0.698	2.00×10^{-4}/psi	4.3	4.0

Case-Bonded Grain, Thermal Shrinkage, $\Delta T = -100°F$

Geometry	Case	Relative Stiffness $Eb/E_c t_c$	Equal Web Fraction			Equal Area			Equivalent Port Fractions			Computer		% Error	
			$(a/b)_W$	σ_T	ϵ_T	$(a/b)_A$	σ_T	ϵ_T	$(a/b)_E$	σ_T	ϵ_T	σ_T	ϵ_T	Stress	Strain
#1	Steel	6.67×10^{-3}	0.800	+183	0.0691	0.312	+2830	0.710	0.729	+285	0.0744	+312	0.0815	8.7	8.5

Free Grain, Internal Pressure Load

Geometry	a/b	Photoelastic	Computer
		σ_T/p_i	σ_T/p_i
#1	0.8	17.2	17.6
#2	0.7	13.0	13.0
#3	0.6	10.0	10.3
#4	0.8	13.4	13.1

Assume the following properties for the propellant and the case:

$E_c = 30 \times 10^6$ psi	$E = 10^3$
$\nu_c = 0.30$	$\nu = 0.49$
$t_c = 0.06"$	$b = 3"$

This problem is identical to the problem used to compare computer solutions obtained by MSC and by Rohm and Haas.[8] Thus the maximum tangential stress and strain are known from an independent source and can be compared to the results obtained using the much simpler methods of this report. The computer solutions give

$$\sigma_T/p_i = -0.698$$

$$\epsilon_T/p_i = 2.0 \times 10^{-4}/\text{psi}$$

In other words, for an internal pressure of 100 psi, the maximum tangential stress is $\sigma_T = -69.8$ psi and the maximum tangential strain is $\epsilon_T = 2\%$.

To illustrate the dependence of the solution on the proper choice of an "equivalent cylinder," the solution will be obtained using the equal web fraction equivalent, the equal area equivalent, and the effective area equivalent defined by equation (27).

For the equal web fraction equivalent, $(a/b)_W = 0.667$. Substituting this value into equation (20), the pressure factor Δ can be calculated as follows

$$\Delta = 0.0260$$

In this example, since $\Delta^3 << \Delta$, the use of only the first two terms in the series is completely justified.

The average interface pressure exerted by the case on the grain can be calculated using equation (19)

$$p' = p_i(1 - [\Delta - \Delta^2])$$

$$= 0.9747\ p_i$$

Thus, for this example, the internal pressure is transmitted with very little loss to the case. This is a typical result for $\nu \approx 0.5$ and a relatively stiff case (i.e., $Eb/E_c t_c << 1$).

The maximum tangential stress (tangent to the star boundary) is calculated from equation (21)

$$\sigma_T = -0.757\ p_i$$

The maximum tangential strain is calculated from equation (24)

$$\sigma_T = 1.54 \times 10^{-4}\ p_i$$

Thus the tangential stress is negative (compressive) while the tangential strain is positive. It should be emphasized that this stress is the maximum (absolute value) value of tangential stress which occurs at the star port surface. The term tangential is used to indicate the direction parallel to the star boundary at the point where the maximum occurs and does not in general mean the "θ" direction, although in this particular example (simple slot) the two directions do coincide.

This maximum tangential stress is not necessarily the maximum stress occurring at the point. In order to check this, the other two principal stresses must be calculated using the boundary condition $\sigma_n = - p_i$ and equation (3)

$$\sigma_{zz} = \nu(\sigma_{xx} + \sigma_{yy}) = \nu(\sigma_n + \sigma_T)$$

$$= - 0.86\ p_i$$

The three-dimensional state of stress for $p_i = 100$ psi is shown below

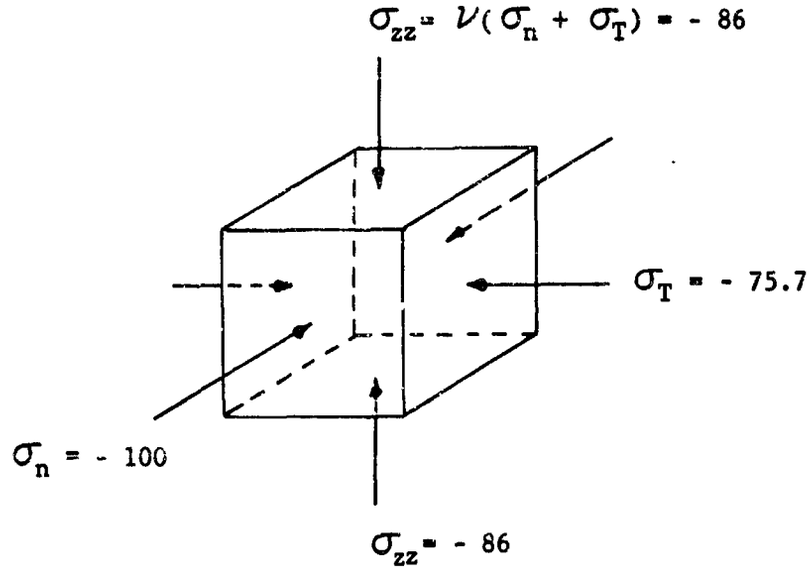

In this example σ_T is the smallest (in absolute value) of the principal stresses.

The same example is now worked out using the equal area equivalent. The port area of the grain is found to be

$$A = 3.64\ in^2$$

Thus an equal port area circular port grain would have a port radius

$$a = 1.08$$

$$\therefore \quad (a/b)_A = 0.36$$

The pressure factor Δ is calculated from equation (20)

$$\Delta = 0.139$$

Thus the interface pressure p' (equation 19) is

$$p' = 0.88\ p_i$$

Equation (21) now gives

$$\sigma_T = 0.122\ p_i$$

The strain ϵ_T is again calculated from equation (24)

$$\epsilon_T = 8.28 \times 10^{-4}\ p_i$$

Note that the calculation based on equal port area gives a very poor estimate of both stress and strain.

As a final example, the calculation will be repeated using the circular port equivalent defined by equation (27)

$$(a/b)_E = 0.618$$

The pressure factor Δ is again calculated from equation (20), using $a/b = 0.618$.

$$\Delta = 0.0336$$

From equation (21)

$$\sigma_T = - 0.688\ p_i$$

and from equation (24)

$$\epsilon_T = 2.08 \times 10^{-4}\ p_i$$

In this particular example, when $(a/b)_E$ is used to calculate p' , the error in stress is 1.4% and the error in strain is 4%, assuming that the computer solution is correct. In all of the comparison problems known to the authors at the present time, $(a/b)_E$ yields the best estimates of stress and strain for a case-bonded grain when compared to the computer solution (Table II).

Thermal Shrinkage. The result of a computer solution for the thermal shrinkage problem can be found in Reference 7. The configuration is a simple slot four star grain with the following parameters:

$a = 8$ in	$t_c = 0.15$ in
$b = 10$ in	$E_c = 30 \times 10^6$ psi
$\sigma = 0.5$ in	$\nu_c = 0.3$
$E = 3 \times 10^3$ psi	$\alpha_T = 6.5 \times 10^{-5}/^\circ F$
$\nu = 0.4987$	$\alpha_c = 6.0 \times 10^{-6}/^\circ F$
$H = 18.2$ (from Figure 8)	$\Delta T = - 100^\circ F$

The computer solution gives the following values for maximum tangential stress and strain

$$\sigma_T = 312 \text{ psi}$$

$$\epsilon_T = 8.15\%$$

For comparison purposes, this problem will be worked out using the methods of this report. To find $(a/b)_E$, note that $(a/b)_W = 0.8$ and $(a/b)_A = 0.318$. Thus using equation (27)

$$(a/b)_E = 0.729$$

Using this value in equation (26), the value of p' is:

$$p' = -15.8 \text{ psi}$$

The maximum tangential stress is now calculated using equation (17) with external pressure p' and internal pressure $p_i = 0$

$$\sigma_T = 285 \text{ psi}$$

This value is in good agreement with the computer solution. On the other hand, when $(a/b)_W$ or $(a/b)_A$ is used in the calculation, the corresponding values of σ_T are

σ_T = 182 psi (equal web fraction)

σ_T = 2,760 psi (equal area)

To continue with the solution, σ_n and σ_{zz} are now calculated. Since the internal pressure is assumed to be zero, $\sigma_n = 0$ and

$$\sigma_{zz} = \nu(\sigma_T + \sigma_n) - E\alpha_T\Delta T$$

$$= 163 \text{ psi}$$

The tangential strain can now be calculated from equations

$$\epsilon_T = \frac{1}{E}\left[\sigma_T - \nu(\sigma_n + \sigma_{zz})\right] + \alpha_T\Delta T$$

$$= 7.46 \times 10^{-2}$$

$$= 7.46\%$$

Thus the strain, calculated using $(a/b)_E$, is in error 8.5% for this problem, assuming that the computer solution is the correct solution.

XII.

EMPIRICAL REPRESENTATION OF EXPERIMENTAL DATA

As was indicated earlier in the section on test results, the data obtained for the simple slot configuration of Figure 7-a may be represented by the empirical equation

$$H = N^{-1/3}\sqrt{\frac{a+b}{b-a}}\left[1 + 2\sqrt{a/\rho}\right] \qquad (28)$$

It would be desirable to determine similar empirical relationships to represent the data for each family tested. It has been shown in the previous sections that the variation with N is adequately described by the $N^{-1/3}$ rule.

Inspection of equation (28) indicates that if N and (a/b) are held constant that a plot of H versus $\sqrt{a/\rho}$ would yield straight lines. This may be seen in Figure 54.

For the slot width effect tests it was shown that the dependence on $N^{-1/3}$ held (see Figure 26); however, no additional simple functional dependency has been observed.

For the positive wedge angle tests the $N^{-1/3}$ rule was shown to hold (Figure 34), and the dependence on the fillet radius factor may be seen in Figure 55. It is seen here that the functional form for the empirical relationship is:

$$H = N^{-1/3}\left[C_1(\alpha, a/b) + C_2(\alpha, a/b)\sqrt{a/\rho}\right]h(\alpha, a/b) \qquad (29)$$

indicating that the dependence on $\sqrt{a/\rho}$ is linear. This is also true for the negative wedge angle family and the elliptical slot tip family as may be seen in Figures 56 and 57.

Judging from the results shown in the figures, it is seen that the functional dependency of H on the parameters N and a/ρ for the simple slot, the positive wedge angle, the negative wedge angle, and the elliptical slot tip tests is adequately represented as described above. The task then remains to determine the unknown functional form of equation (29) for the latter three familes. This work is presently underway and will hopefully be reported in a later report.

XIII.

CONCLUSIONS

Parametric photoelastic investigations of four families of internally perforated rocket grains have been conducted. The results are presented in graphical form showing the stress factor H as a function of the four geometrical parameters necessary to describe each family. Good correlation of these data with previous work of the authors and analytical and numerical solutions is shown.

Methods of applying the experimentally obtained data to other problems of interest have been discussed. In particular the problem of a case-bonded grain subjected to both pressure and thermal loads has been considered. An engineering "rule of thumb" is suggested which allows quite accurate calculations of the stress and strain problems considered.

A limited number of numerical solutions for problems similar to those discussed here have recently been published in Reference 7. A comparison of these and all other known numerical solutions was made with those obtained using data obtained from this study. In general good agreement was obtained. In all cases the disagreement was less than 10% in stress and 15% in strain.

Empirical formulas are derived in some cases to represent the variation of the stress factor as a function of the various parameters. In all cases the variation with the number of star points has been shown to be $N^{-1/3}$. In all cases other than the slot width tests the functional dependency on the fillet radius factor has been shown to be linear with $\sqrt{a/\rho}$.

REFERENCES

1. D. D. Ordahl and M. L. Williams, "Preliminary Photoelastic Design Data for Stresses in Rocket Grains," Jet Propulsion, June 1957.

2. Durelli and Lake, "Device for Applying Uniform Loading to Boundaries of Complicated Shape," Proceedings of the Society for Experimental Stress Analysis, Vol. II, no. 1, 1953.

3. M. E. Fourney and R. R. Parmerter, "Stress Concentrations for Internally Perforated Star Grains," NAVWEPS Report 7758, 1961.

4. S. Timoshinko and J. N. Goodier, Theory of Elasticity, McGraw-Hill Book Company, Inc., New York, 1951.

5. Worthing and Geffner, Treatment of Experimental Data, Wiley, 1943.

6. M. L. Williams, P. J. Blatz, and R. A. Schapery, "Fundamental Studies Relating to Systems Analysis of Solid Propellants," GALCIT SM 61-5, California Institute of Technology, 1961.

7. E. B. Becker and J. J. Brisbare, "Application of the Finite Element Method to Stress Analysis of Solid Propellant Rocket Grains," Rohm and Haas Report No. S-76, November 18, 1965.

8. Private Communication, "Mathematical Sciences Corporation - Rohm and Haas Company Comparison Problem," November, 1965.

9. "Engineering Methods for Grain Structural Integrity Analysis," Lockheed Propulsion Company Report No. 578/556-F-3, May, 1963.

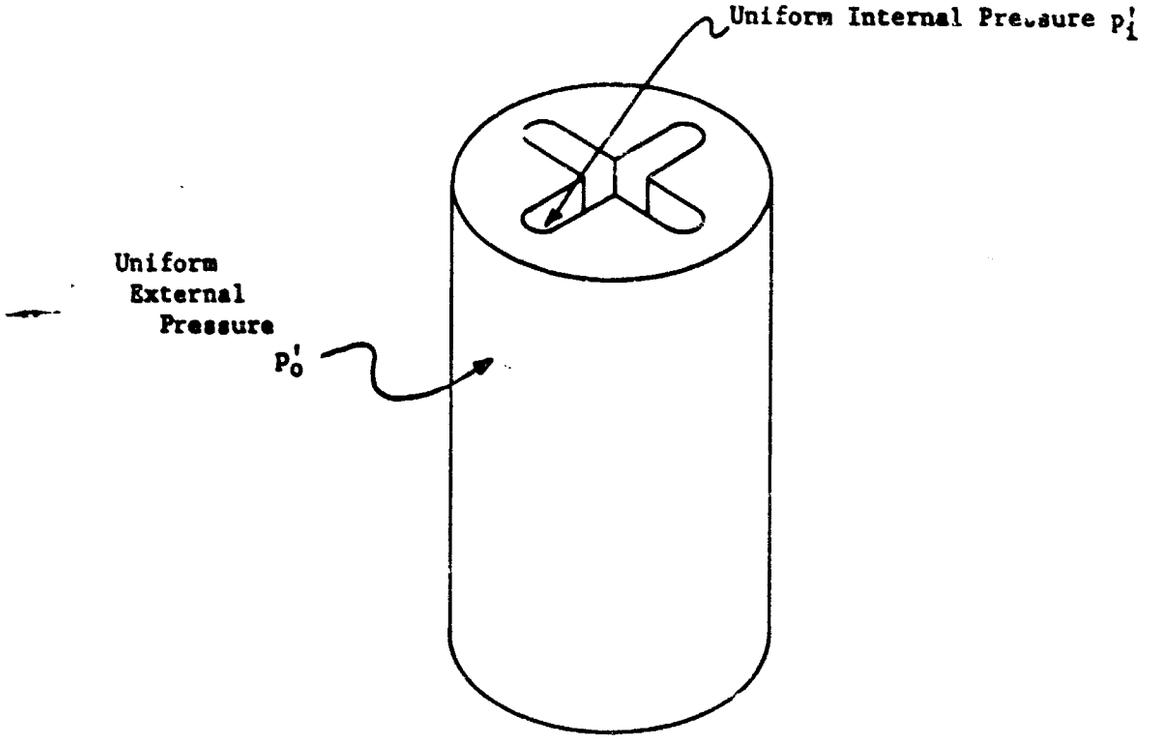

-a-
Plane Strain Problem

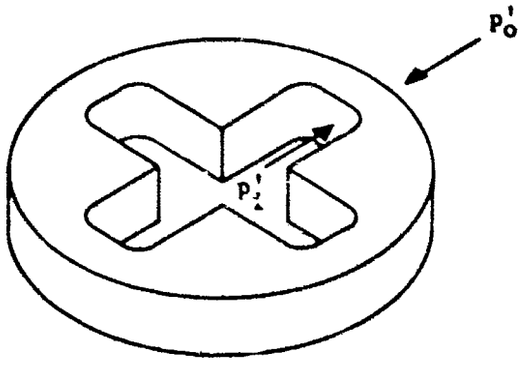

-b-
Plane Stress Problem

FIGURE 1

GEOMETRY AND LOADING CONDITIONS FOR GENERAL PROBLEMS

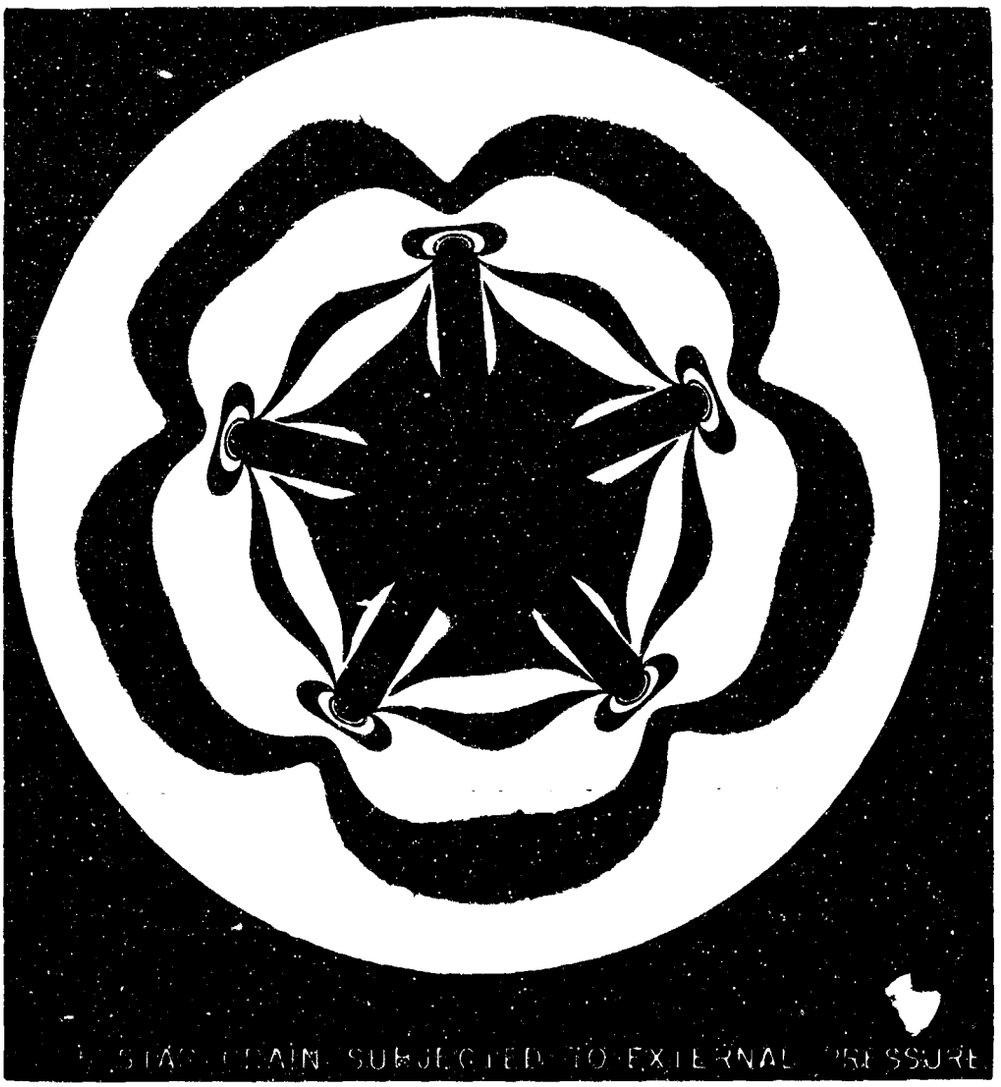

FIGURE 2

ISOCHROMATIC FRINGE PATTERN
FOR TYPICAL SIMPLE SLOT CONFIGURATION

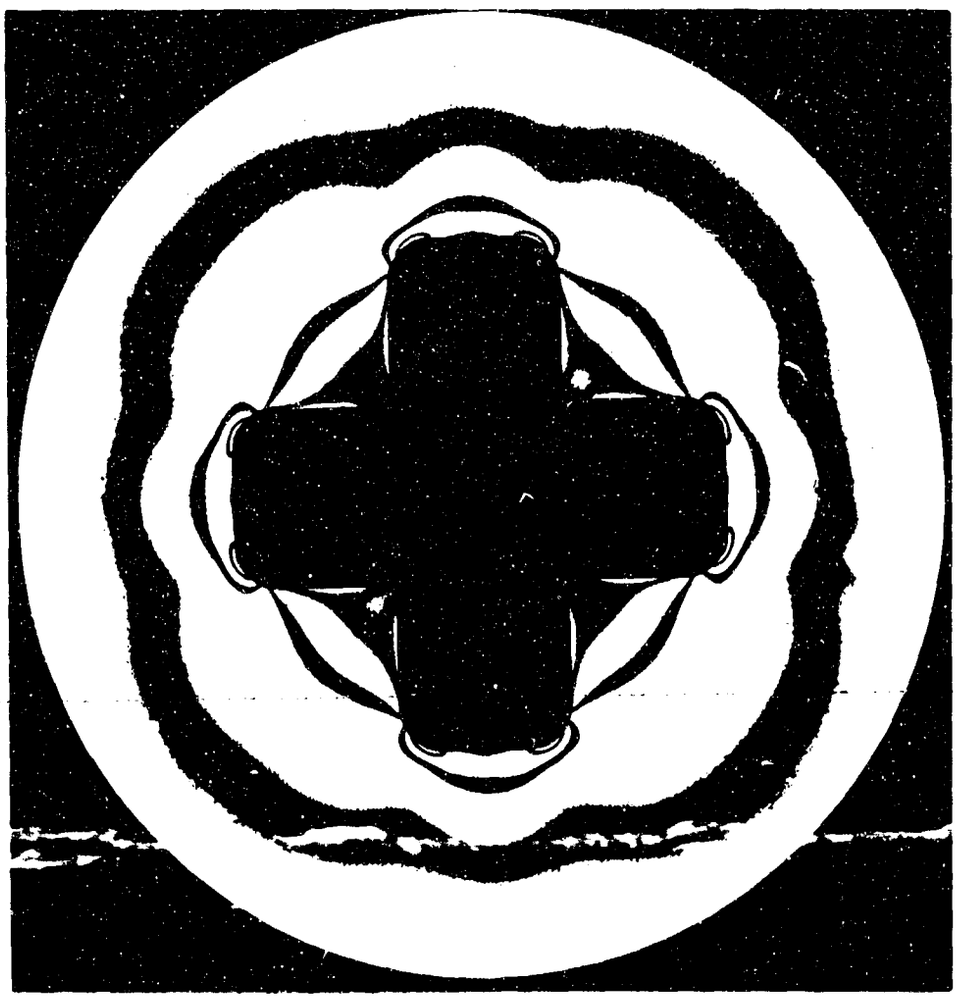

FIGURE 3

ISOCHROMATIC FRINGE PATTERN
FOR TYPICAL SLOT WIDTH TEST CONFIGURATION

$N = 4$, $d/2\rho = 2$, $a/b = 70\%$, $a/\rho = 7.98$, $H = 8.46$

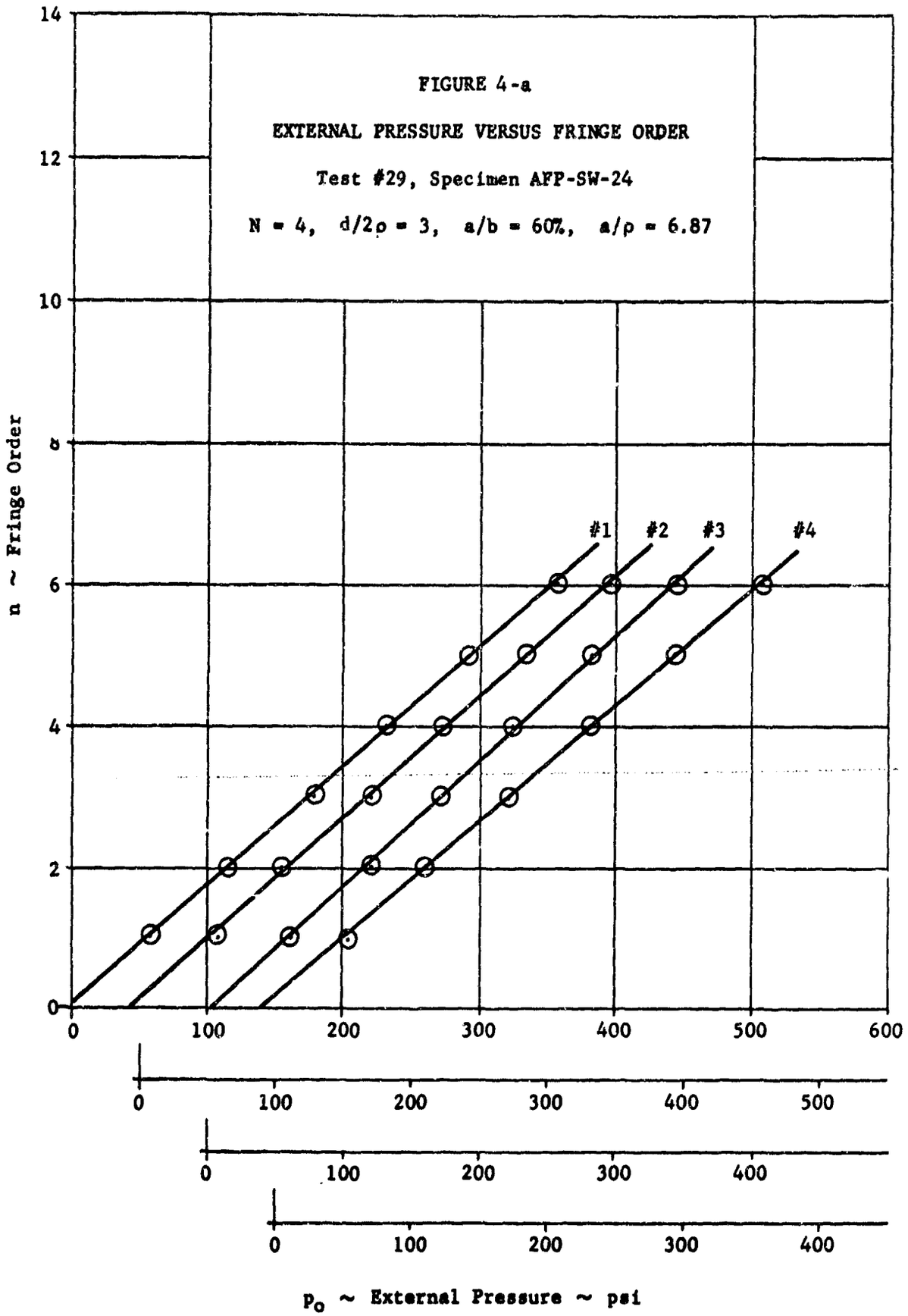
FIGURE 4-a
EXTERNAL PRESSURE VERSUS FRINGE ORDER
Test #29, Specimen AFP-SW-24
N = 4, d/2ρ = 3, a/b = 60%, a/ρ = 6.87
n ~ Fringe Order
#1
#2
#3
#4
0
2
4
6
8
10
12
14
0
100
200
300
400
500
600
p_o ~ External Pressure ~ psi

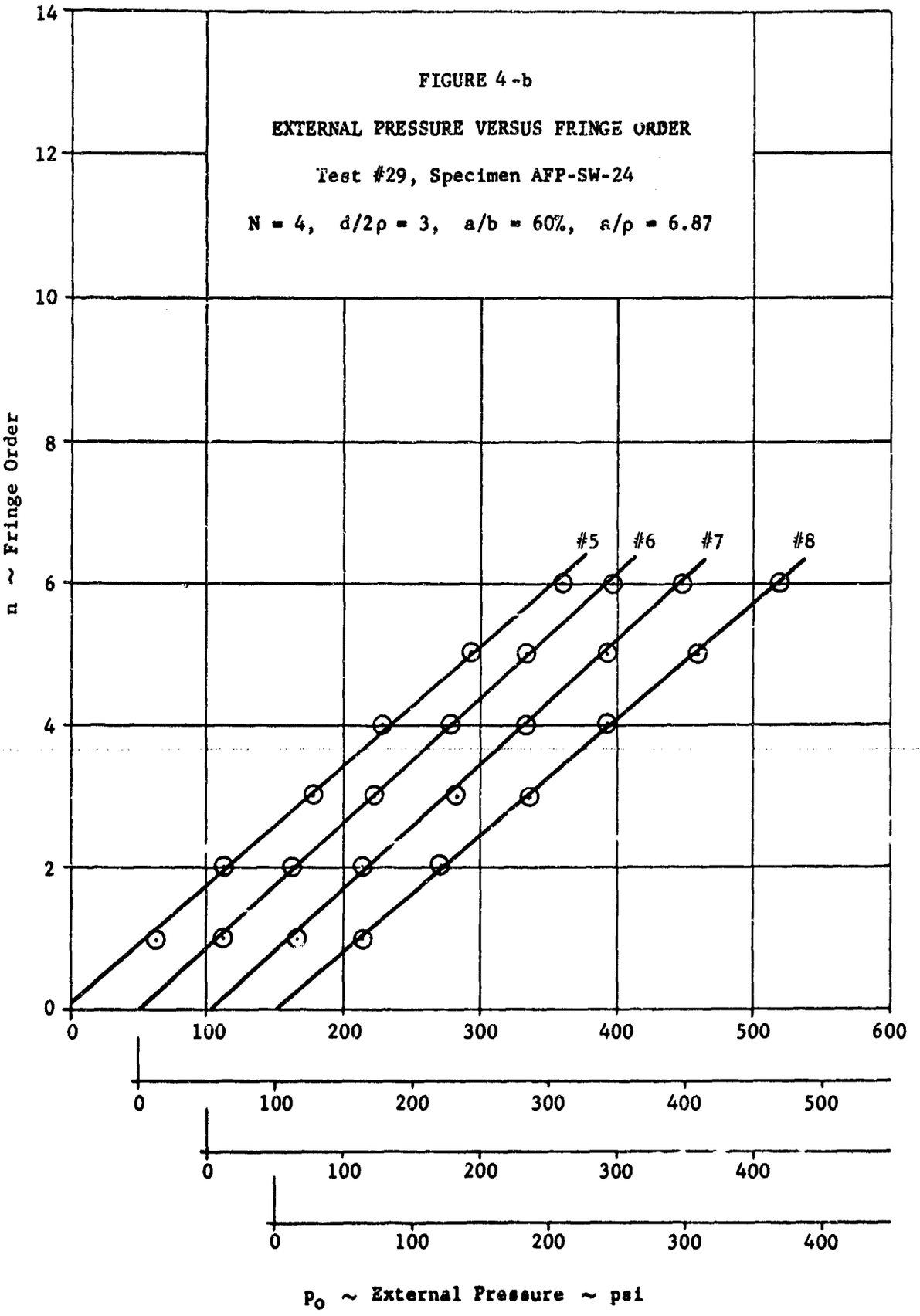
FIGURE 4-b
EXTERNAL PRESSURE VERSUS FRINGE ORDER
Test #29, Specimen AFP-SW-24
N = 4, d/2ρ = 3, a/b = 60%, ε/ρ = 6.87
n ~ Fringe Order
#5
#6
#7
#8
0
2
4
6
8
10
12
14
0
100
200
300
400
500
600
p_o ~ External Pressure ~ psi

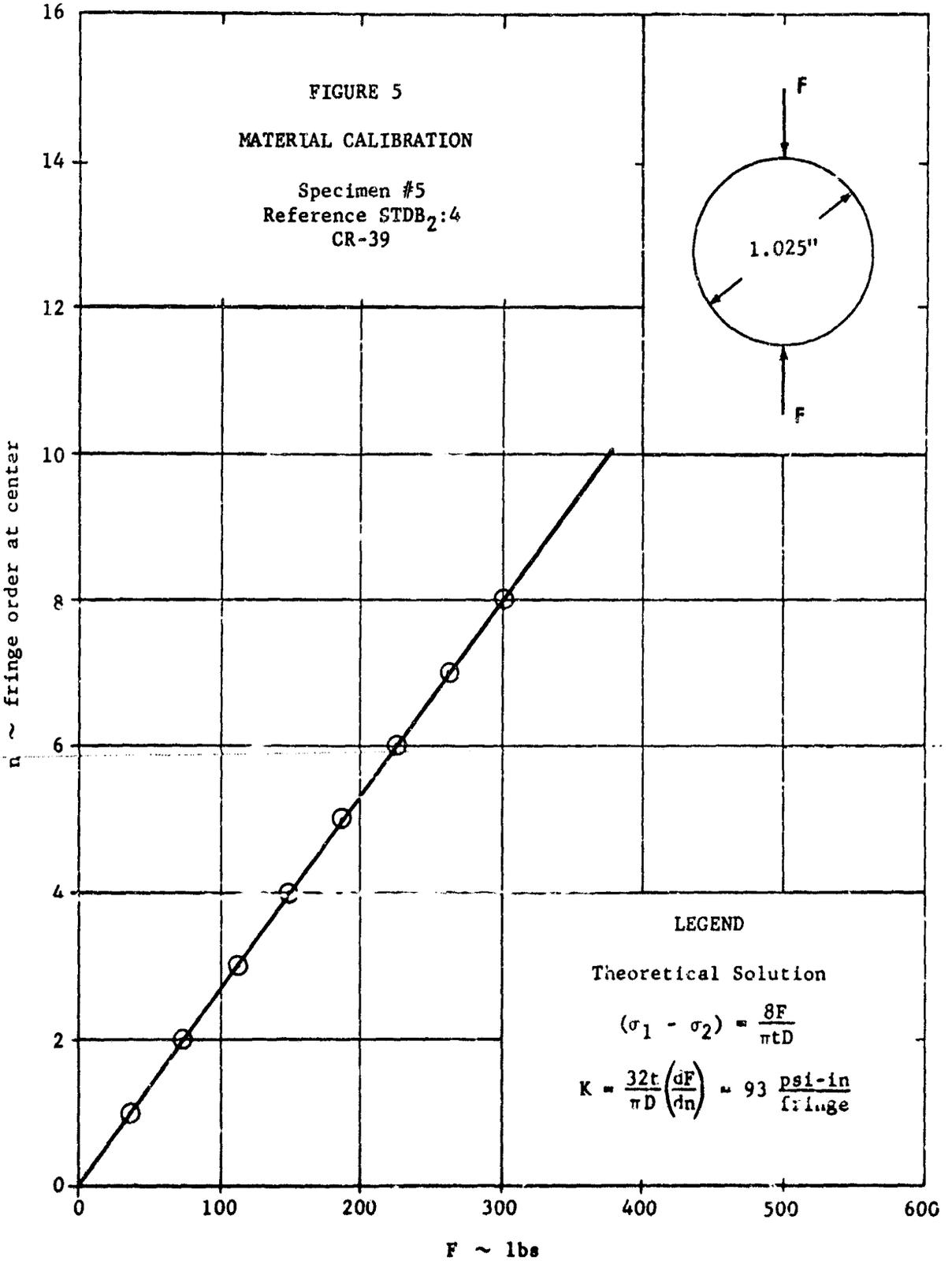
FIGURE 5
MATERIAL CALIBRATION
Specimen #5
Reference STDB2:4
CR-39
F
1.025"
F
LEGEND
Theoretical Solution
$(\sigma_1 - \sigma_2) = \frac{8F}{\pi tD}$
$K = \frac{32t}{\pi D}\left(\frac{dF}{dn}\right) = 93 \frac{psi\text{-}in}{fringe}$
n ~ fringe order at center
F ~ lbs
0
2
4
6
8
10
12
14
16
0
100
200
300
400
500
600

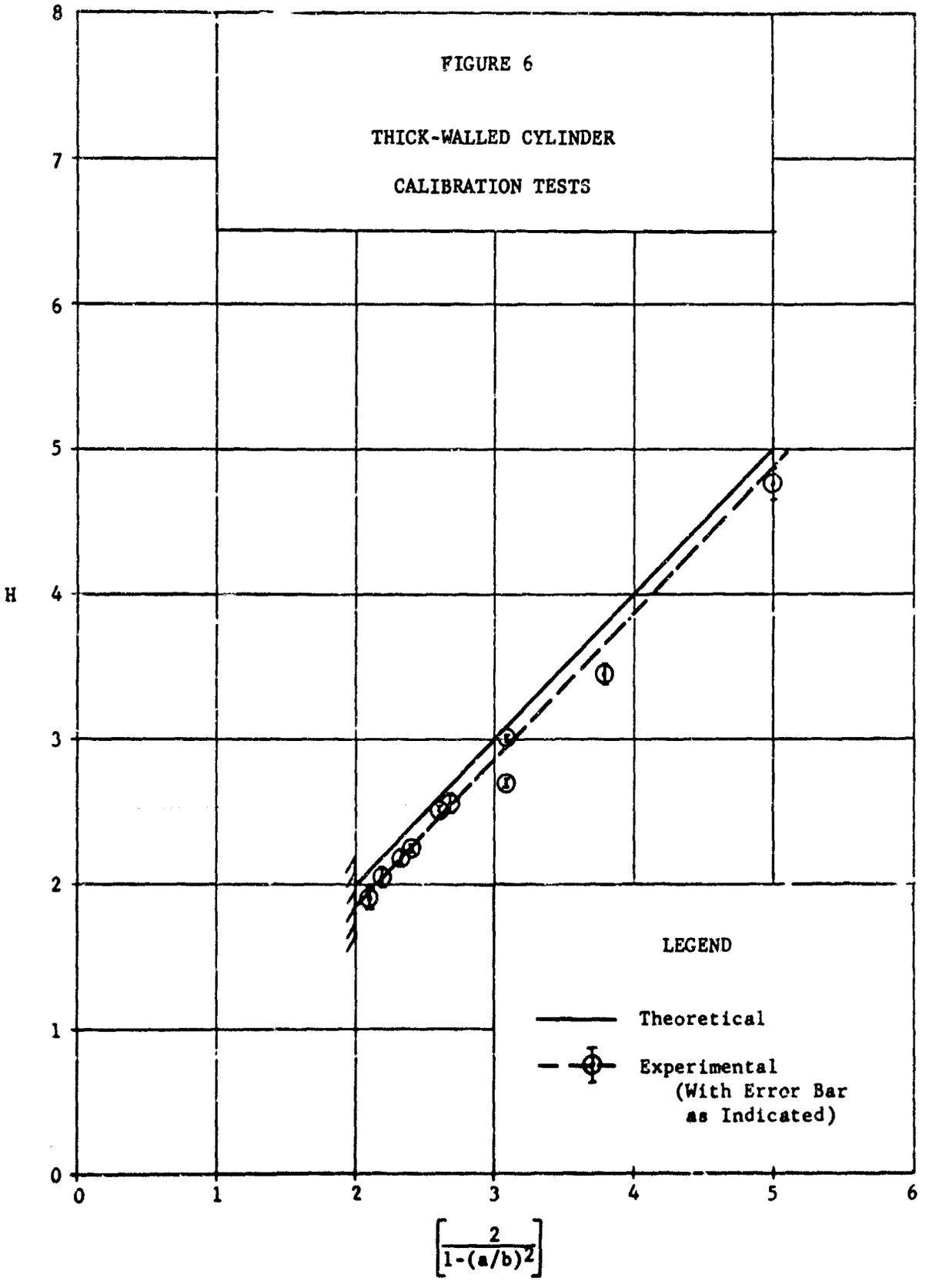
FIGURE 6
THICK-WALLED CYLINDER
CALIBRATION TESTS
H
0
1
2
3
4
5
6
7
8
$\left[\frac{2}{1-(a/b)^2}\right]$
LEGEND
Theoretical
Experimental
(With Error Bar
as Indicated)

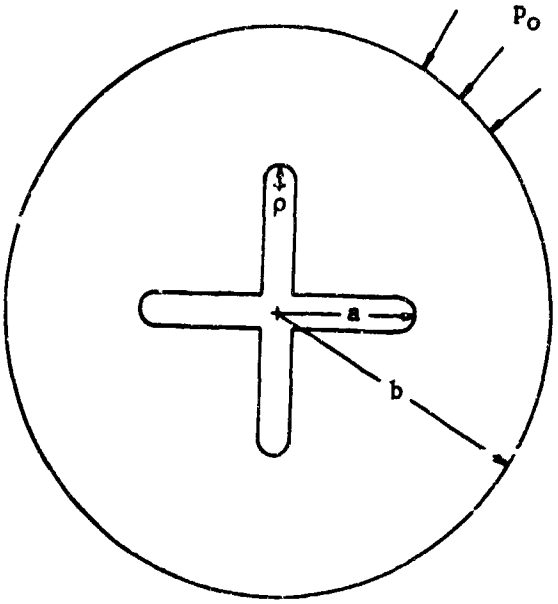

-a-
Simple Slotted Grains
$d/2\rho = 1$ (NOTS Data)

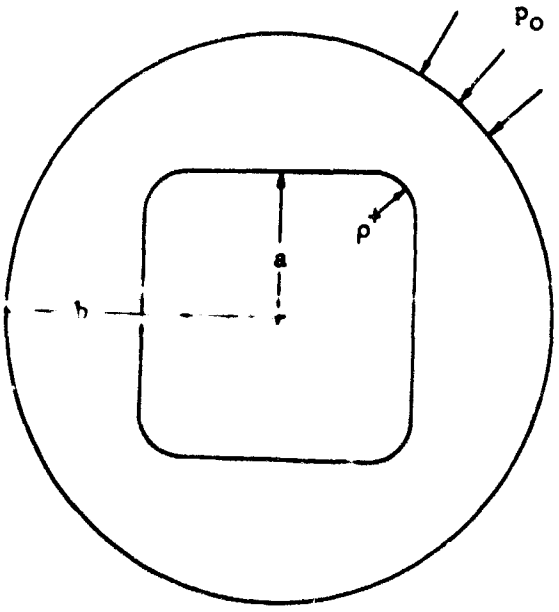

-b-
Limit Squares

FIGURE 7
GEOMETRY OF LIMIT CASES

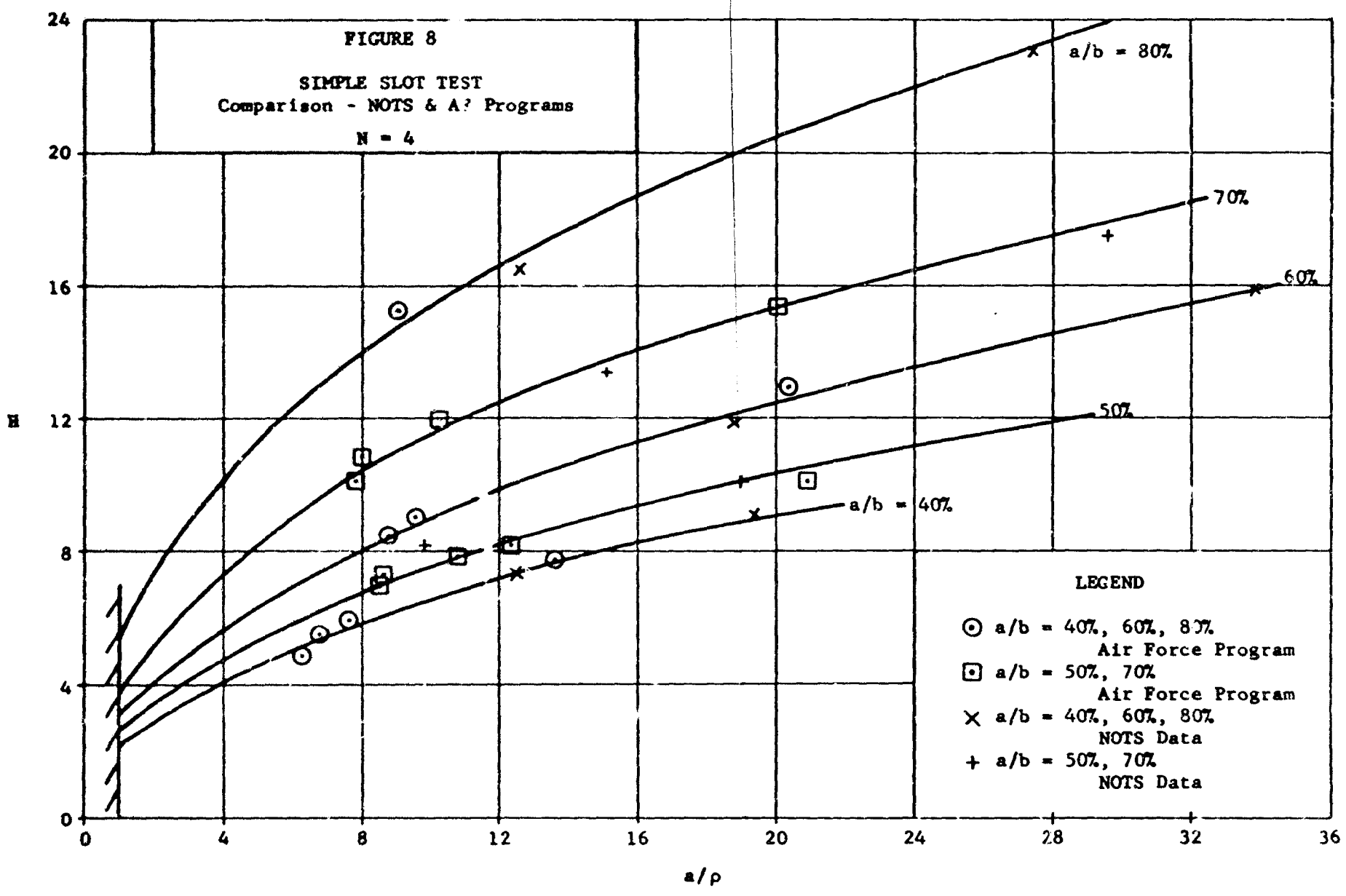
FIGURE 8
SIMPLE SLOT TEST
Comparison - NOTS & AF Programs
N = 4
a/b = 80%
70%
60%
50%
a/b = 40%
H
a/ρ
0
4
8
12
16
20
24
28
32
36
LEGEND
a/b = 40%, 60%, 80%
Air Force Program
a/b = 50%, 70%
Air Force Program
a/b = 40%, 60%, 80%
NOTS Data
a/b = 50%, 70%
NOTS Data

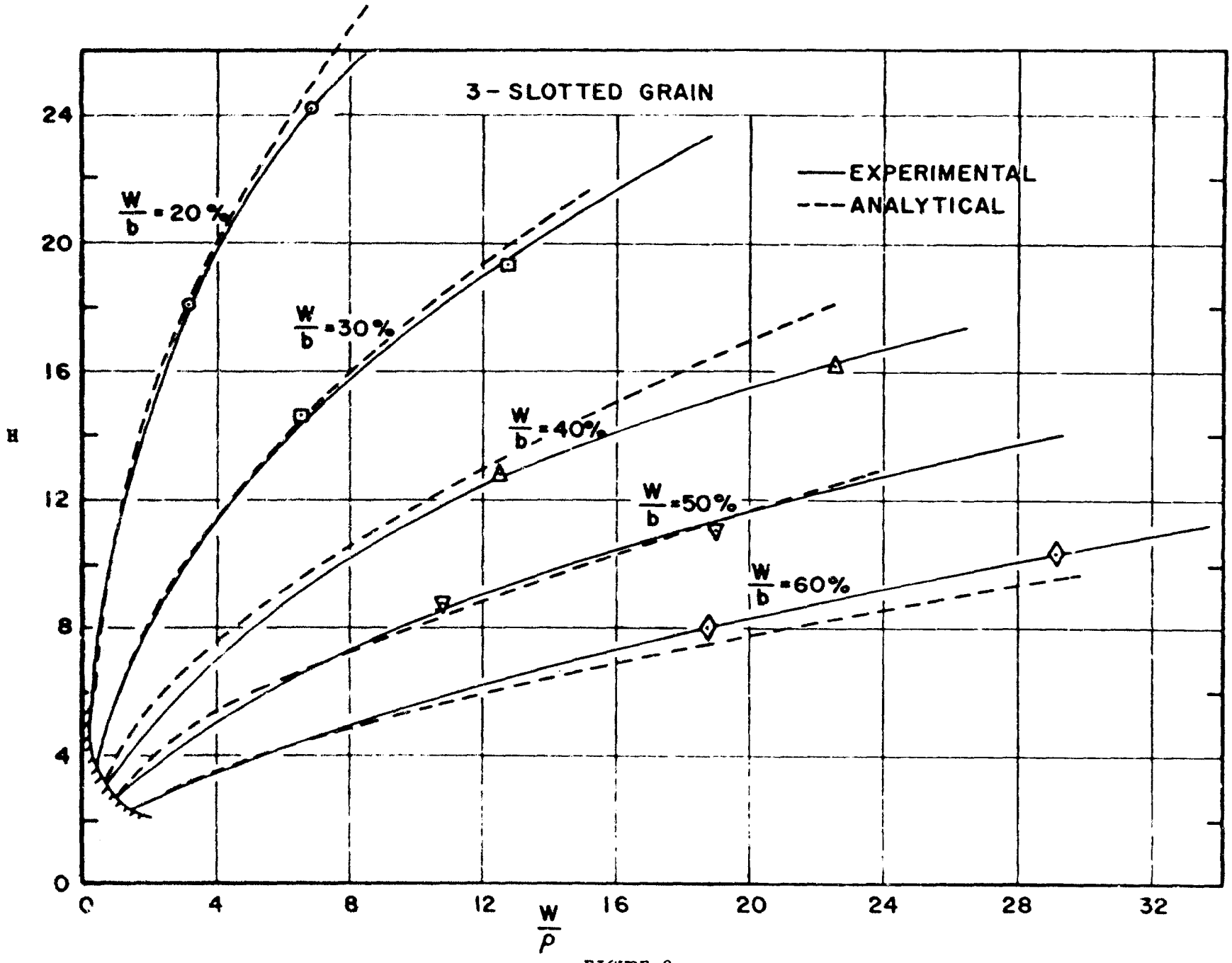
3 - SLOTTED GRAIN
EXPERIMENTAL
ANALYTICAL
W/b = 20%
W/b = 30%
W/b = 40%
W/b = 50%
W/b = 60%
H
W/ρ
0
4
8
12
16
20
24
28
32

FIGURE 9

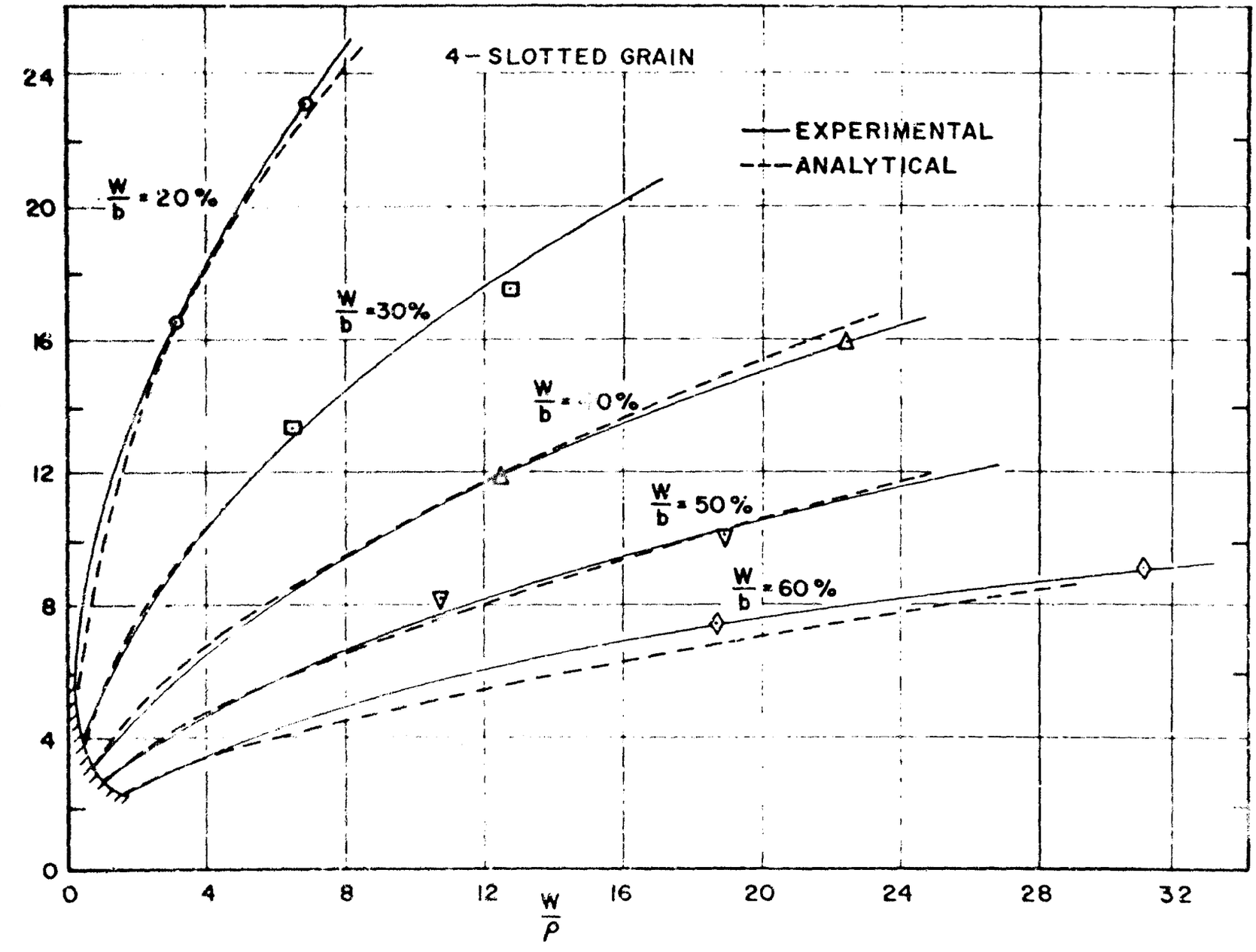
4-SLOTTED GRAIN
EXPERIMENTAL
ANALYTICAL
W/b = 20%
W/b = 30%
W/b = 40%
W/b = 50%
W/b = 60%
0
4
8
12
16
20
24
28
32
W/ρ

FIGURE 10

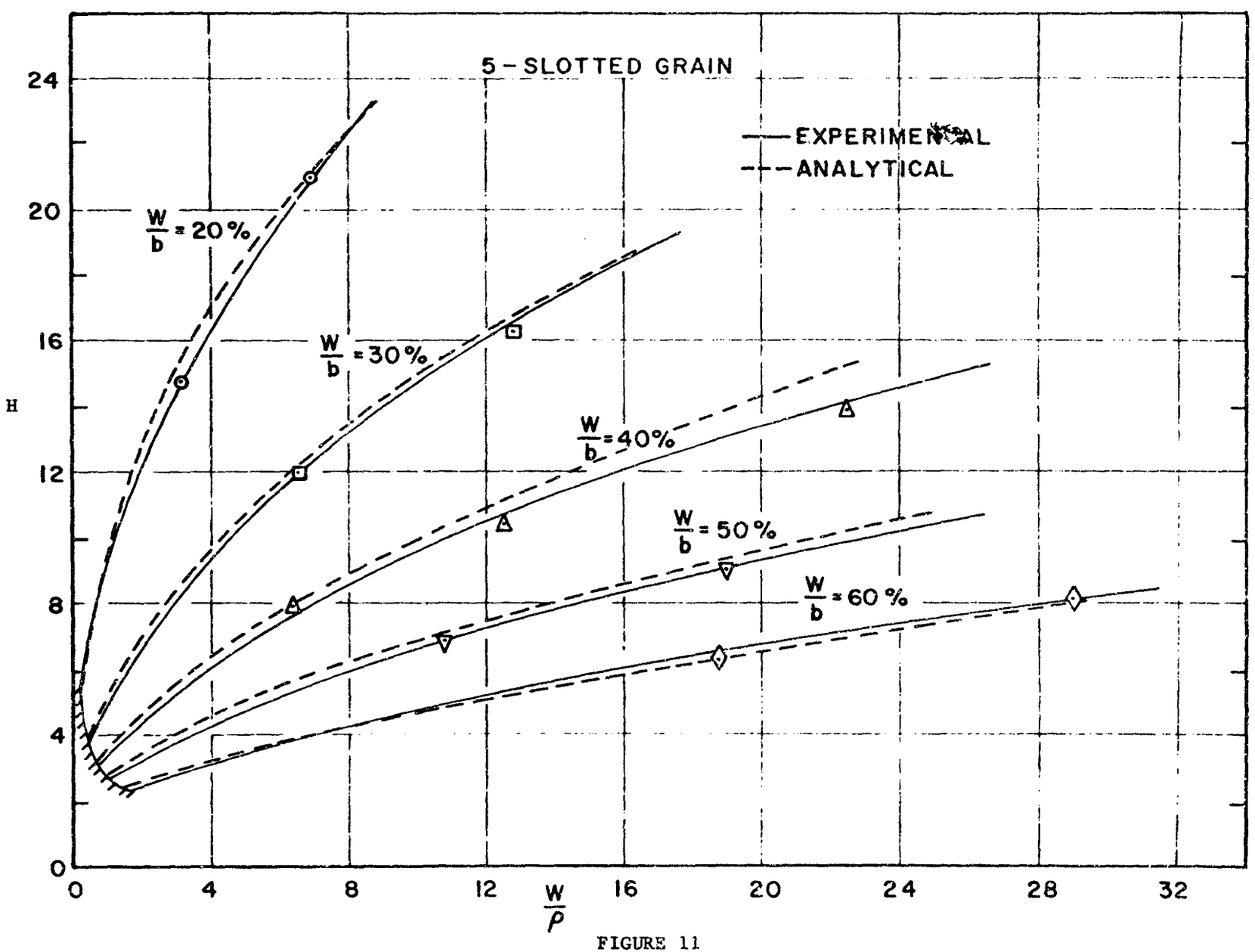
5 - SLOTTED GRAIN
EXPERIMENTAL
ANALYTICAL
W/b = 20%
W/b = 30%
W/b = 40%
W/b = 50%
W/b = 60%
H
W/ρ
0
4
8
12
16
20
24
28
32

FIGURE 11

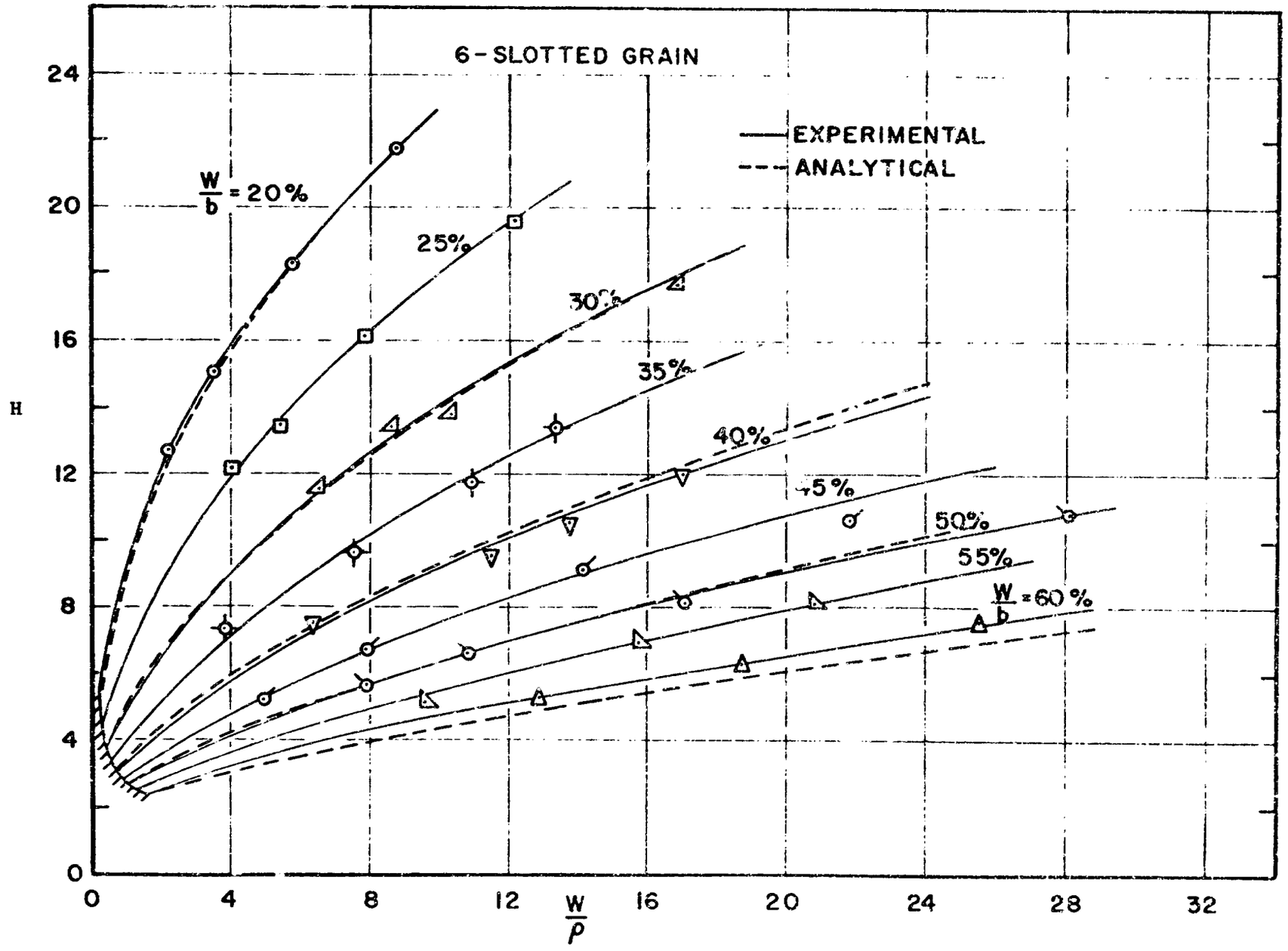
6-SLOTTED GRAIN
EXPERIMENTAL
ANALYTICAL
W/b = 20%
25%
30%
35%
40%
45%
50%
55%
W/b = 60%
H
W/P
0
4
8
12
16
20
24
28
32

FIGURE 12

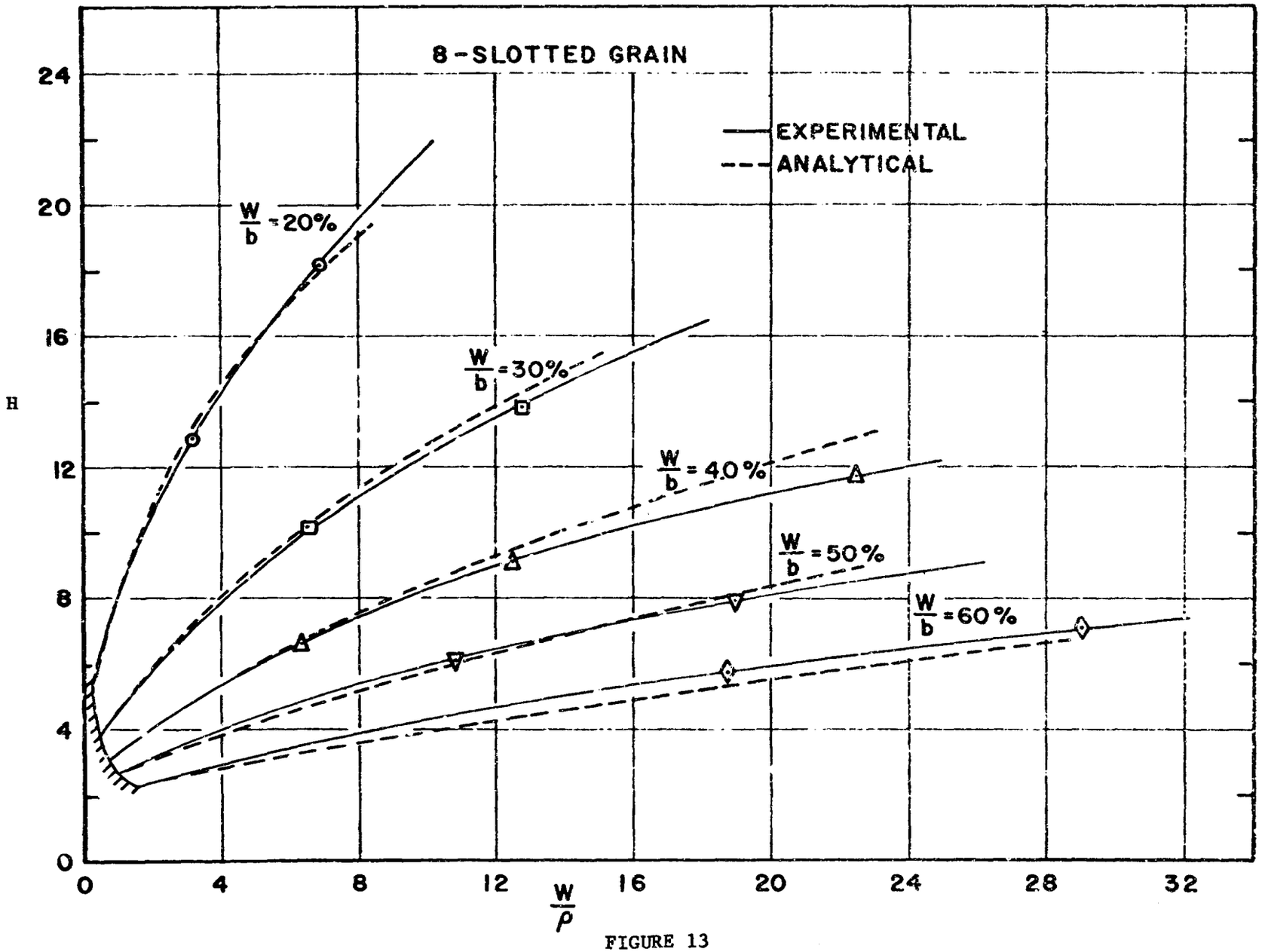
8-SLOTTED GRAIN
EXPERIMENTAL
ANALYTICAL
W/b = 20%
W/b = 30%
W/b = 40%
W/b = 50%
W/b = 60%
H
W/ρ
0
4
8
12
16
20
24
28
32

FIGURE 13

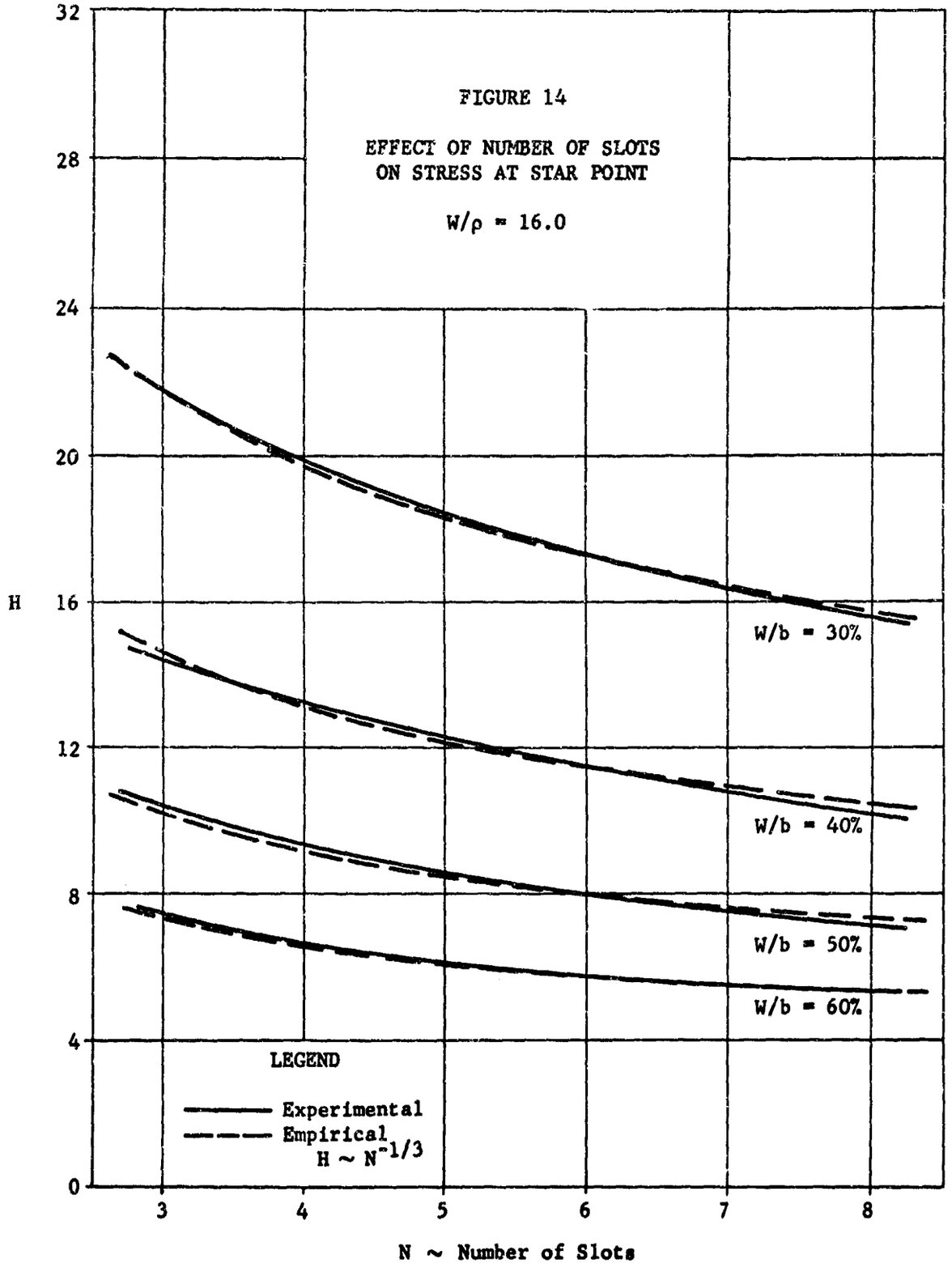
FIGURE 14
EFFECT OF NUMBER OF SLOTS ON STRESS AT STAR POINT
W/ρ = 16.0
H
32
28
24
20
16
12
8
4
0
3
4
5
6
7
8
N ~ Number of Slots
W/b = 30%
W/b = 40%
W/b = 50%
W/b = 60%
LEGEND
Experimental
Empirical
H ~ N^-1/3

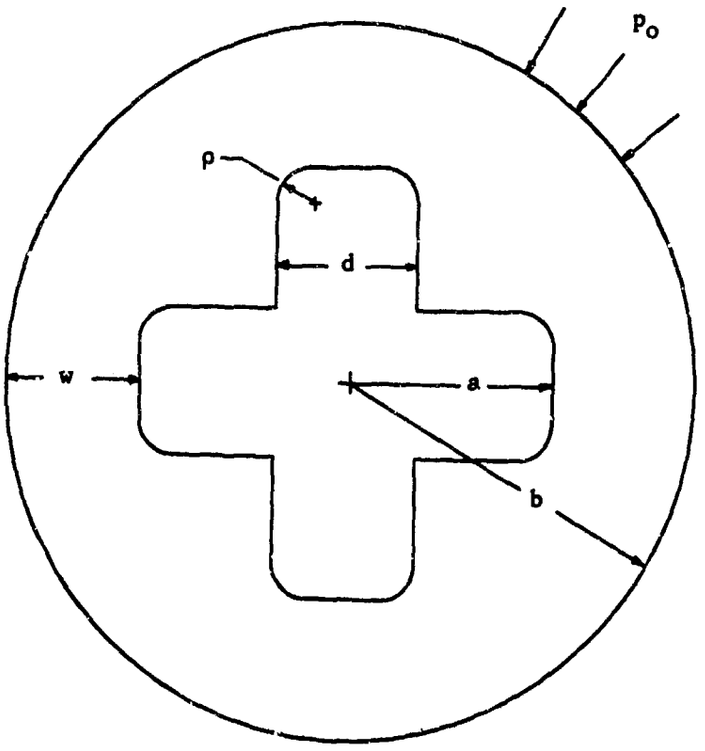

FIGURE 15

GEOMETRY OF TYPICAL CROSS SECTION

FOR SLOT WIDTH EFFECT TESTS

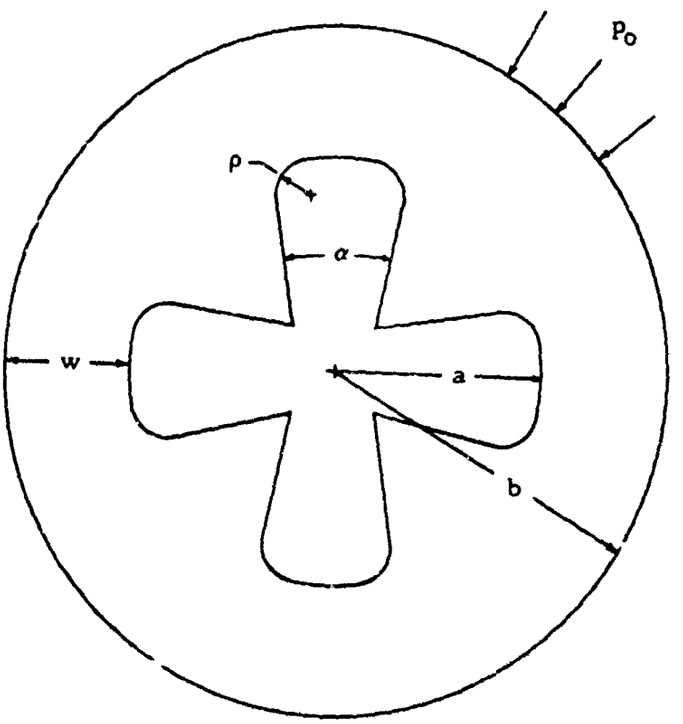

FIGURE 16

GEOMETRY OF TYPICAL CROSS SECTION

FOR POSITIVE WEDGE ANGLE TESTS

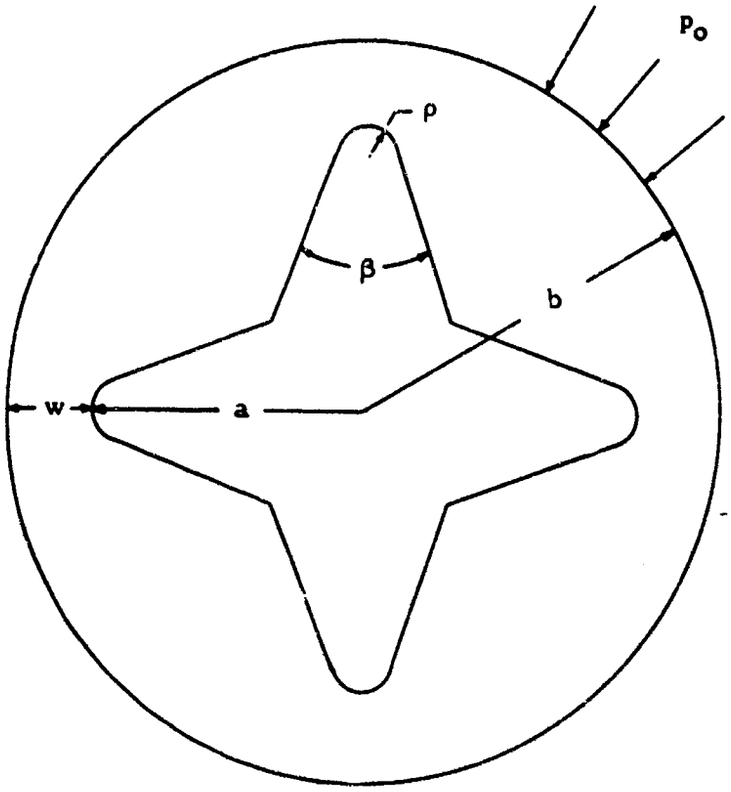

FIGURE 17

GEOMETRY OF TYPICAL CROSS SECTION

FOR NEGATIVE WEDGE ANGLE TESTS

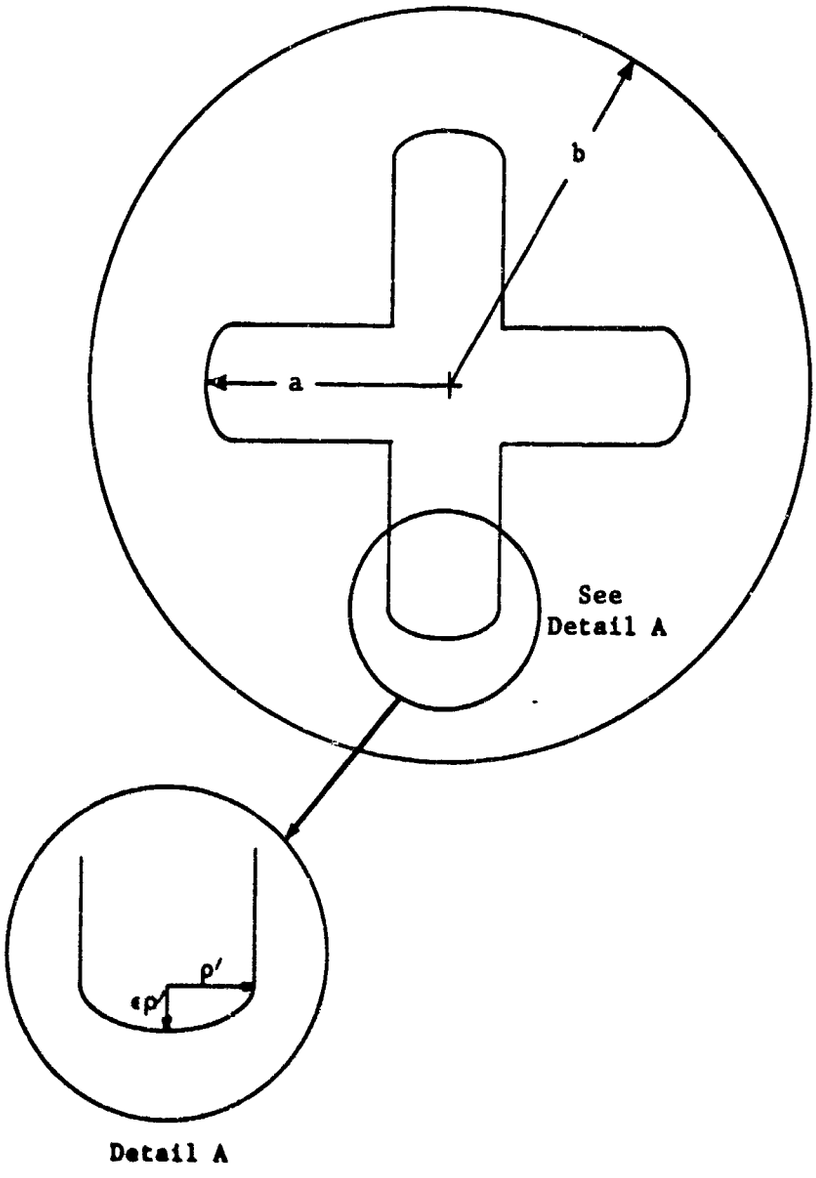

FIGURE 18

GEOMETRY OF TYPICAL CROSS SECTION

FOR ELLIPTICAL SLOT TIP TESTS

FIGURE 19

SLOT WIDTH EFFECT TESTS

N = 4, $d/2\rho = 2$

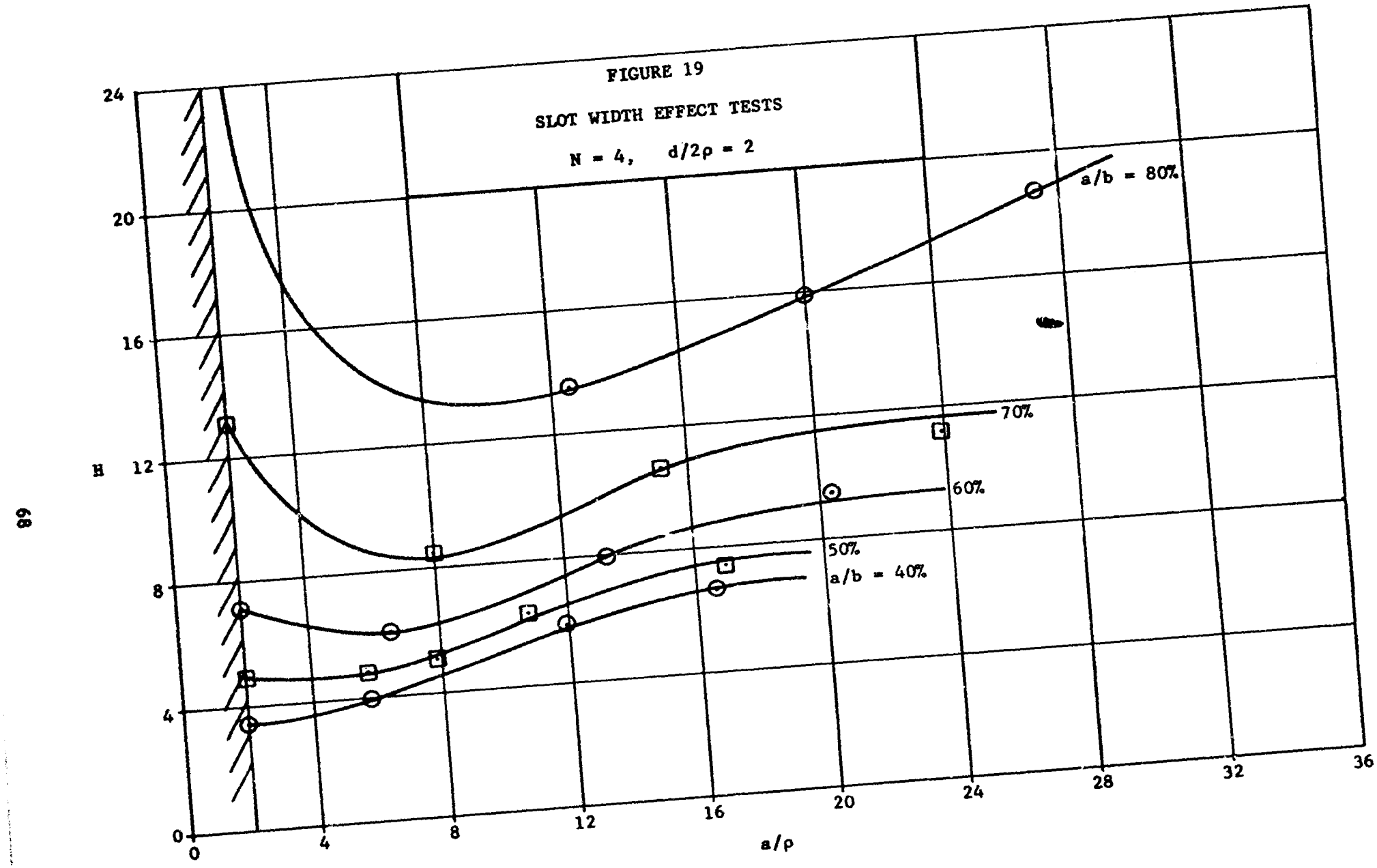

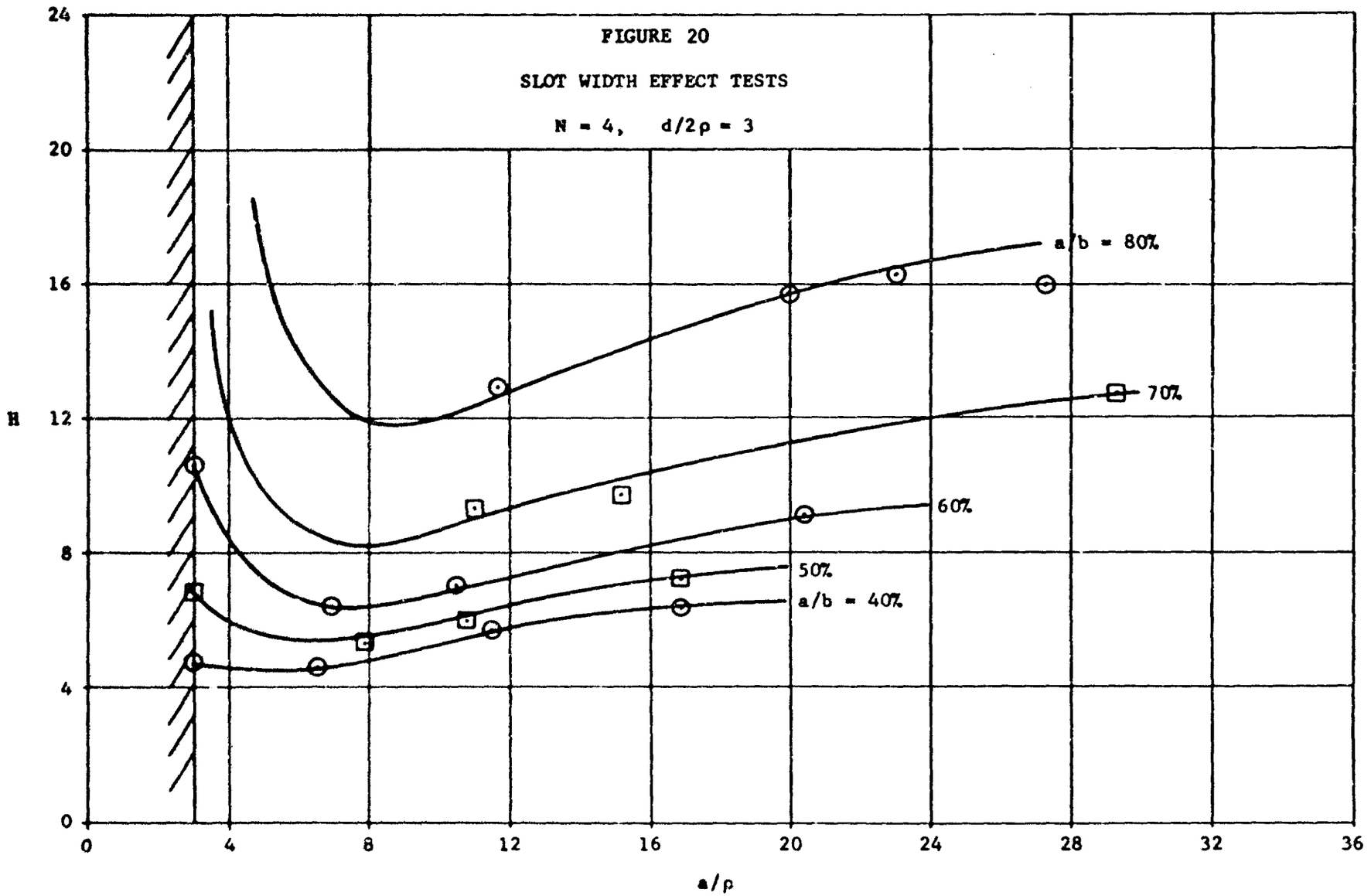
FIGURE 20
SLOT WIDTH EFFECT TESTS
N = 4, d/2ρ = 3
H
a/ρ
a/b = 80%
70%
60%
50%
a/b = 40%
0
4
8
12
16
20
24
28
32
36

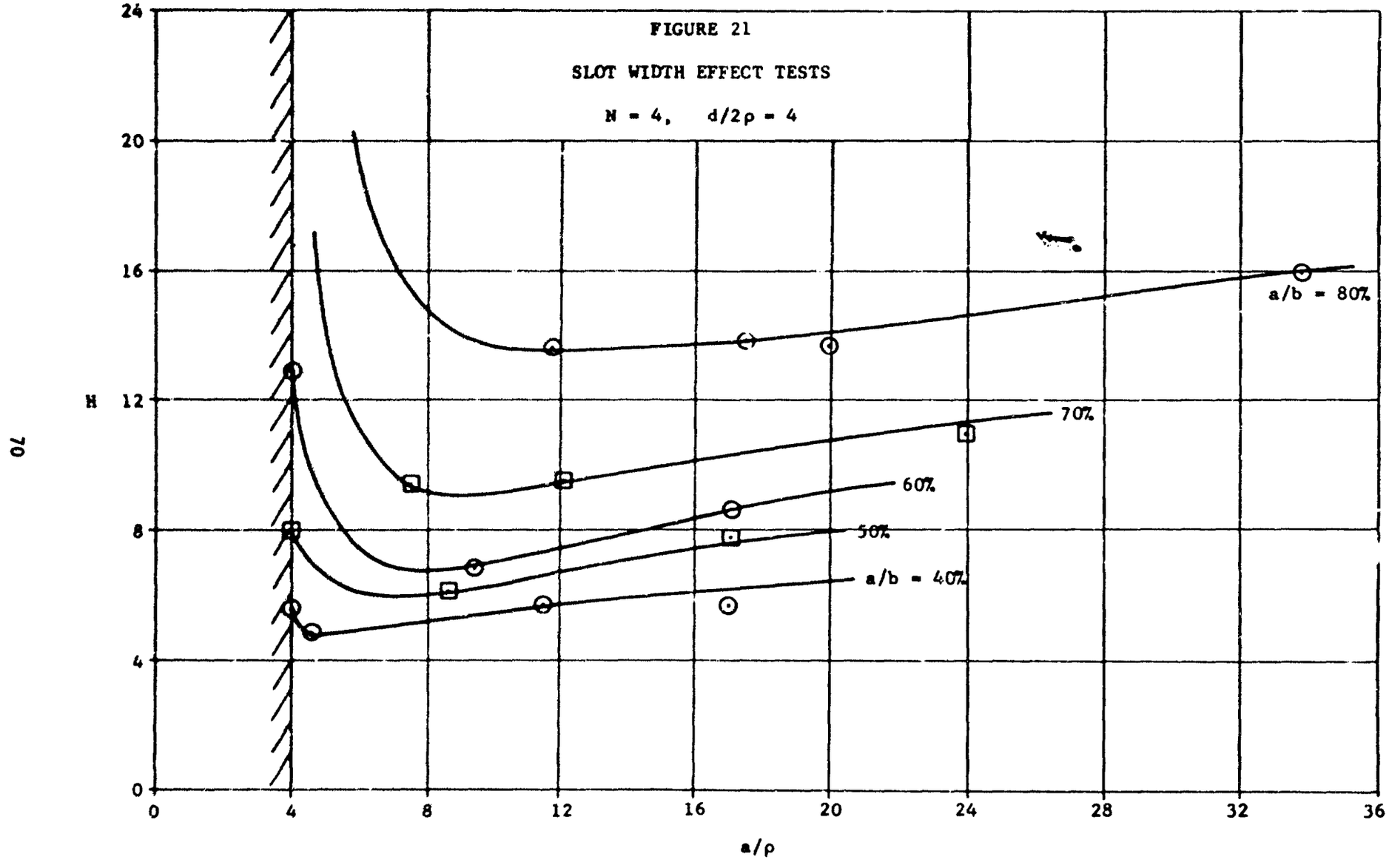
FIGURE 21
SLOT WIDTH EFFECT TESTS
N = 4, d/2ρ = 4
24
20
16
12
8
4
0
H
0
4
8
12
16
20
24
28
32
36
a/ρ
a/b = 80%
70%
60%
50%
a/b = 40%

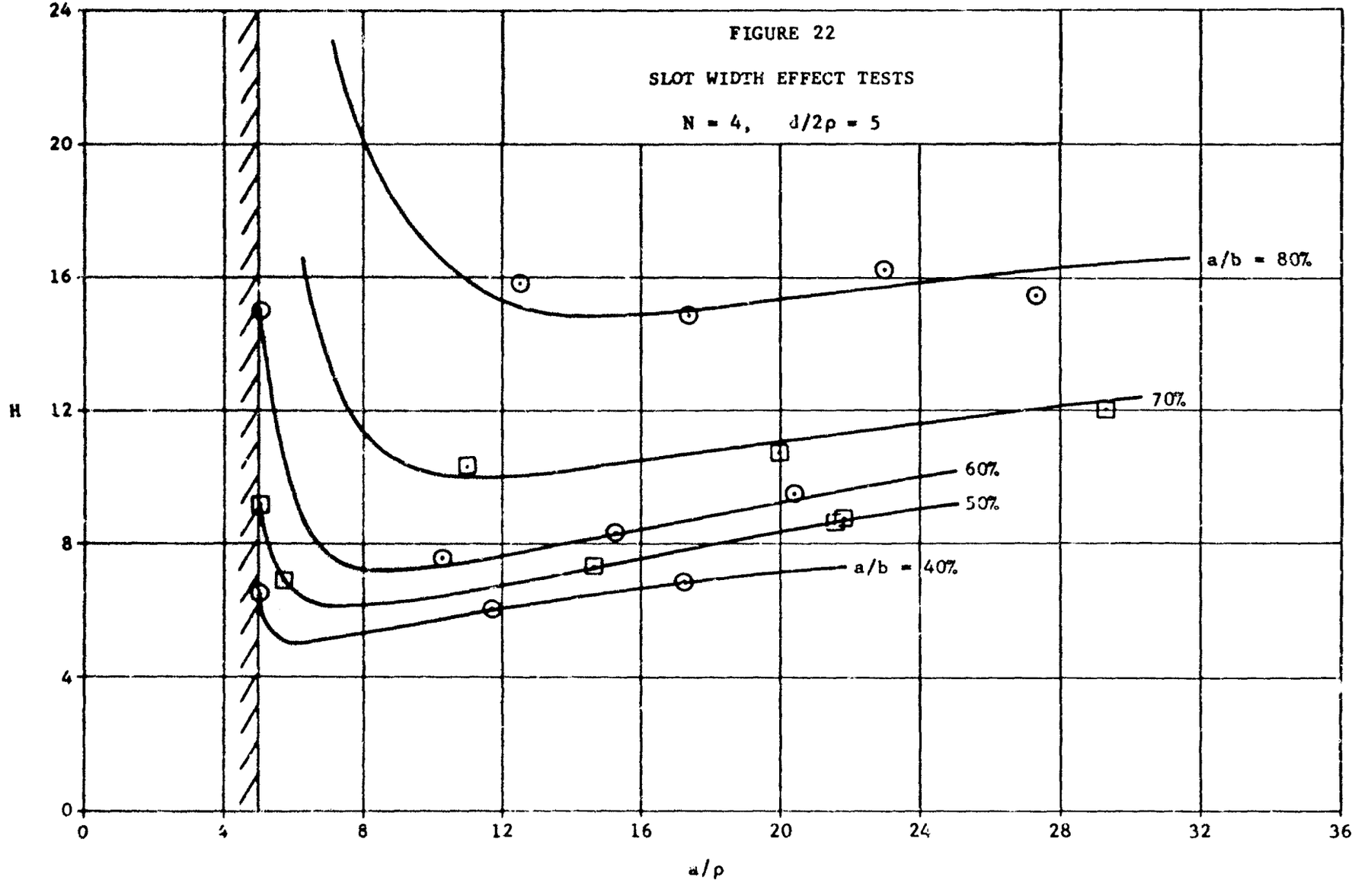
FIGURE 22
SLOT WIDTH EFFECT TESTS
N = 4, d/2ρ = 5
H
a/ρ
a/b = 80%
70%
60%
50%
a/b = 40%
0
4
8
12
16
20
24
28
32
36

FIGURE 23

SLOT WIDTH EFFECT
LIMIT POINT TESTS

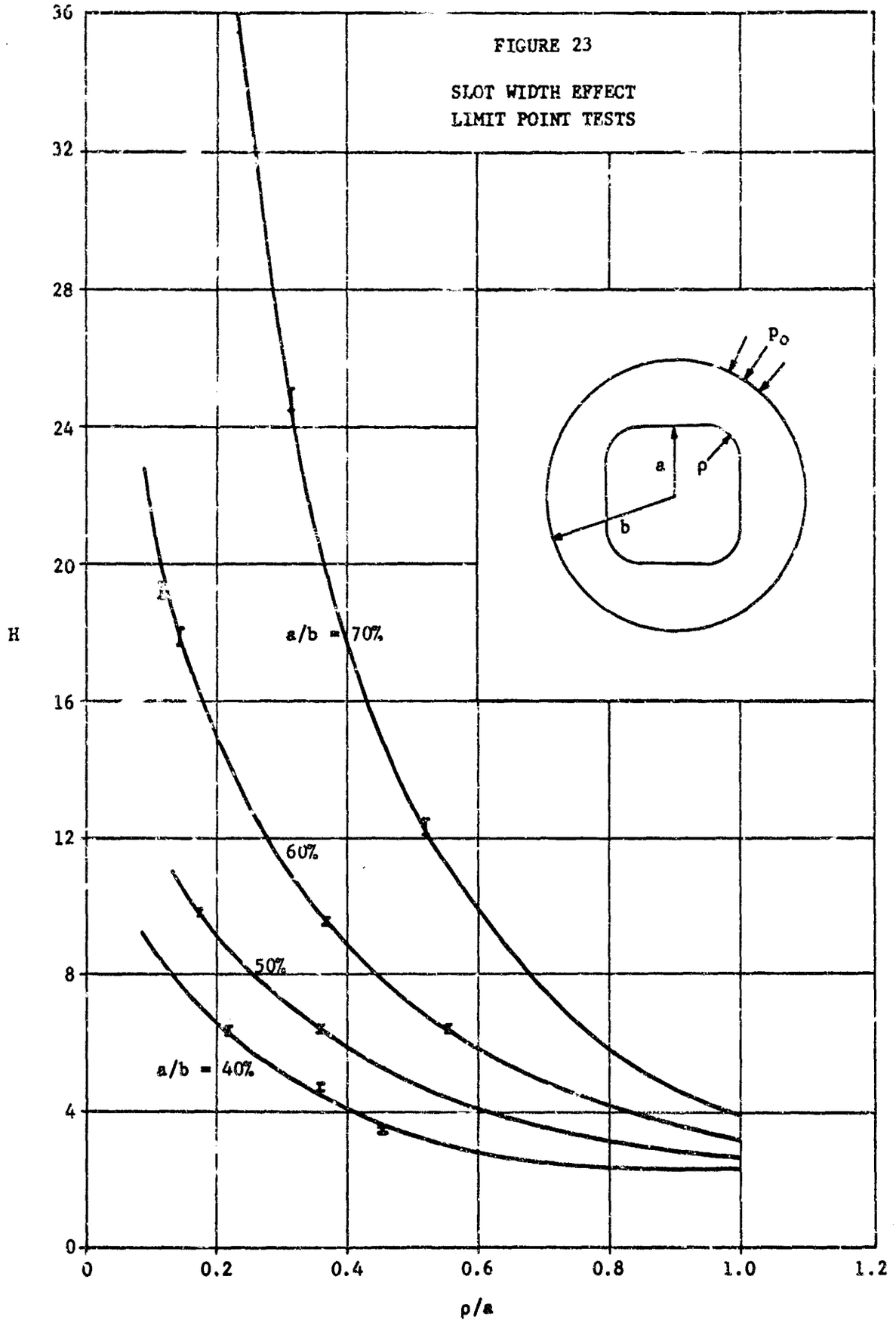

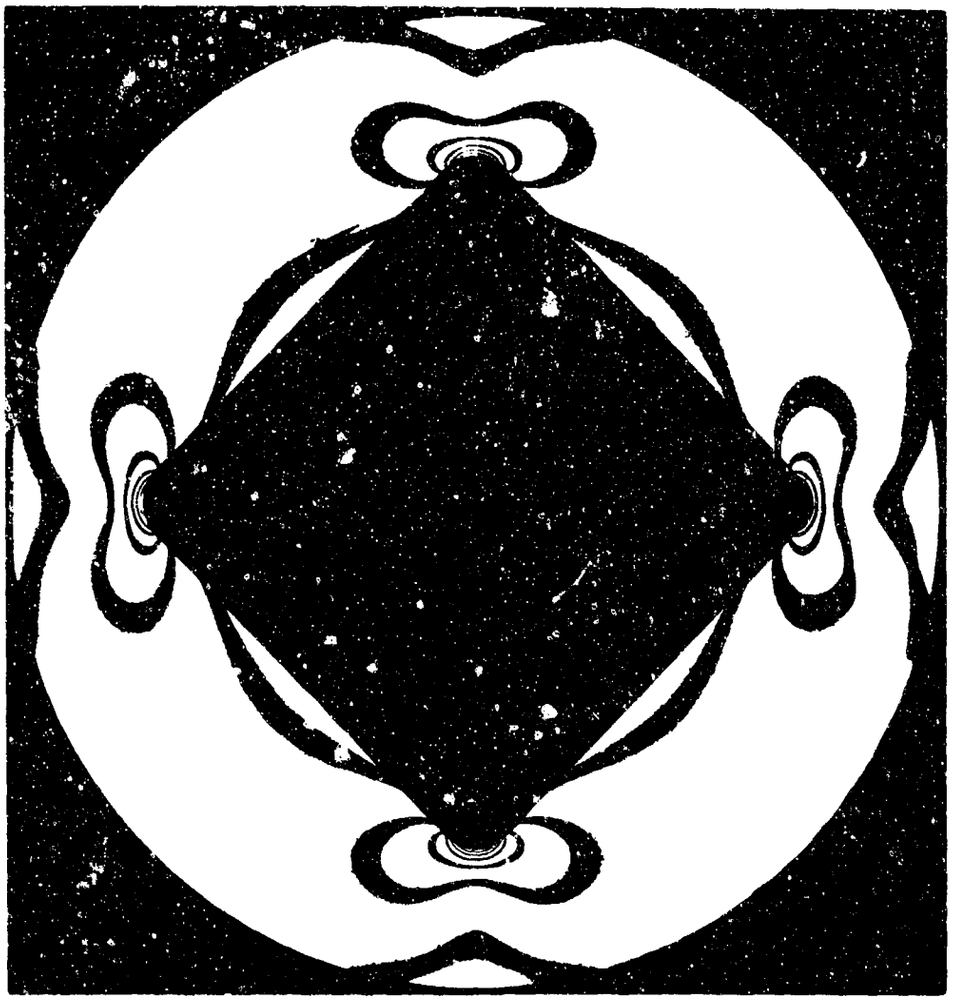

FIGURE 24

ISOCHROMATIC FRINGE PATTERN FOR LIMITING SQUARE

$a/b = 60\%$, $a/\rho = 8.72$, $H = 19.6$

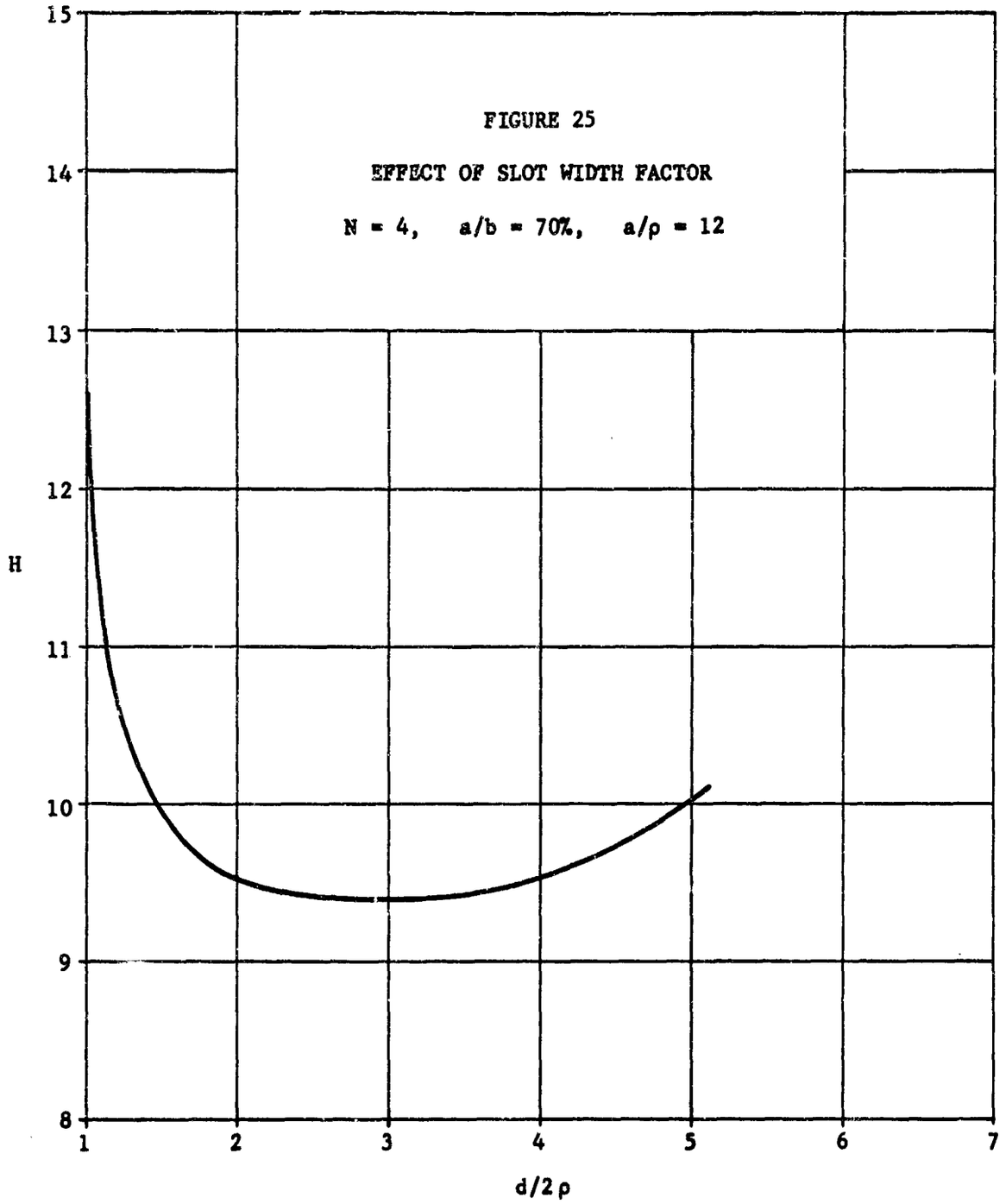

FIGURE 25

EFFECT OF SLOT WIDTH FACTOR

N = 4, a/b = 70%, a/ρ = 12

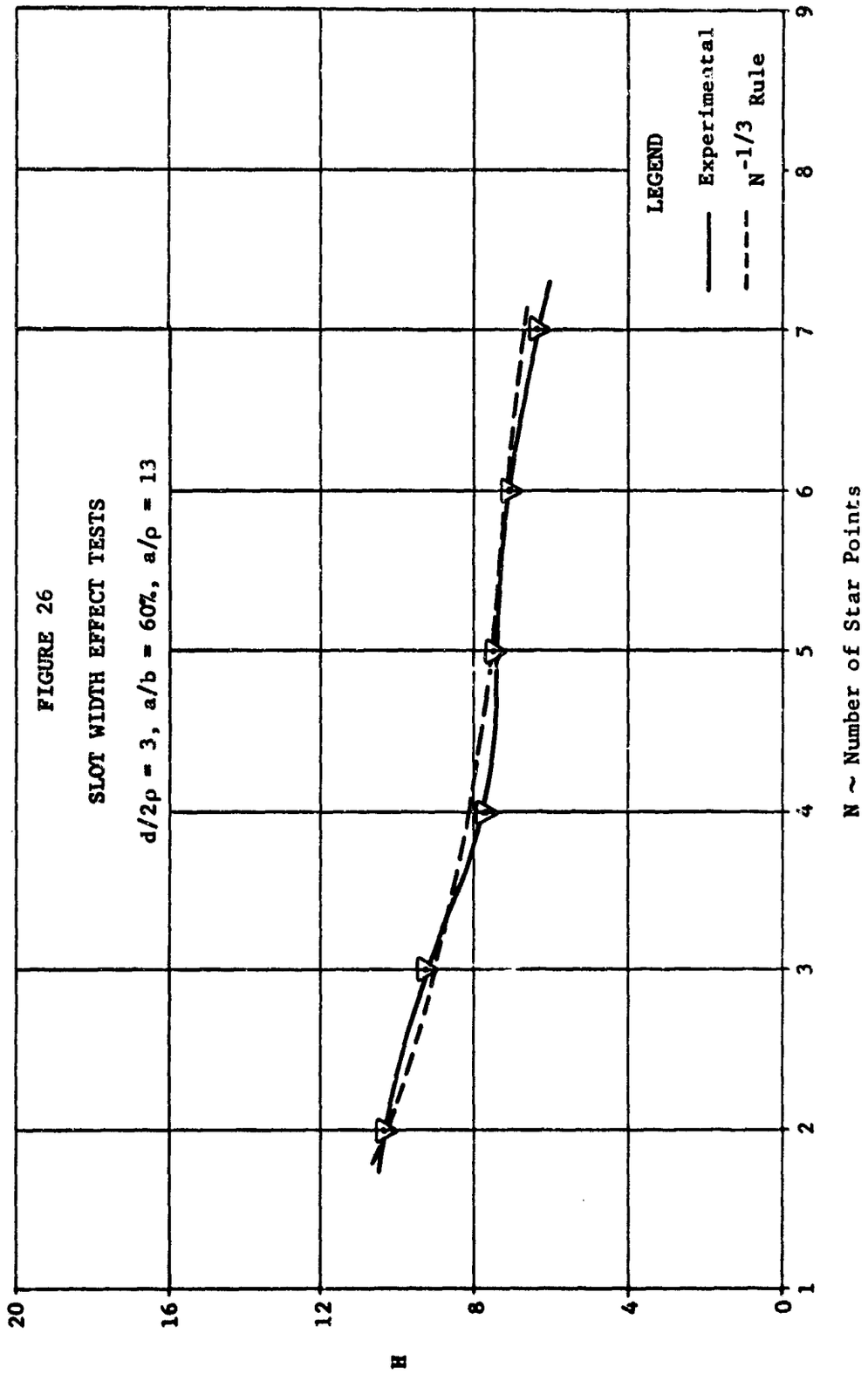
FIGURE 26
SLOT WIDTH EFFECT TESTS
d/2ρ = 3, a/b = 60%, a/ρ = 13
LEGEND
Experimental
N^-1/3 Rule
H
N ~ Number of Star Points
0
4
8
12
16
20
1
2
3
4
5
6
7
8
9

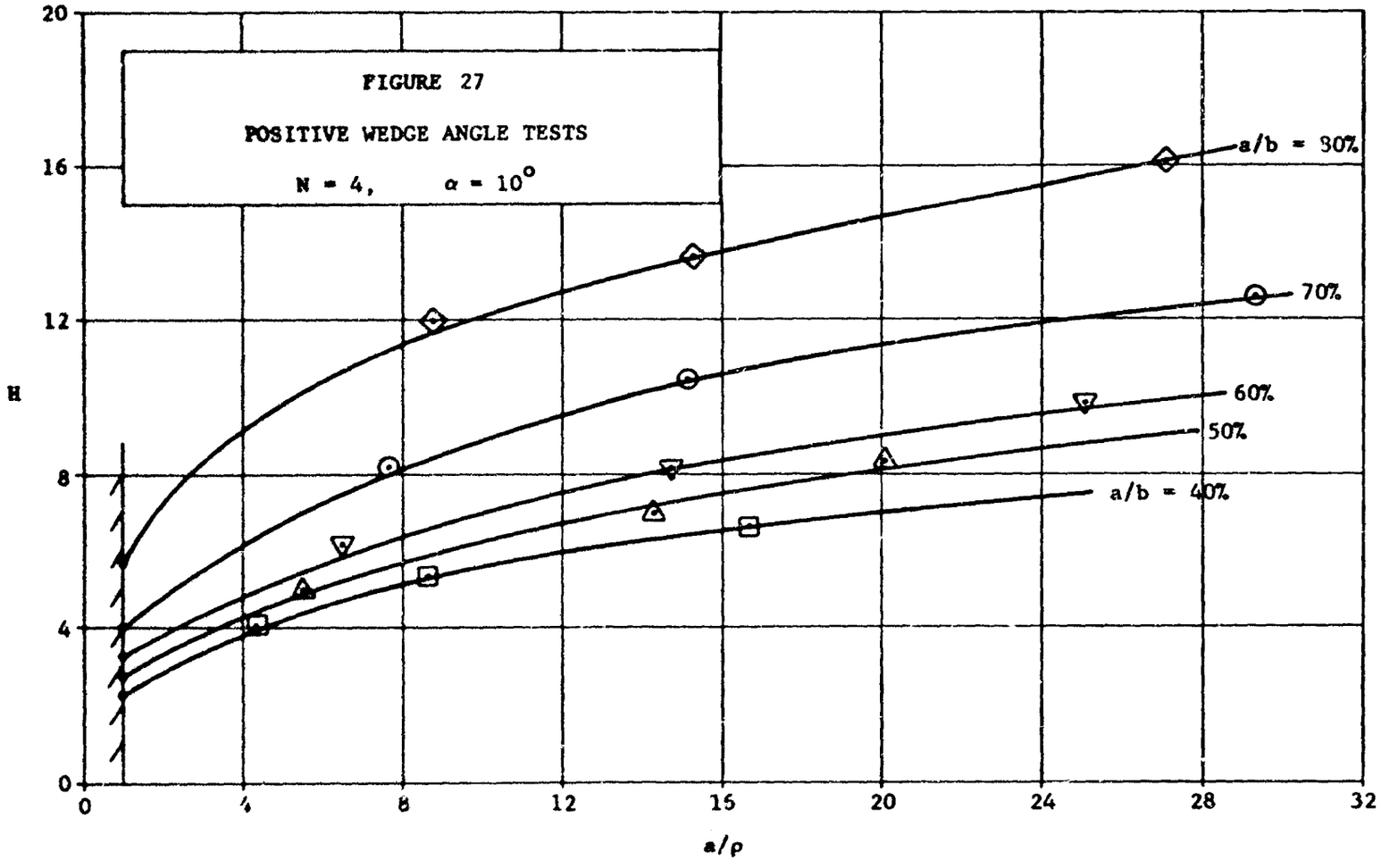
FIGURE 27
POSITIVE WEDGE ANGLE TESTS
N = 4, α = 10°
H
a/ρ
a/b = 80%
70%
60%
50%
a/b = 40%
0
4
8
12
16
20
0
4
8
12
15
20
24
28
32

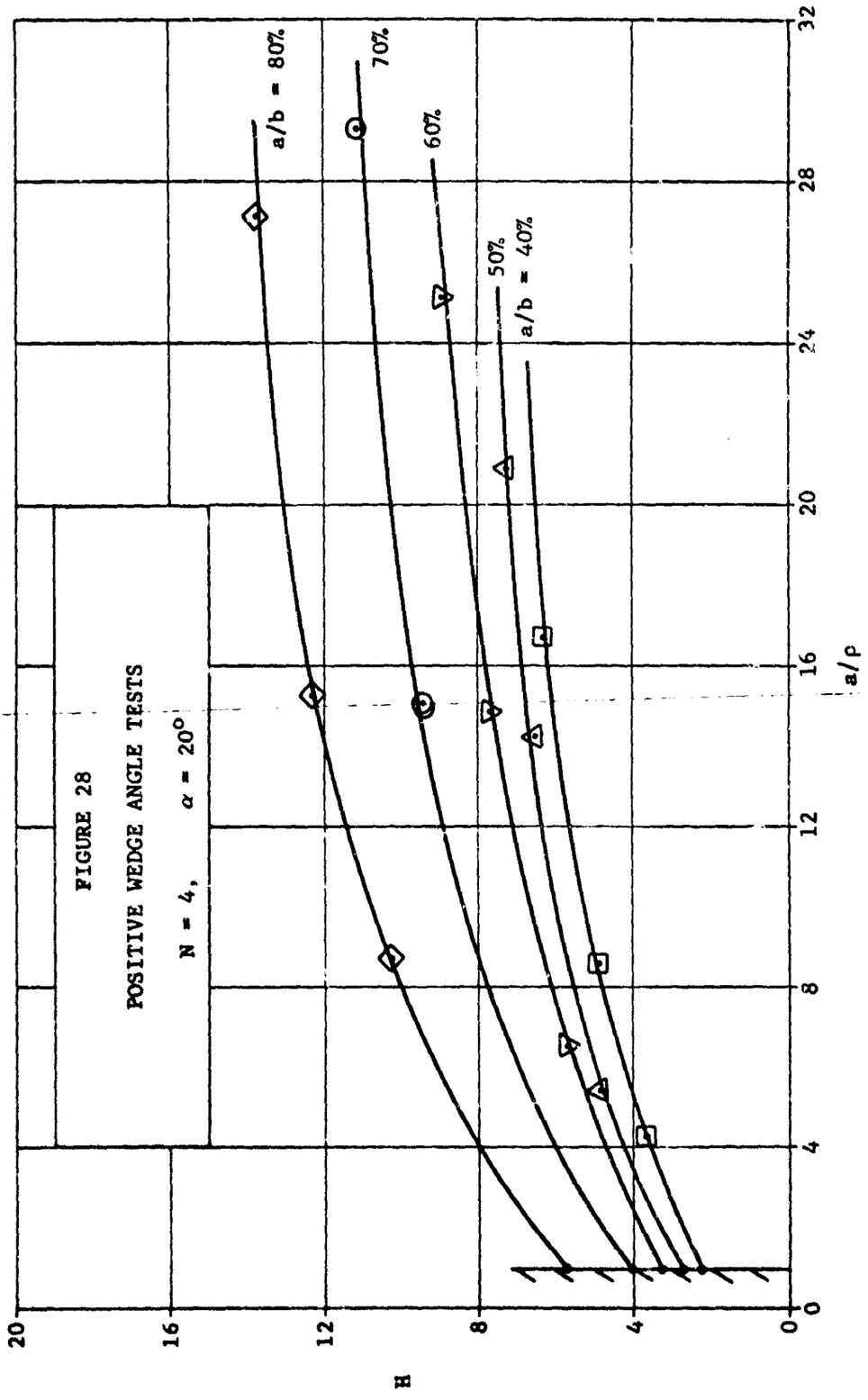
a/b = 80%
70%
60%
50%
a/b = 40%
FIGURE 28
POSITIVE WEDGE ANGLE TESTS
N = 4, α = 20°
H
a/ρ
0
4
8
12
16
20
24
28
32

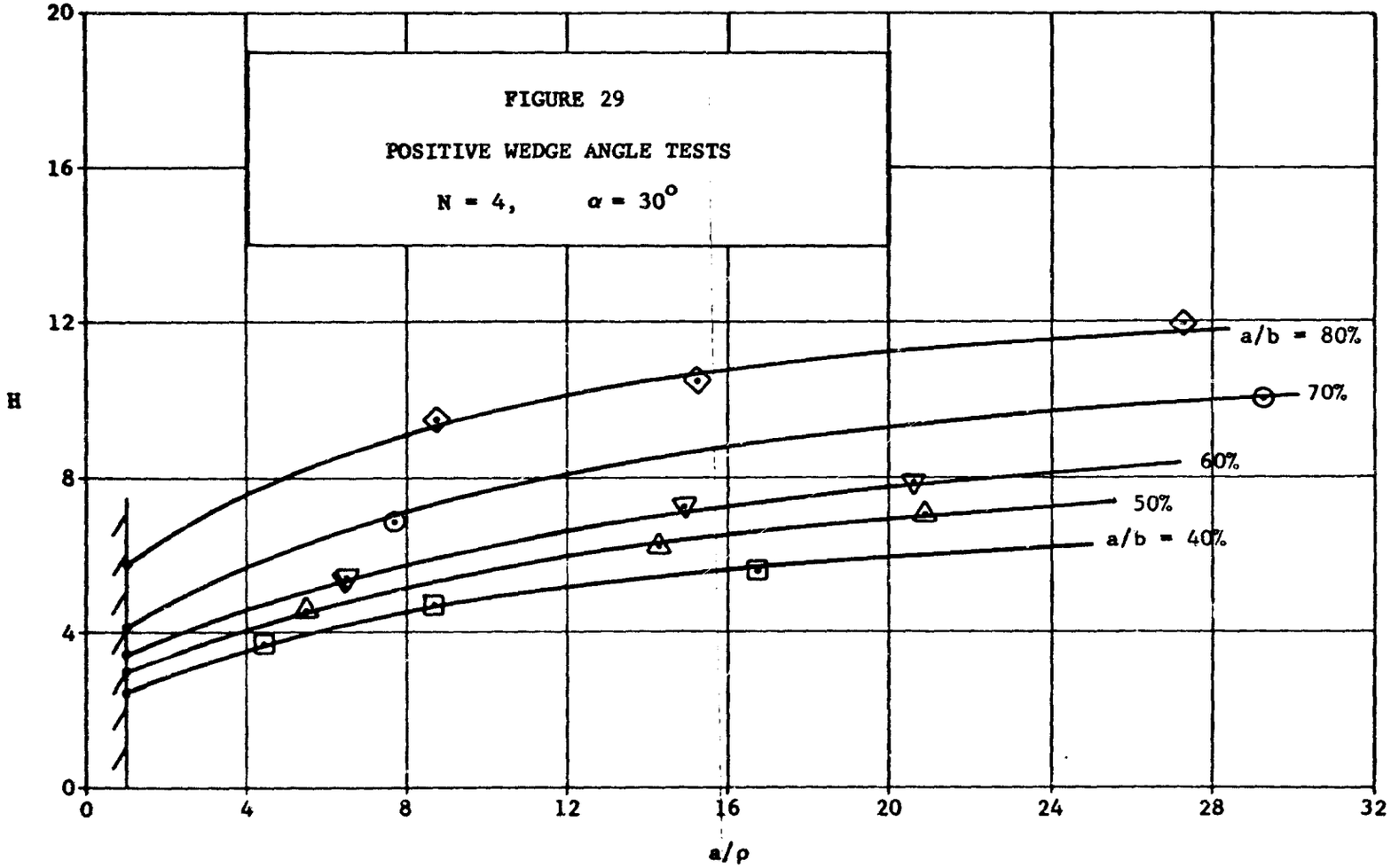
FIGURE 29
POSITIVE WEDGE ANGLE TESTS
N = 4, α = 30°
H
a/ρ
a/b = 80%
70%
60%
50%
a/b = 40%
0
4
8
12
16
20
24
28
32

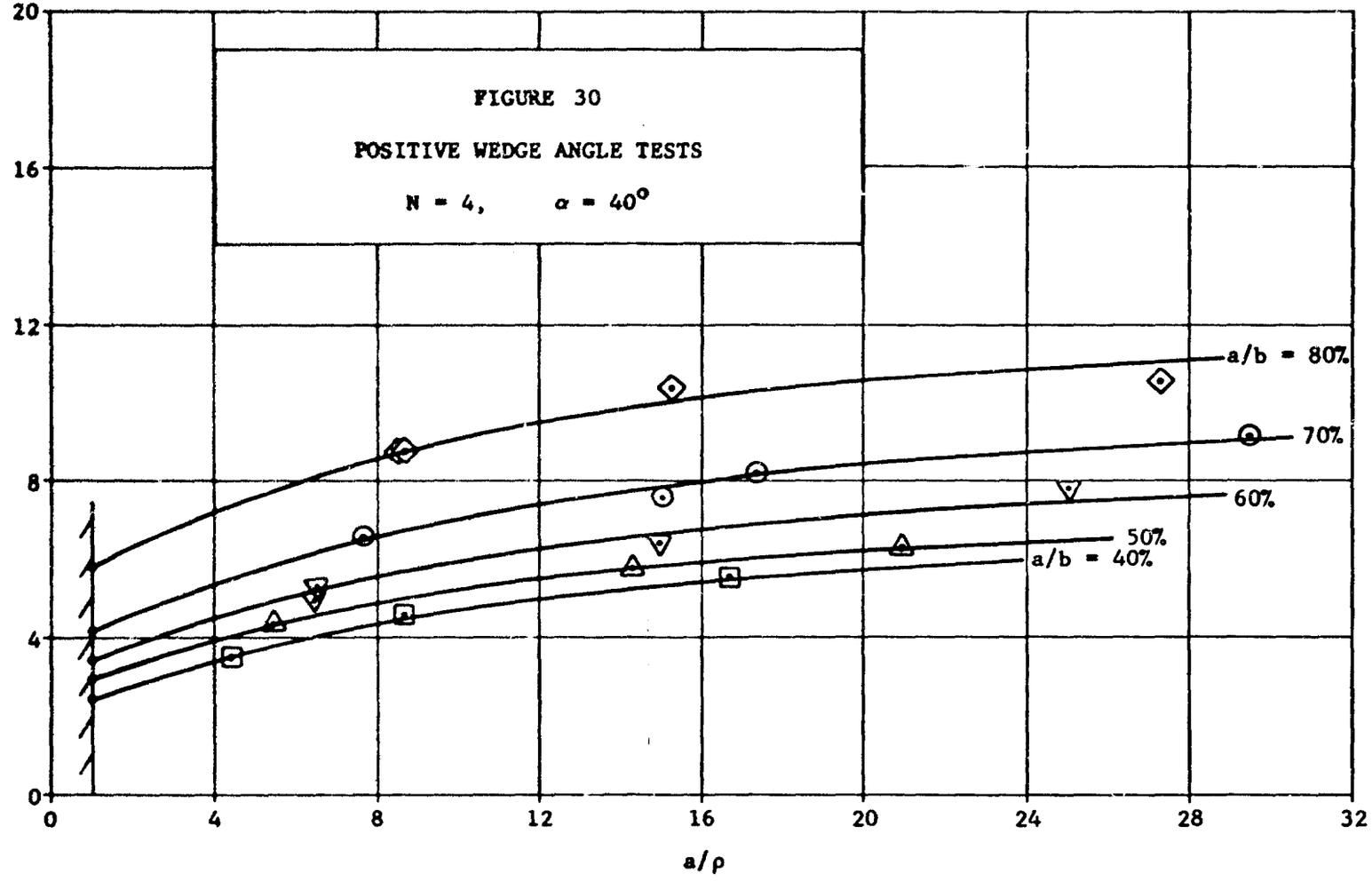
FIGURE 30
POSITIVE WEDGE ANGLE TESTS
N = 4, α = 40°
H
a/ρ
a/b = 80%
70%
60%
50%
a/b = 40%
0
4
8
12
16
20
24
28
32

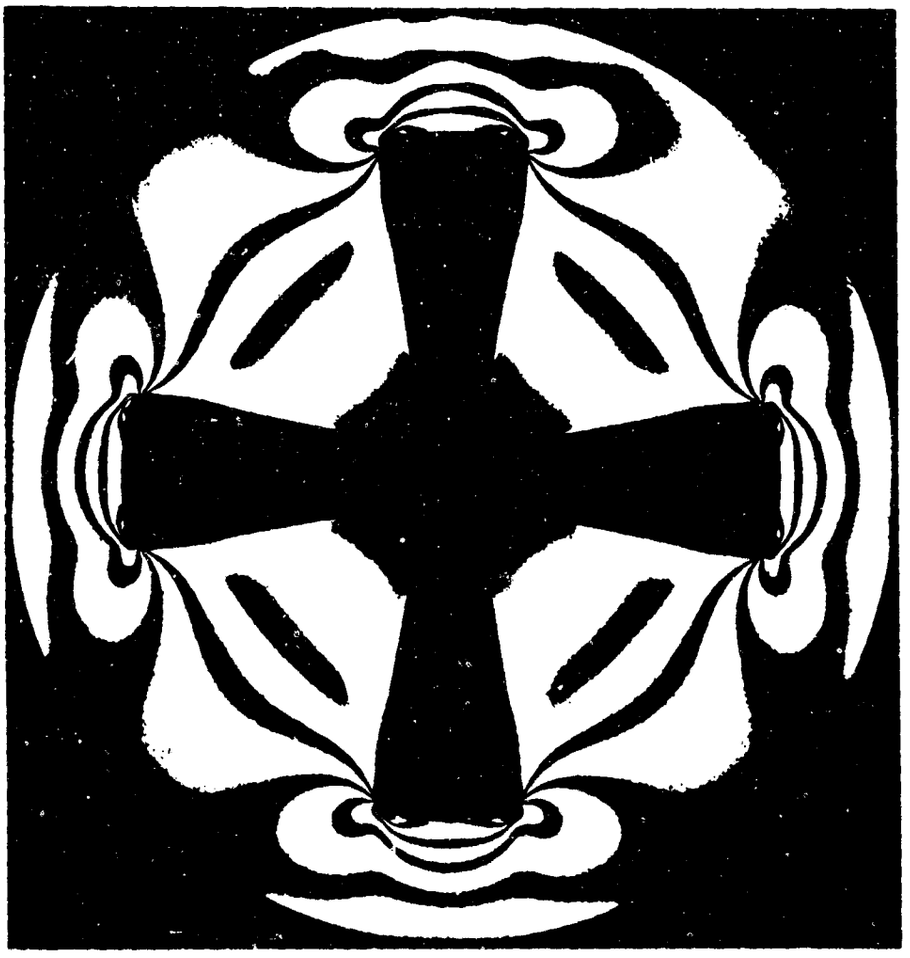

FIGURE 31

ISOCHROMATIC FRINGE PATTERN
OF TYPICAL POSITIVE WEDGE ANGLE CONFIGURATION

$N = 4$, $\alpha = 20^{\circ}$, $a/b = 70\%$, $a/\rho = 15.12$

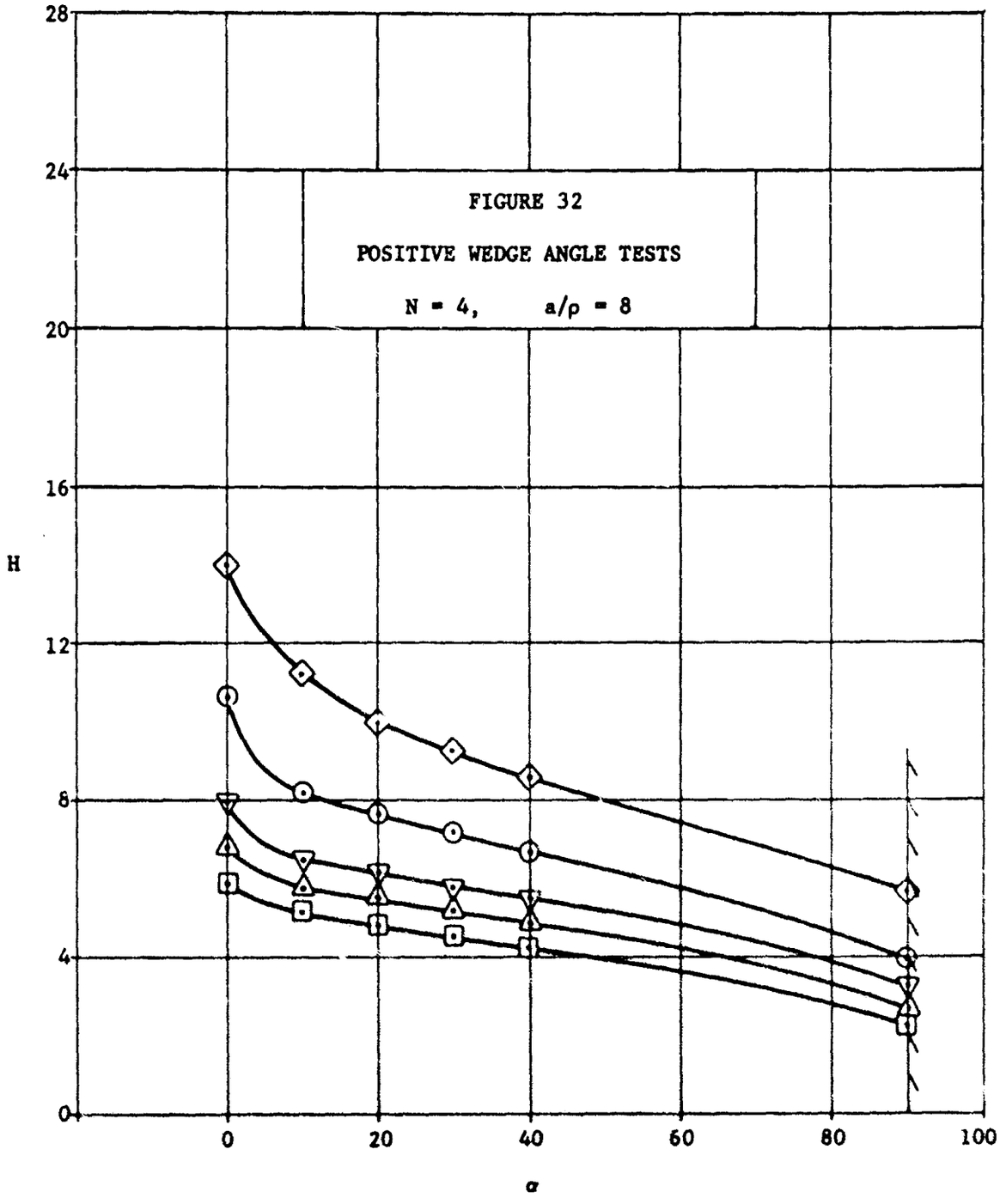
FIGURE 32
POSITIVE WEDGE ANGLE TESTS
N = 4, a/ρ = 8
H
α
28
24
20
16
12
8
4
0
0
20
40
60
80
100

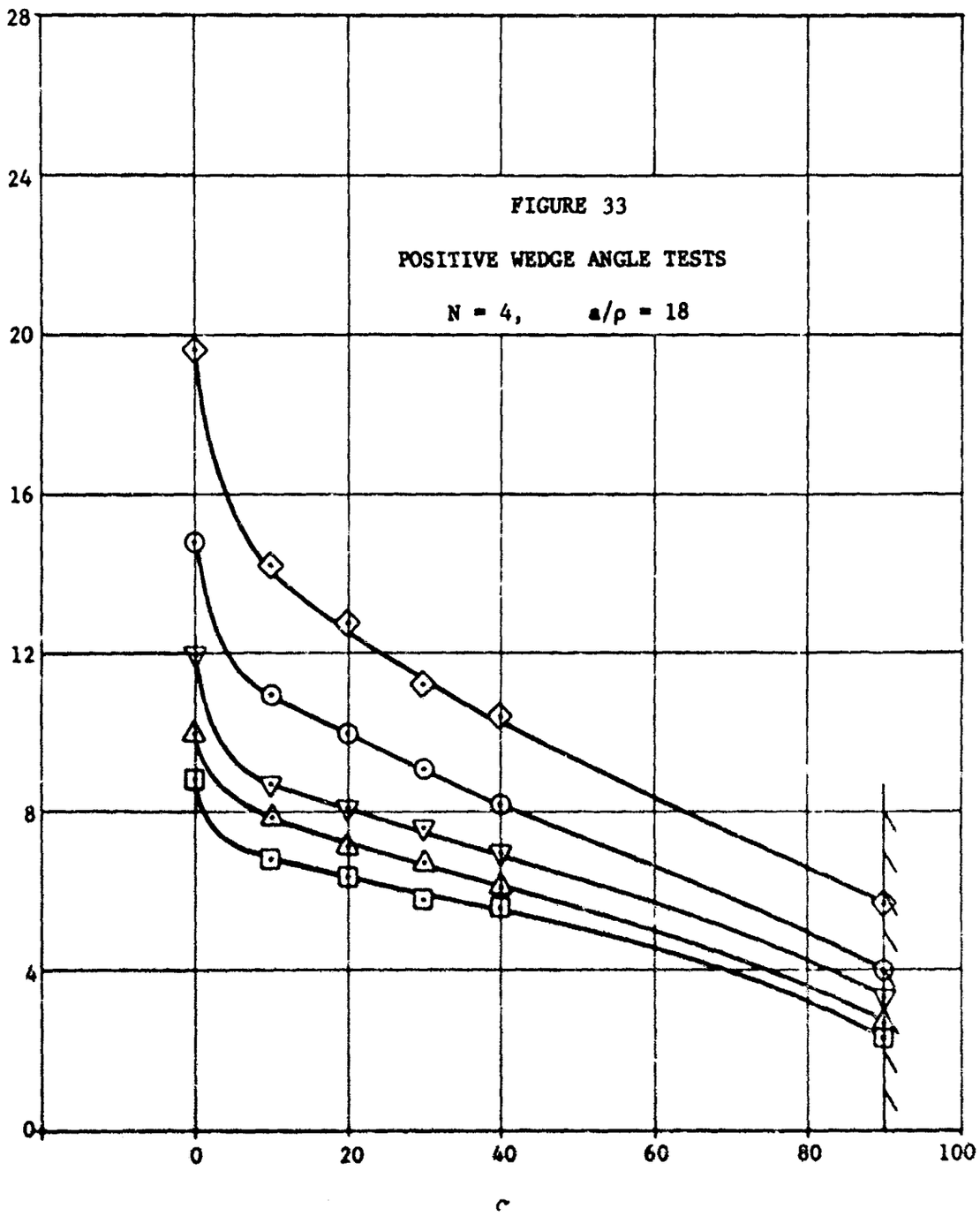

FIGURE 33

POSITIVE WEDGE ANGLE TESTS

N = 4, a/ρ = 18

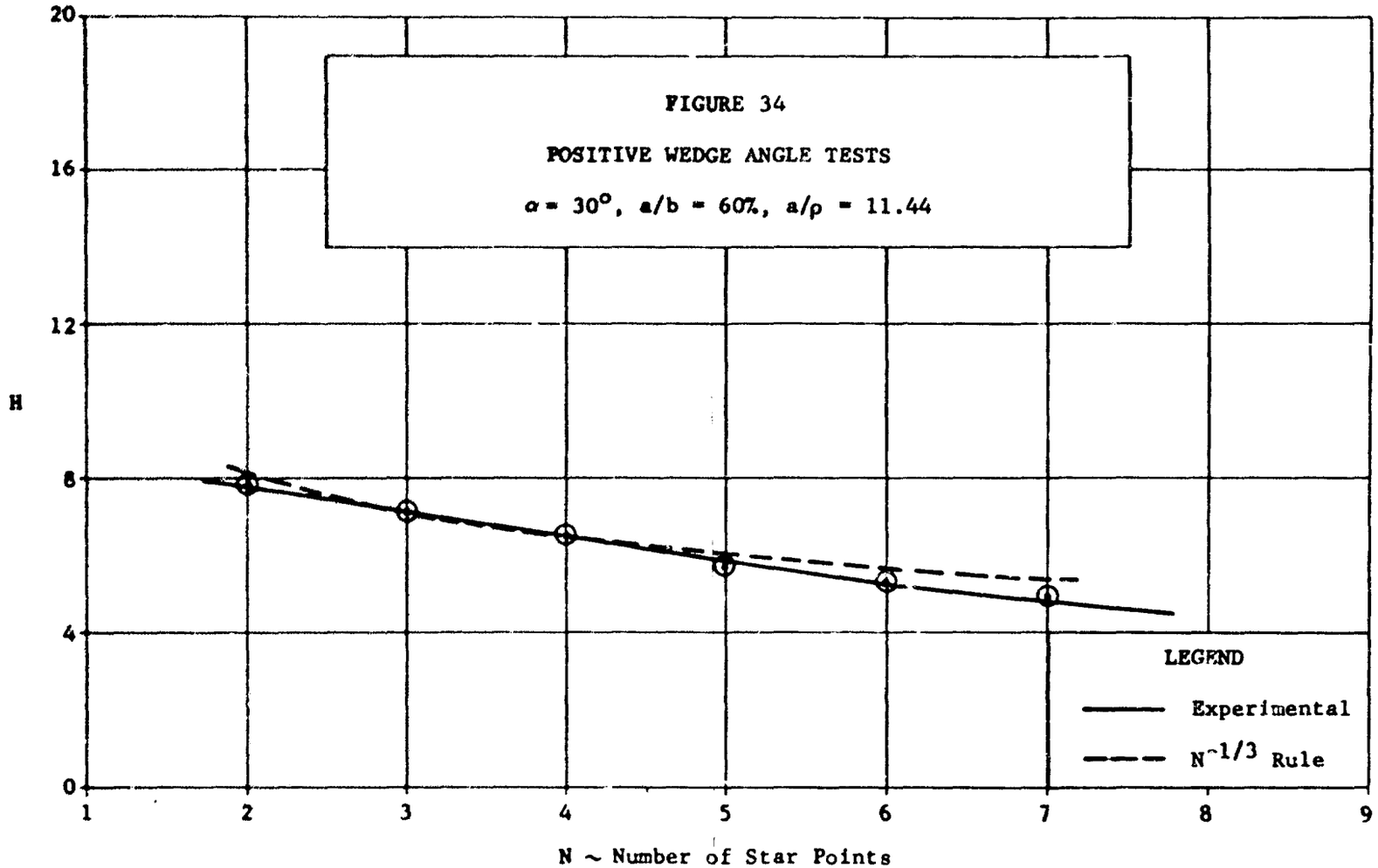
FIGURE 34
POSITIVE WEDGE ANGLE TESTS
α = 30°, a/b = 60%, a/ρ = 11.44
H
20
16
12
8
4
0
1
2
3
4
5
6
7
8
9
N ~ Number of Star Points
LEGEND
Experimental
N^-1/3 Rule

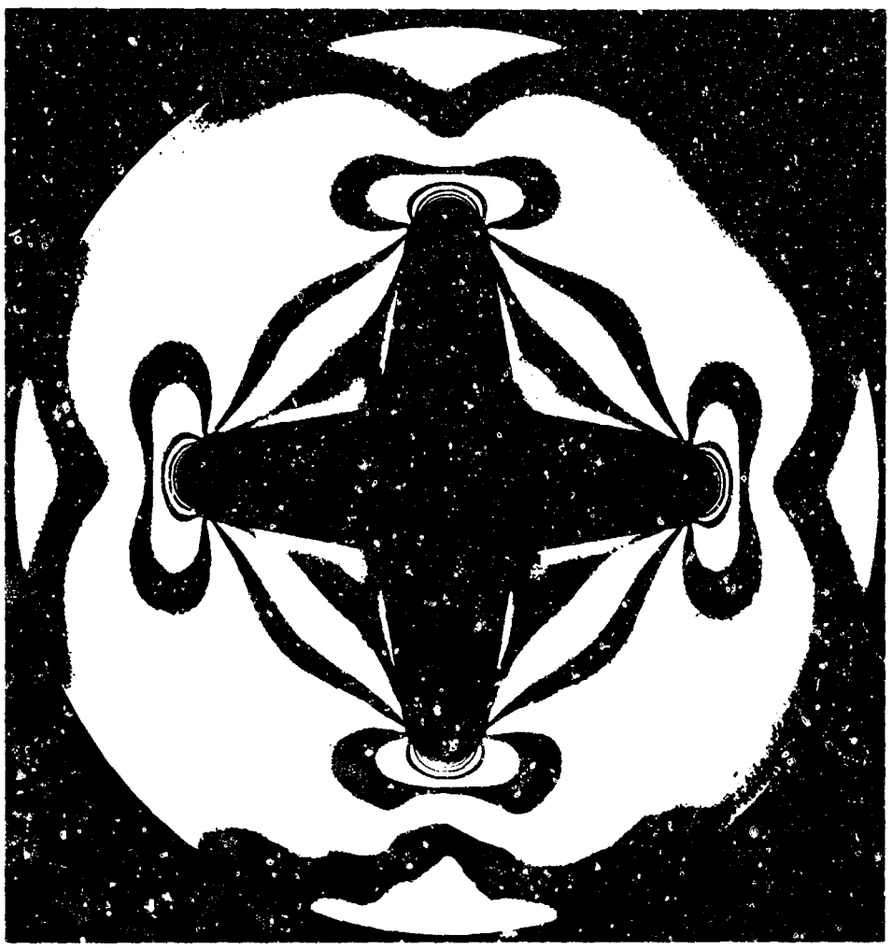

FIGURE 35

ISOCHROMATIC FRINGE PATTERN
OF TYPICAL NEGATIVE WEDGE ANGLE CONFIGURATION

$N = 4$, $\beta = 20^{\circ}$, $e/b = 58\%$, $a/\rho = 6.33$, $H = 7.22$, $p_o = 300$ psi

(NOTE: Distortion of fringe pattern on bottom extremity of model was due to delamination of lens in optical bench.)

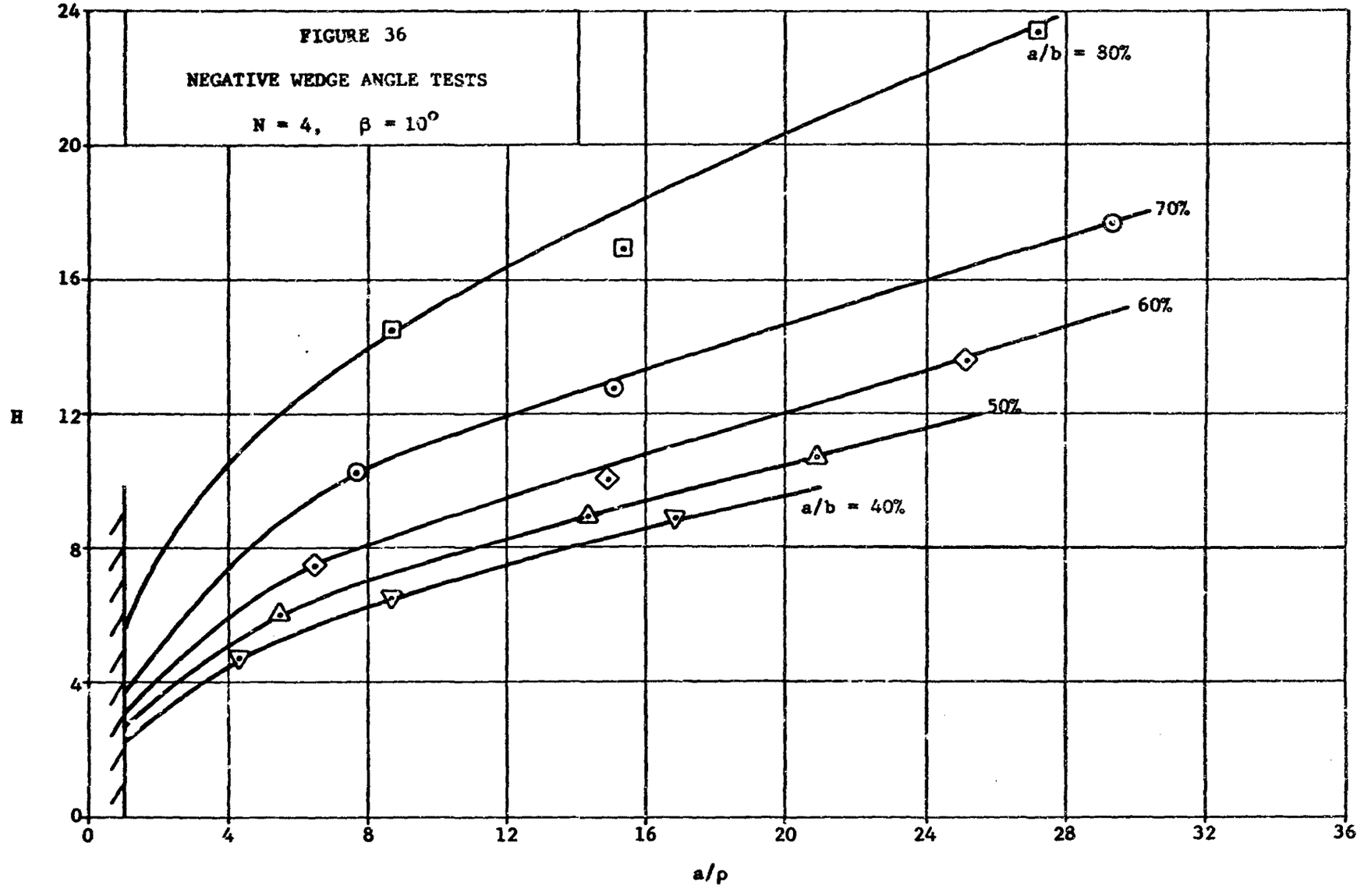
FIGURE 36
NEGATIVE WEDGE ANGLE TESTS
N = 4, β = 10°
a/b = 80%
70%
60%
50%
a/b = 40%
H
a/ρ
0
4
8
12
16
20
24
28
32
36

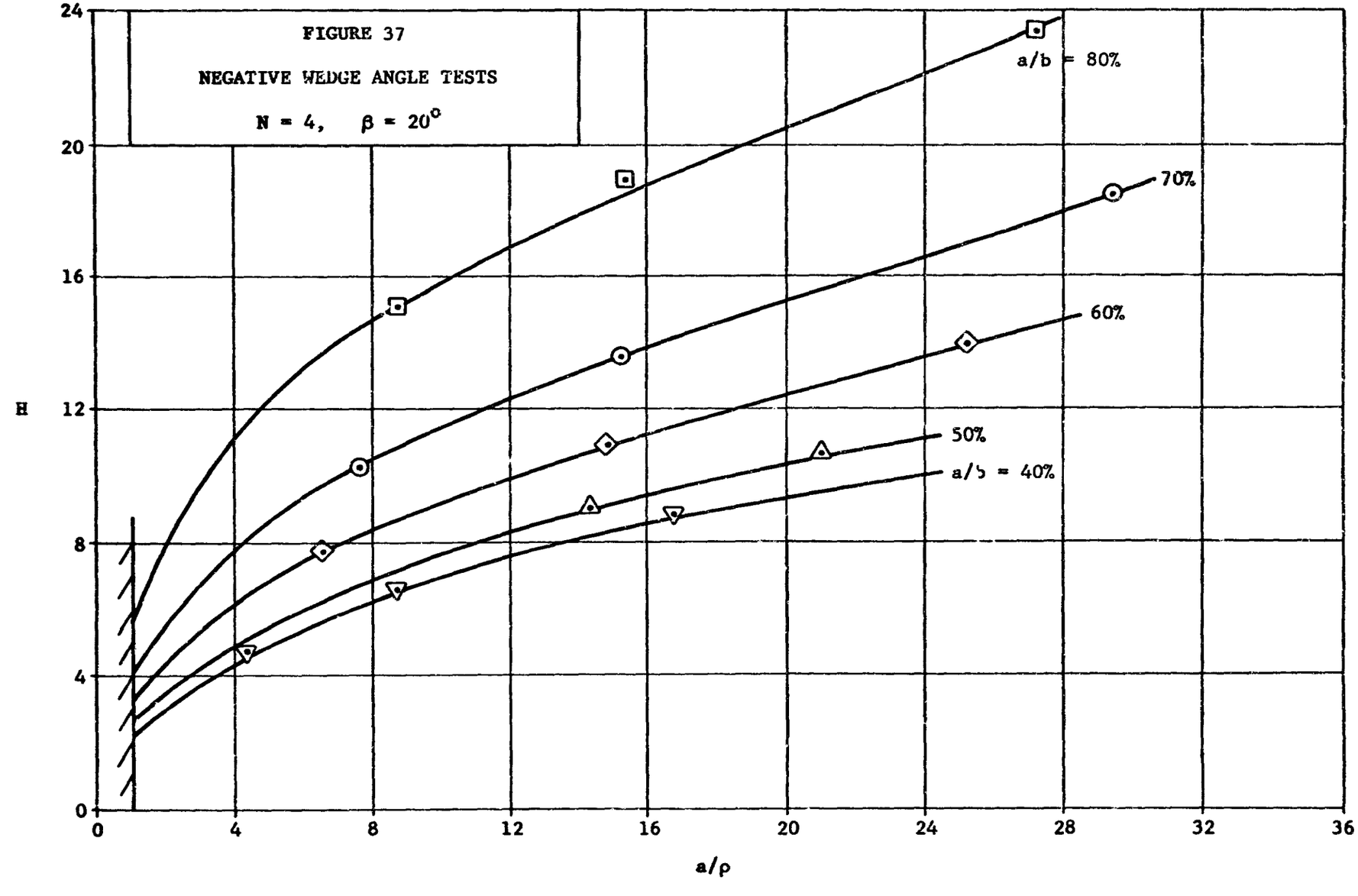
FIGURE 37
NEGATIVE WEDGE ANGLE TESTS
N = 4, β = 20°
a/b = 80%
70%
60%
50%
a/b = 40%
H
a/ρ
0
4
8
12
16
20
24
28
32
36

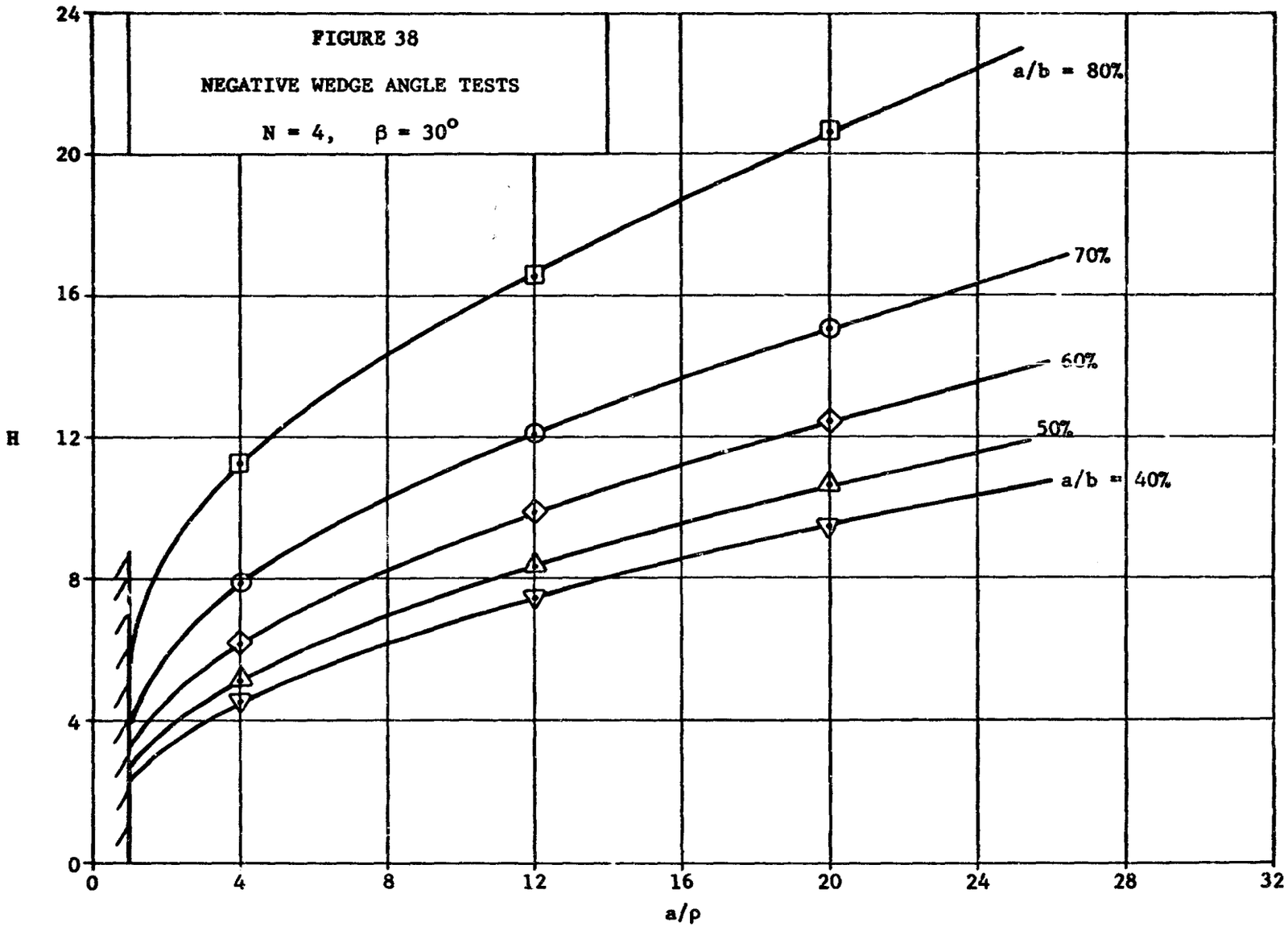
FIGURE 38
NEGATIVE WEDGE ANGLE TESTS
N = 4, β = 30°
a/b = 80%
70%
60%
50%
a/b = 40%
H
a/ρ
0
4
8
12
16
20
24
28
32

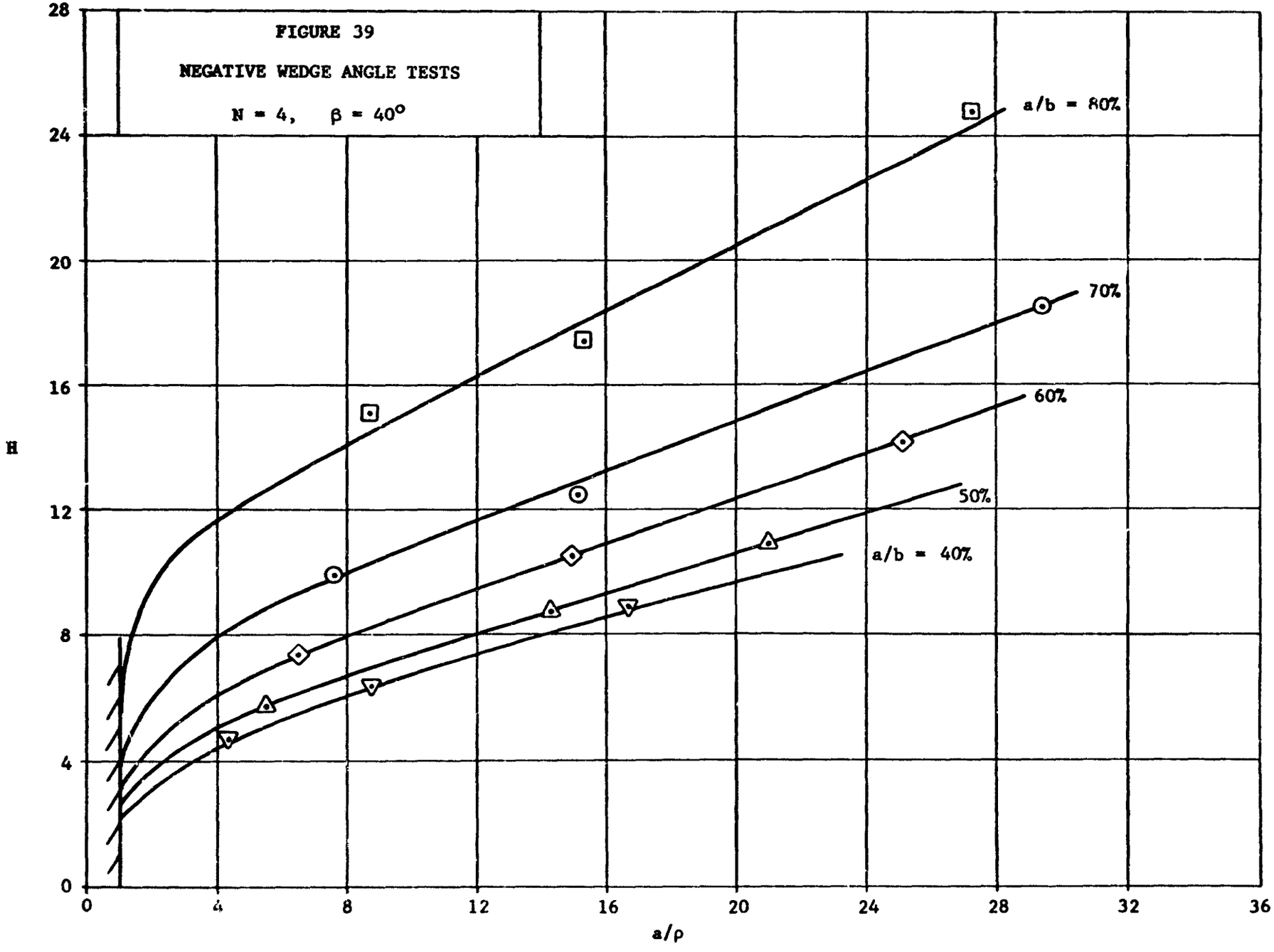
FIGURE 39
NEGATIVE WEDGE ANGLE TESTS
N = 4, β = 40°
a/b = 80%
70%
60%
50%
a/b = 40%
H
a/ρ
0
4
8
12
16
20
24
28
32
36

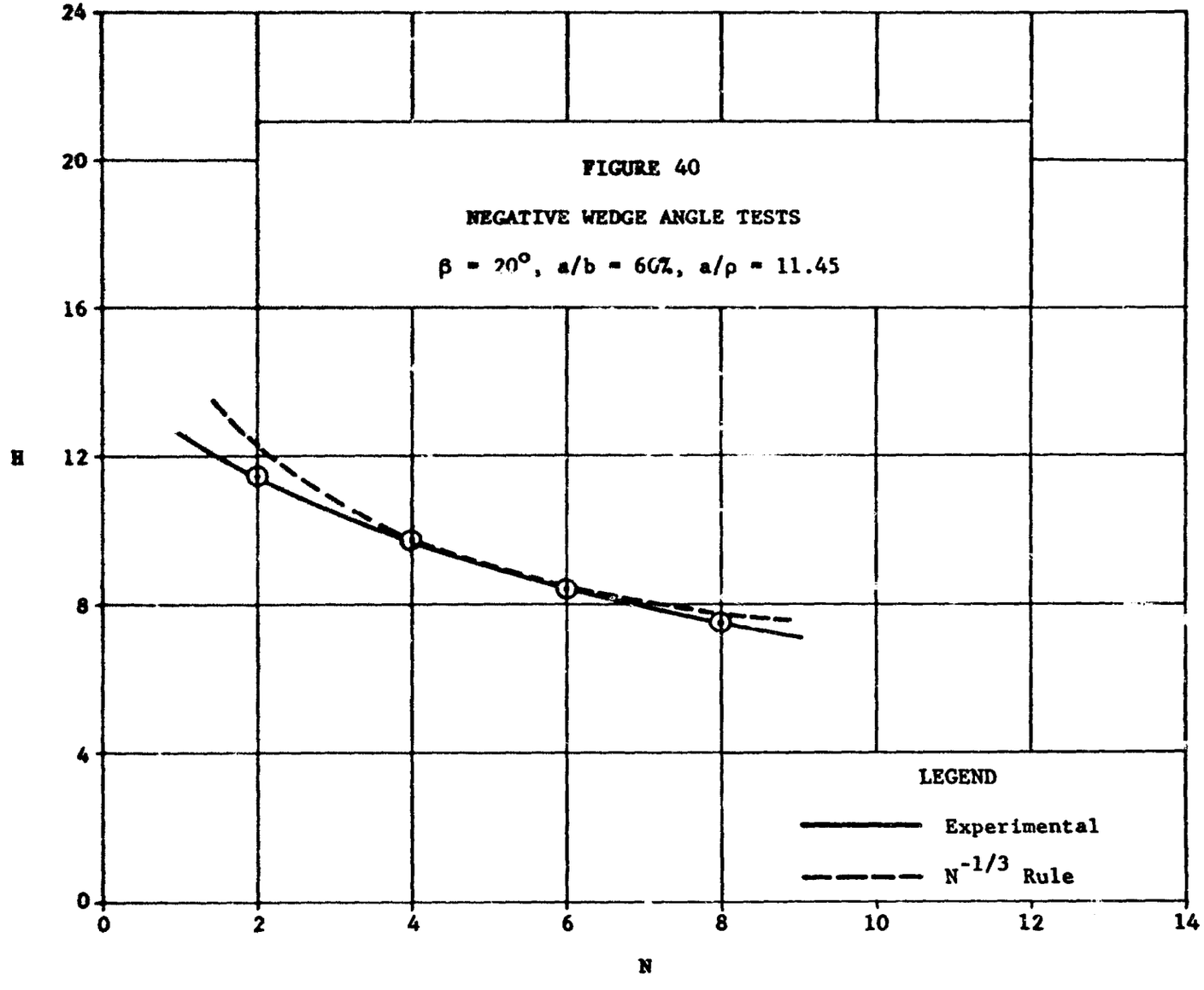
FIGURE 40
NEGATIVE WEDGE ANGLE TESTS
β = 20°, a/b = 60%, a/ρ = 11.45
H
N
0
4
8
12
16
20
24
0
2
4
6
8
10
12
14
LEGEND
Experimental
N^-1/3 Rule

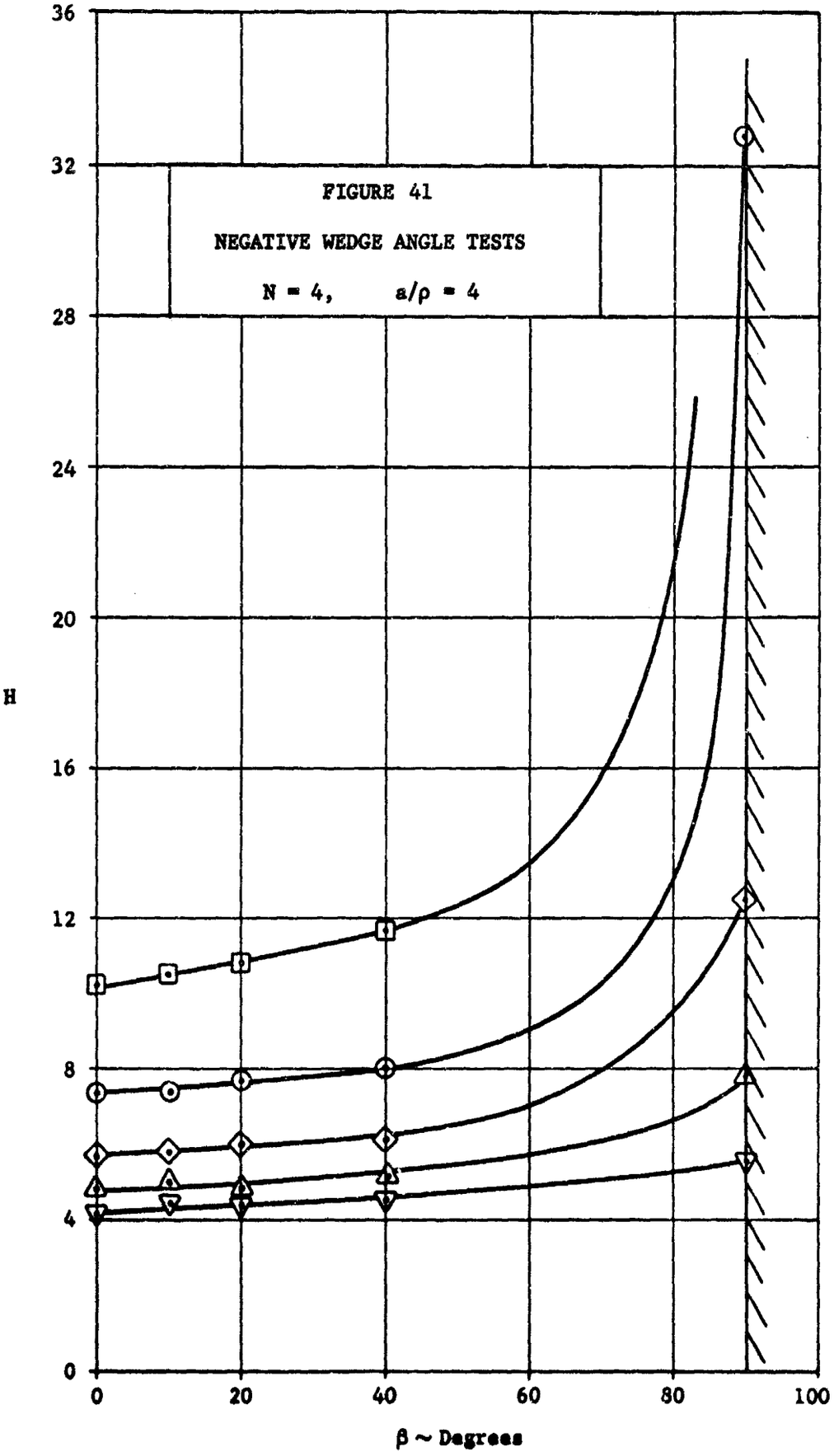
FIGURE 41
NEGATIVE WEDGE ANGLE TESTS
N = 4, a/ρ = 4
H
36
32
28
24
20
16
12
8
4
0
0
20
40
60
80
100
β ~ Degrees

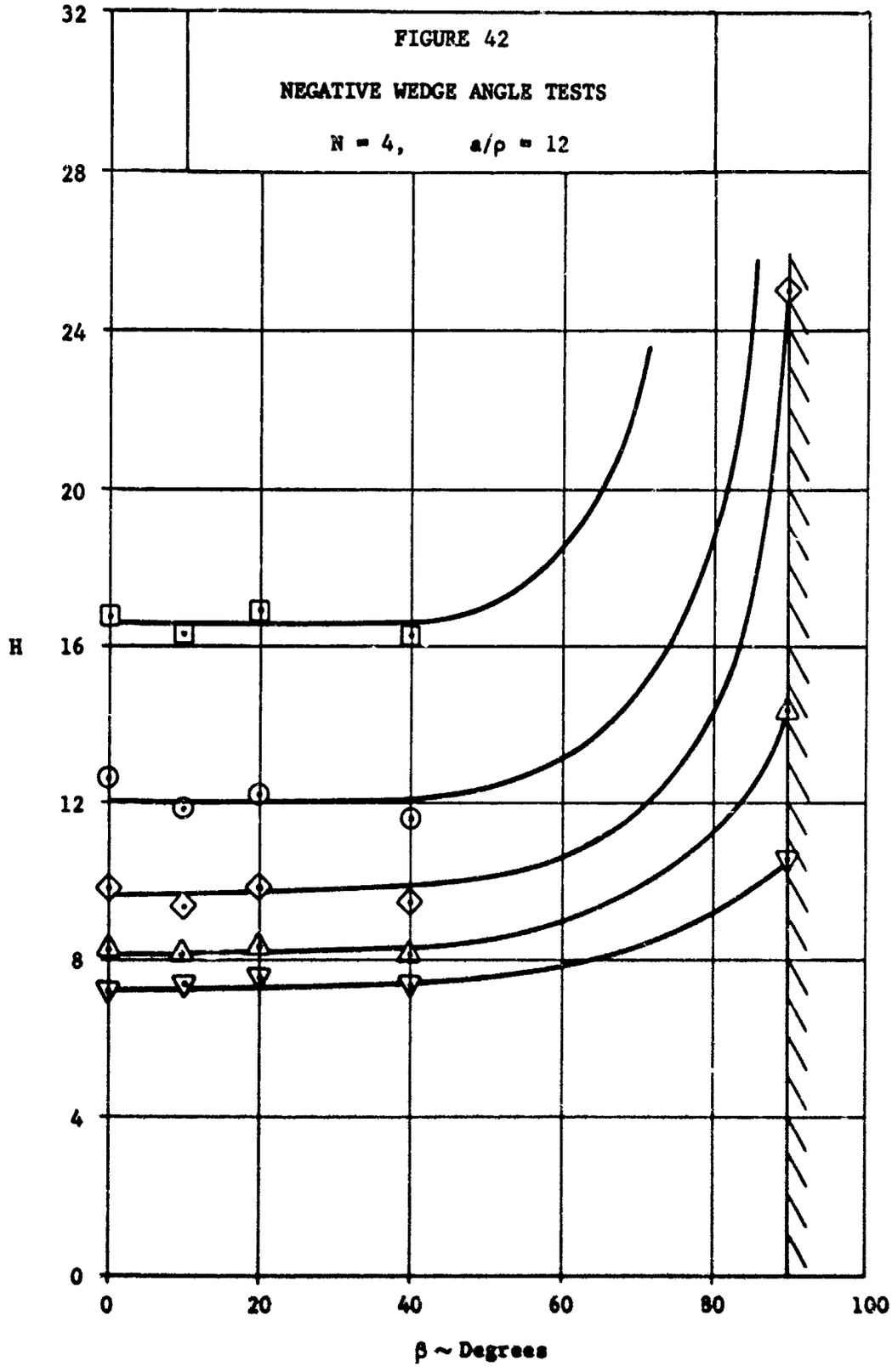
FIGURE 42
NEGATIVE WEDGE ANGLE TESTS
N = 4, a/ρ = 12
H
32
28
24
20
16
12
8
4
0
0
20
40
60
80
100
β ~ Degrees

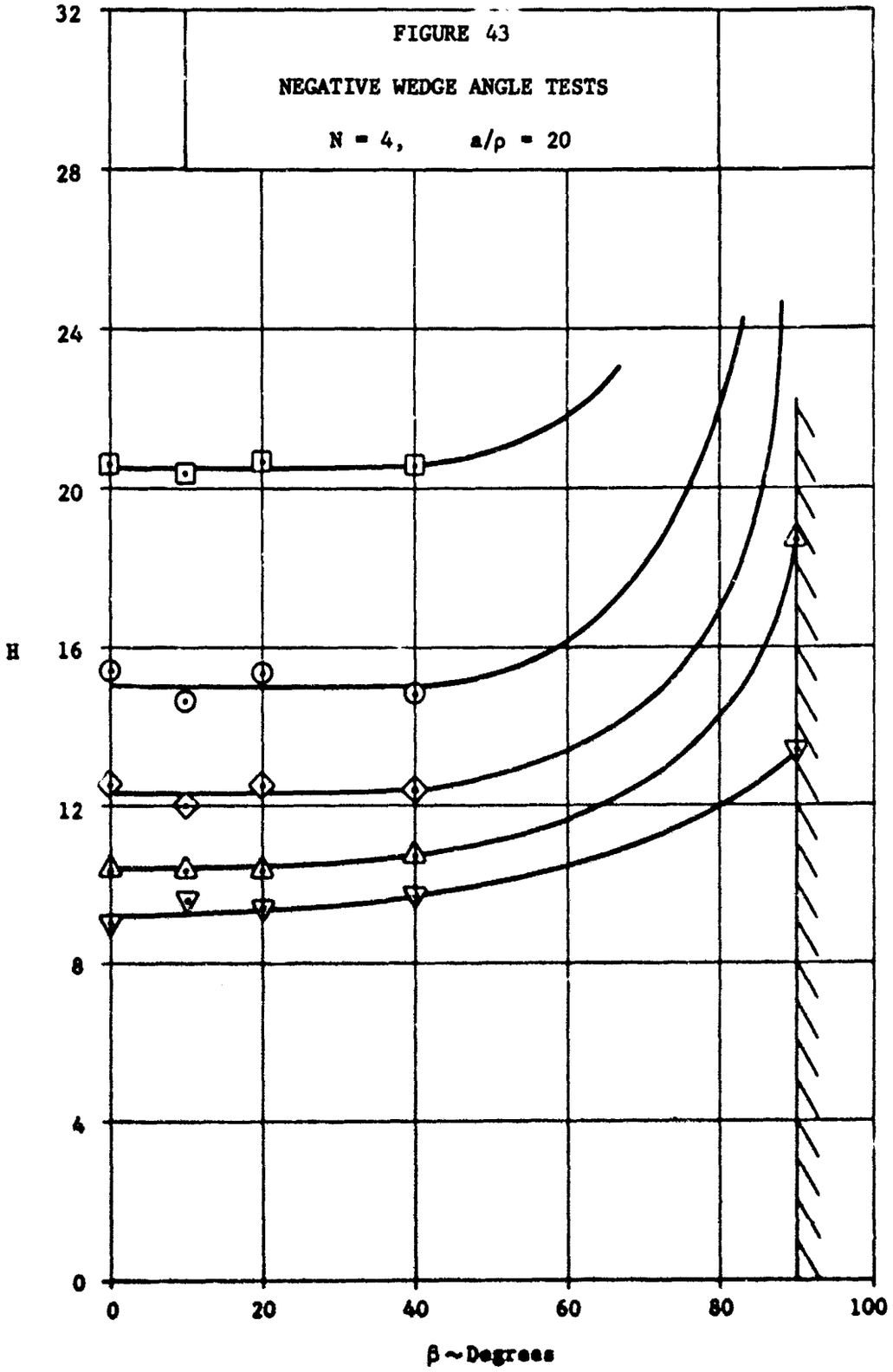
FIGURE 43
NEGATIVE WEDGE ANGLE TESTS
N = 4, a/ρ = 20
H
32
28
24
20
16
12
8
4
0
0
20
40
60
80
100
β ~ Degrees

$\epsilon = 1.0, \quad 2\rho = 0.753$

$\epsilon = 0.8, \quad 2\rho = 0.753$

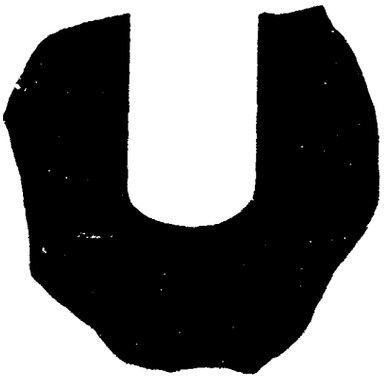

$\epsilon = 0.6, \quad 2\rho = 0.753$

$\epsilon = 0.4, \quad 2\rho = 0.753$

FIGURE 44

DETAIL OF ELLIPTICAL SLOT TIP GEOMETRY
FOR VARIOUS ECCENTRICITIES

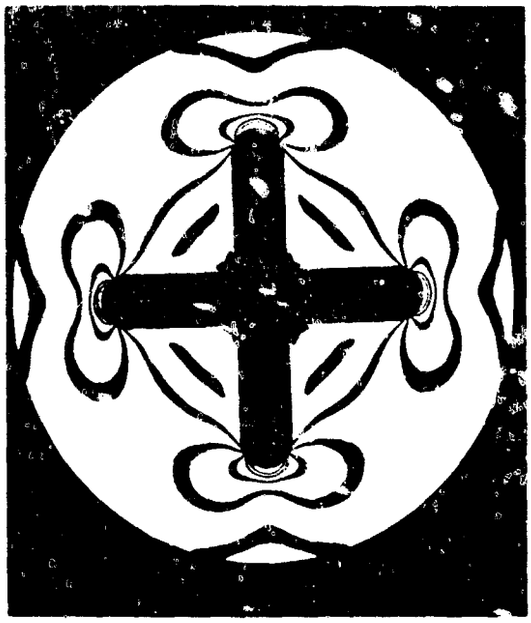

-a- $\epsilon = 1.0$

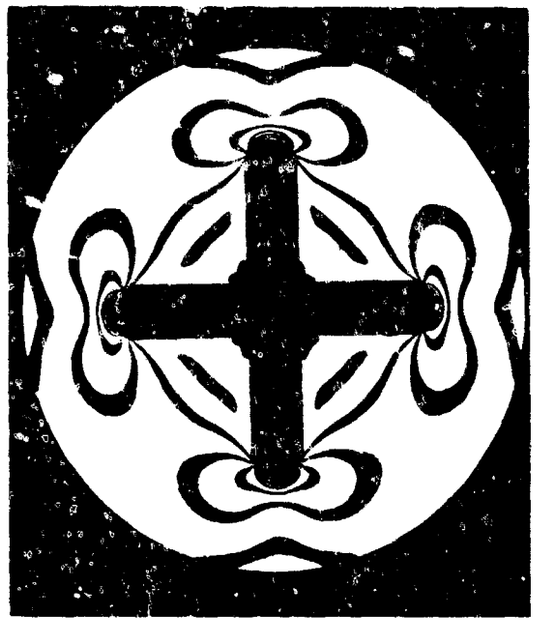

-b- $\epsilon = 0.8$

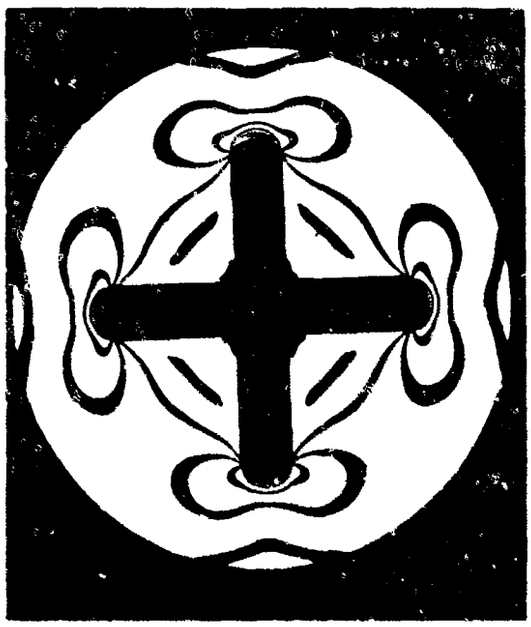

-c- $\epsilon = 0.6$

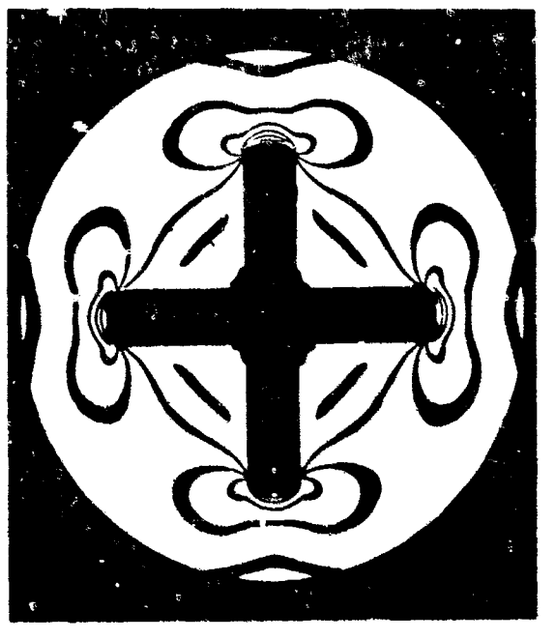

-d- $\epsilon = 0.4$

FIGURE 45

VARIATION OF ISOCHROMATIC FRINGE PATTERN WITH ECCENTRICITY

p_o = 350 psi, a/b = 60%, 2ρ = 0.5"

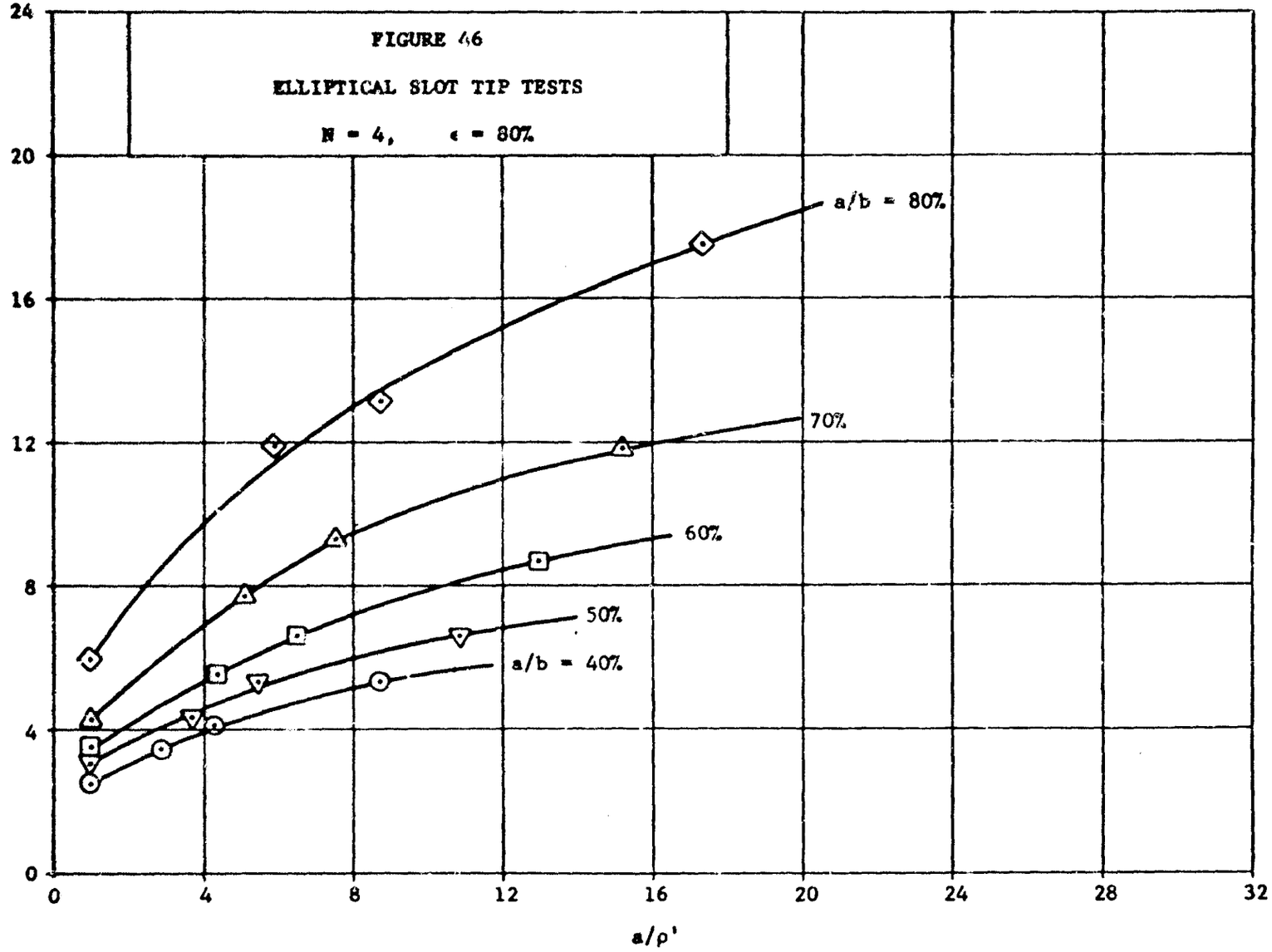
FIGURE 46
ELLIPTICAL SLOT TIP TESTS
N = 4, ε = 80%
H
a/ρ'
a/b = 80%
70%
60%
50%
a/b = 40%
0
4
8
12
16
20
24
28
32

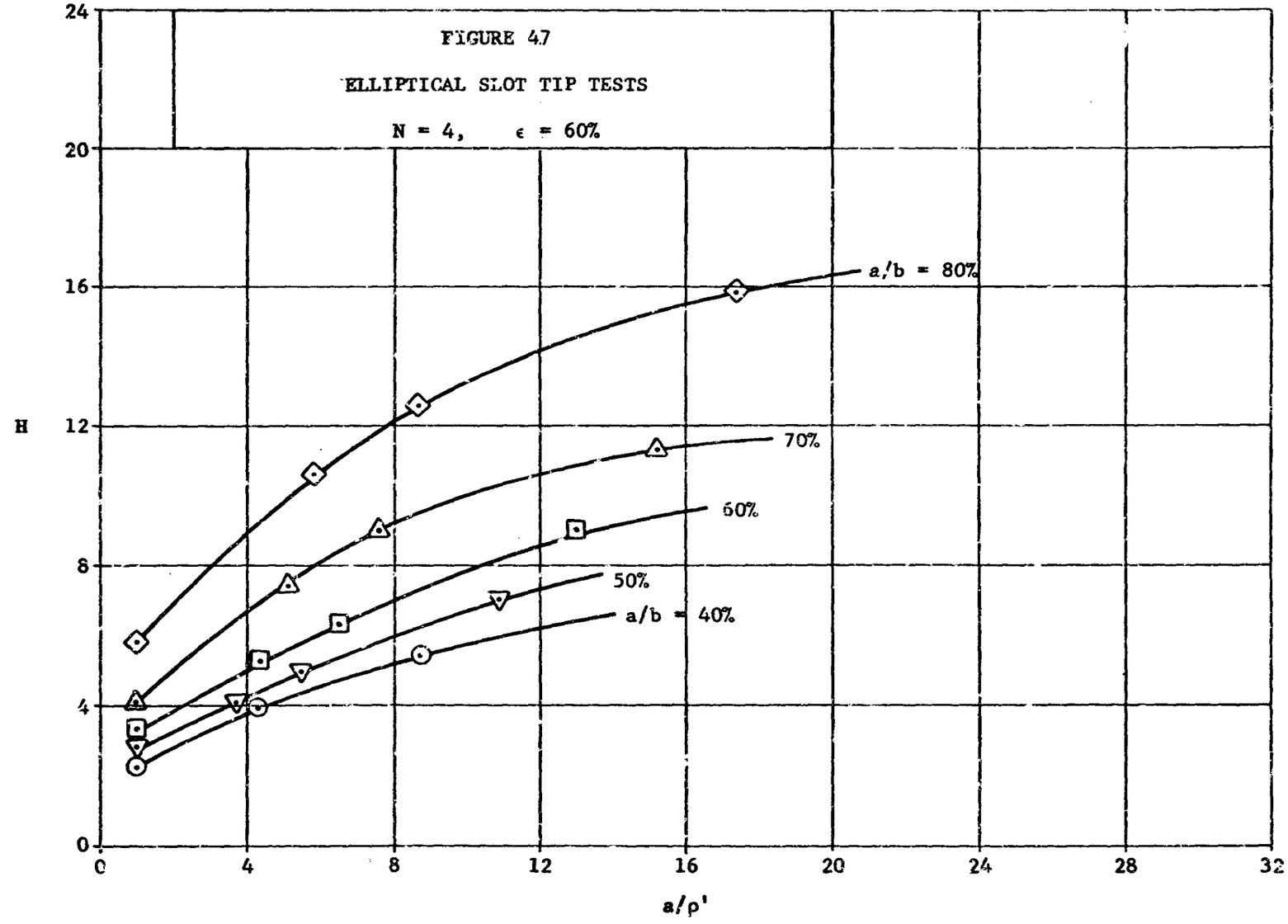
FIGURE 47
ELLIPTICAL SLOT TIP TESTS
N = 4, ϵ = 60%
H
a/ρ'
a/b = 80%
70%
60%
50%
a/b = 40%
0
4
8
12
16
20
24
28
32

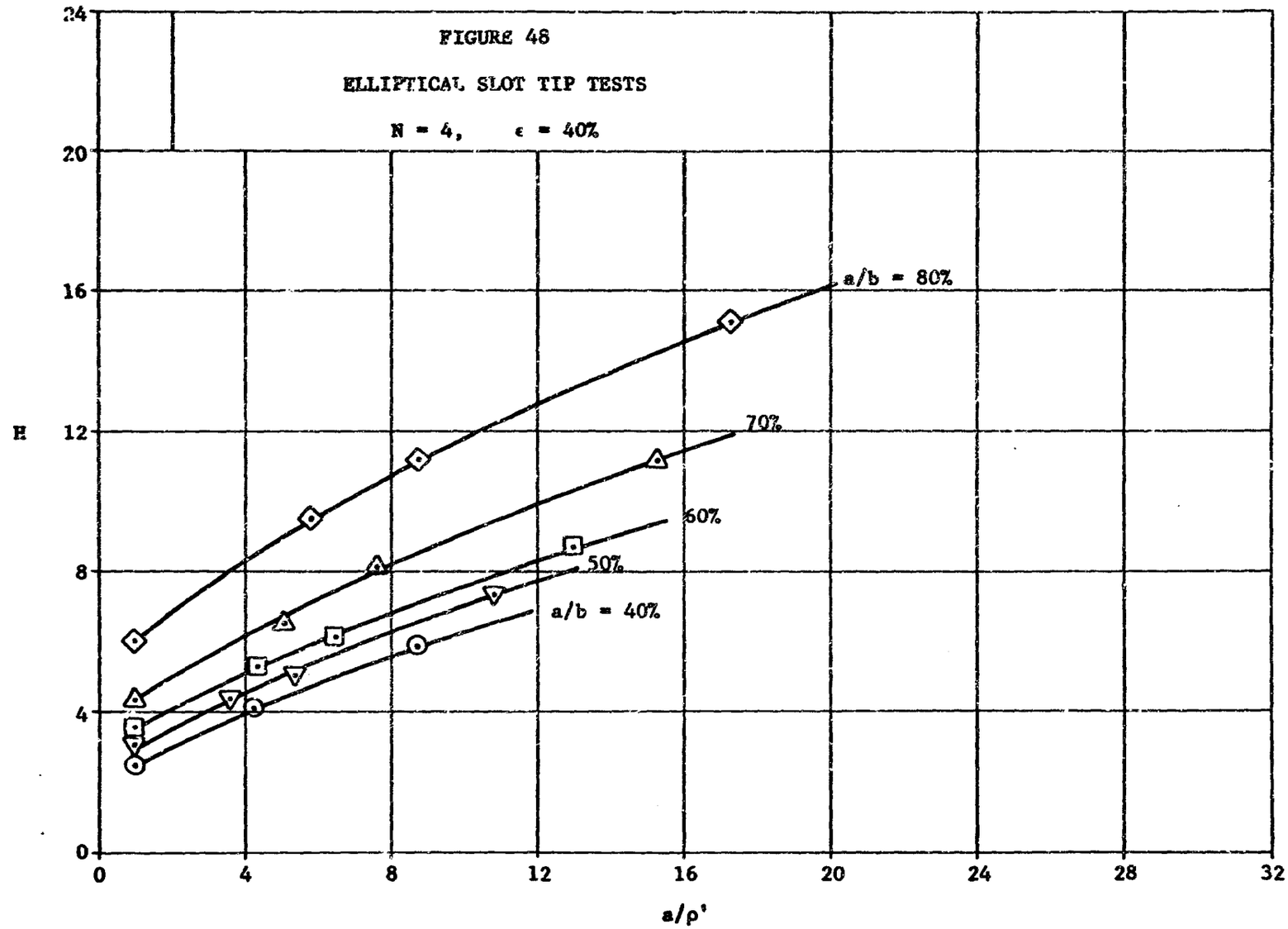
FIGURE 48
ELLIPTICAL SLOT TIP TESTS
N = 4, ε = 40%
H
a/ρ'
a/b = 80%
70%
60%
50%
a/b = 40%
0
4
8
12
16
20
24
28
32

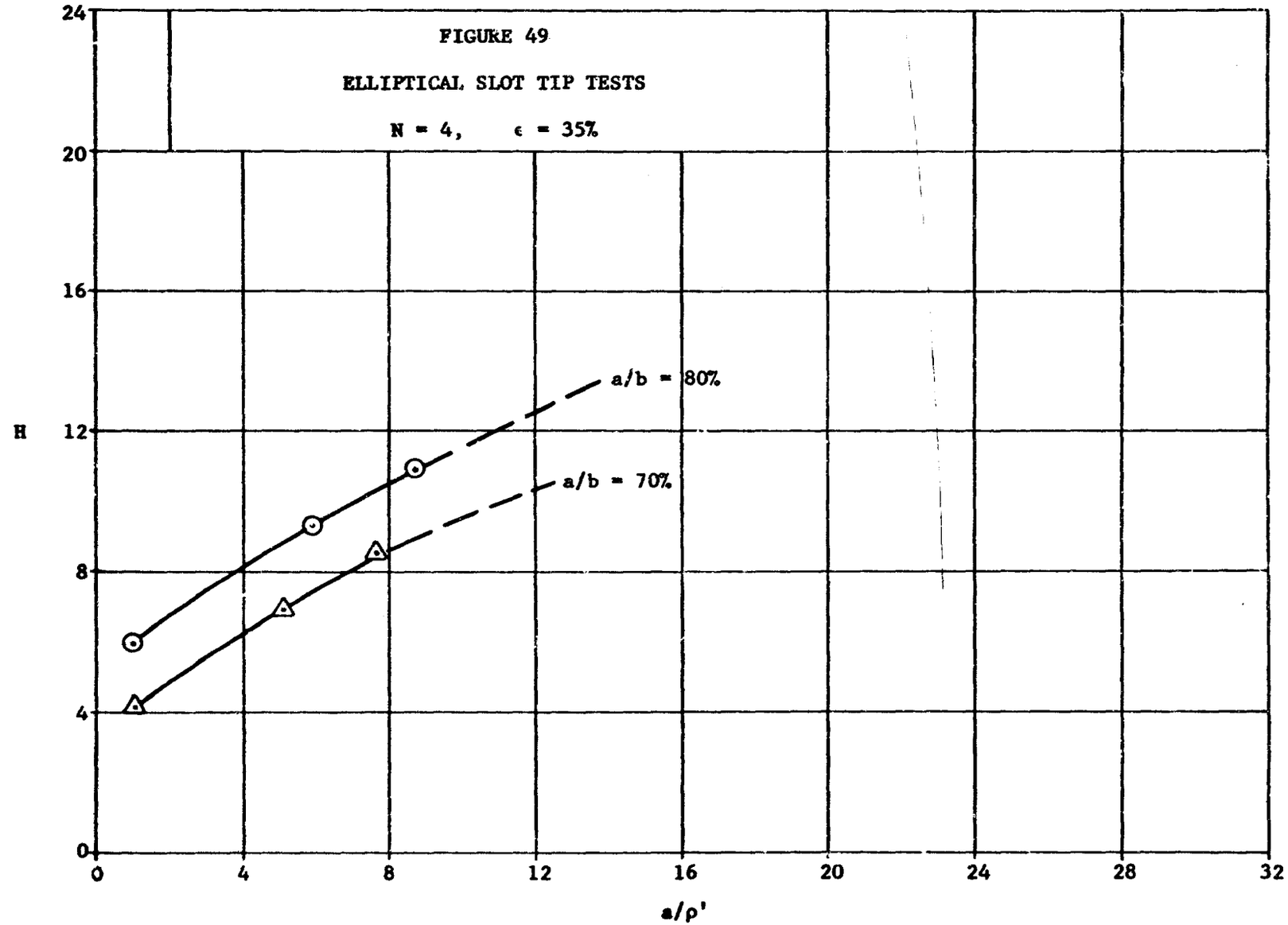
FIGURE 49
ELLIPTICAL SLOT TIP TESTS
N = 4, ϵ = 35%
a/b = 80%
a/b = 70%
H
a/ρ'
0
4
8
12
16
20
24
28
32

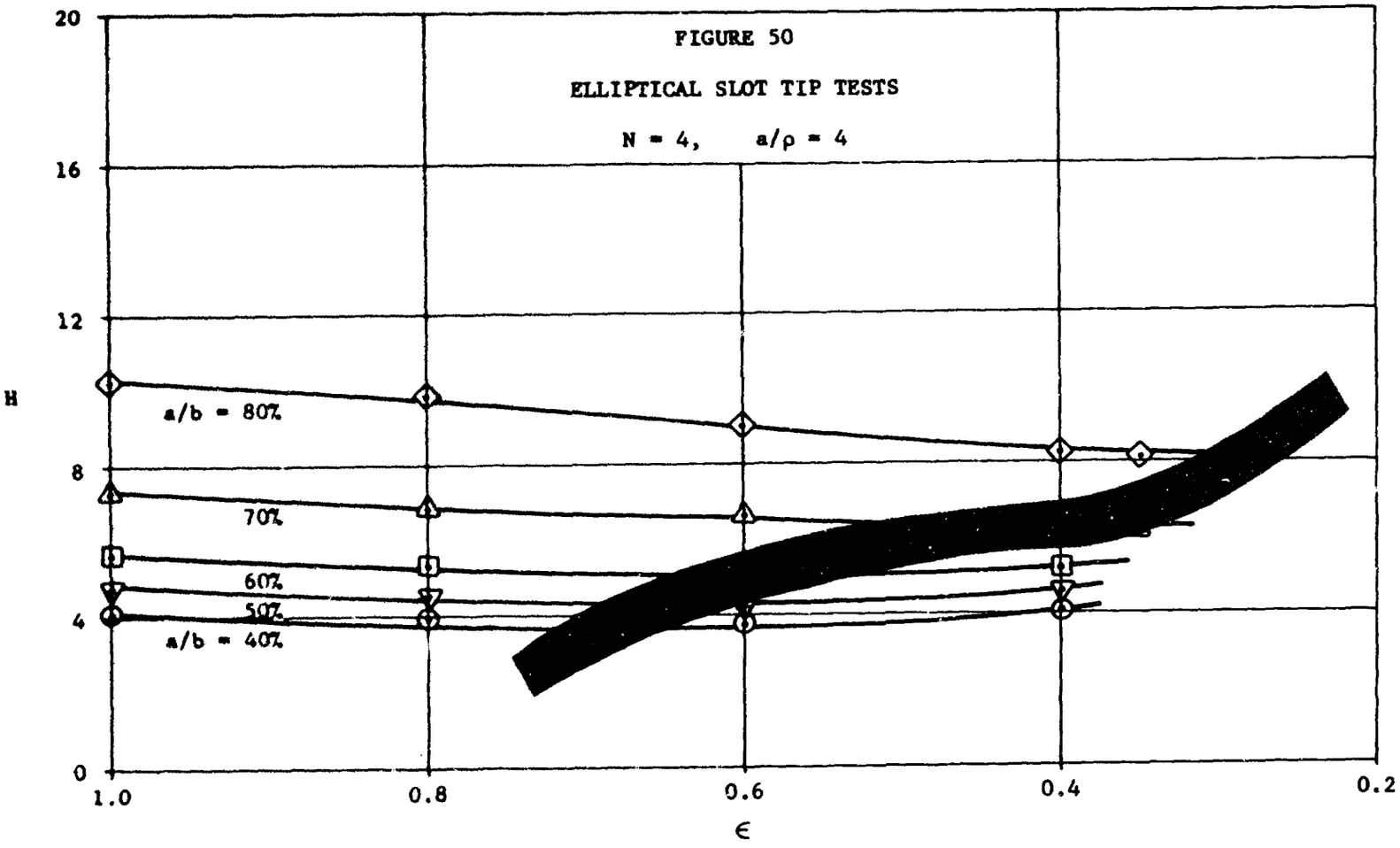
FIGURE 50
ELLIPTICAL SLOT TIP TESTS
N = 4, a/ρ = 4
20
16
12
8
4
0
H
a/b = 80%
70%
60%
50%
a/b = 40%
1.0
0.8
0.6
0.4
0.2
ϵ

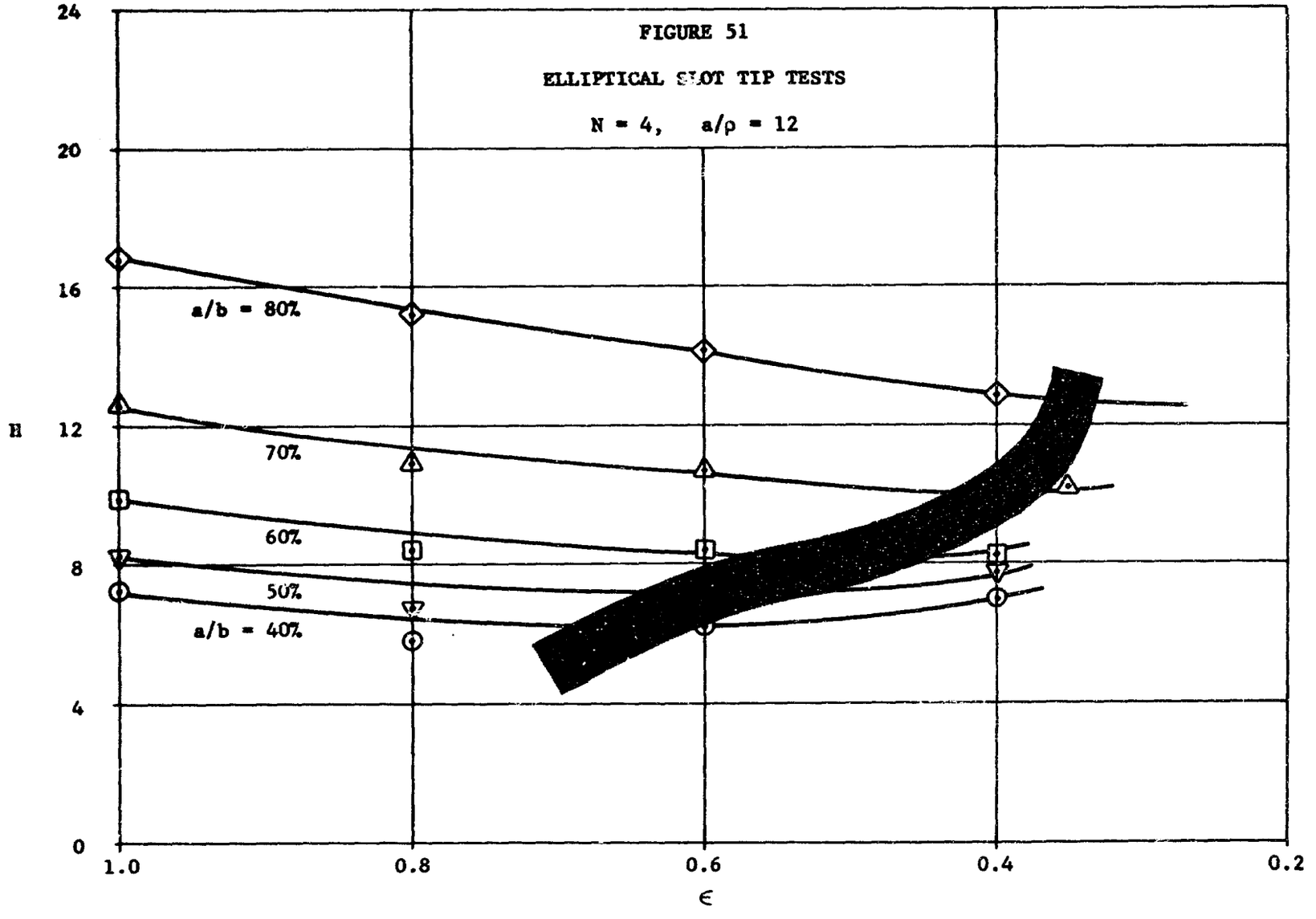
FIGURE 51
ELLIPTICAL SLOT TIP TESTS
N = 4, a/ρ = 12
24
20
16
12
8
4
0
H
a/b = 80%
70%
60%
50%
a/b = 40%
1.0
0.8
0.6
0.4
0.2
∈

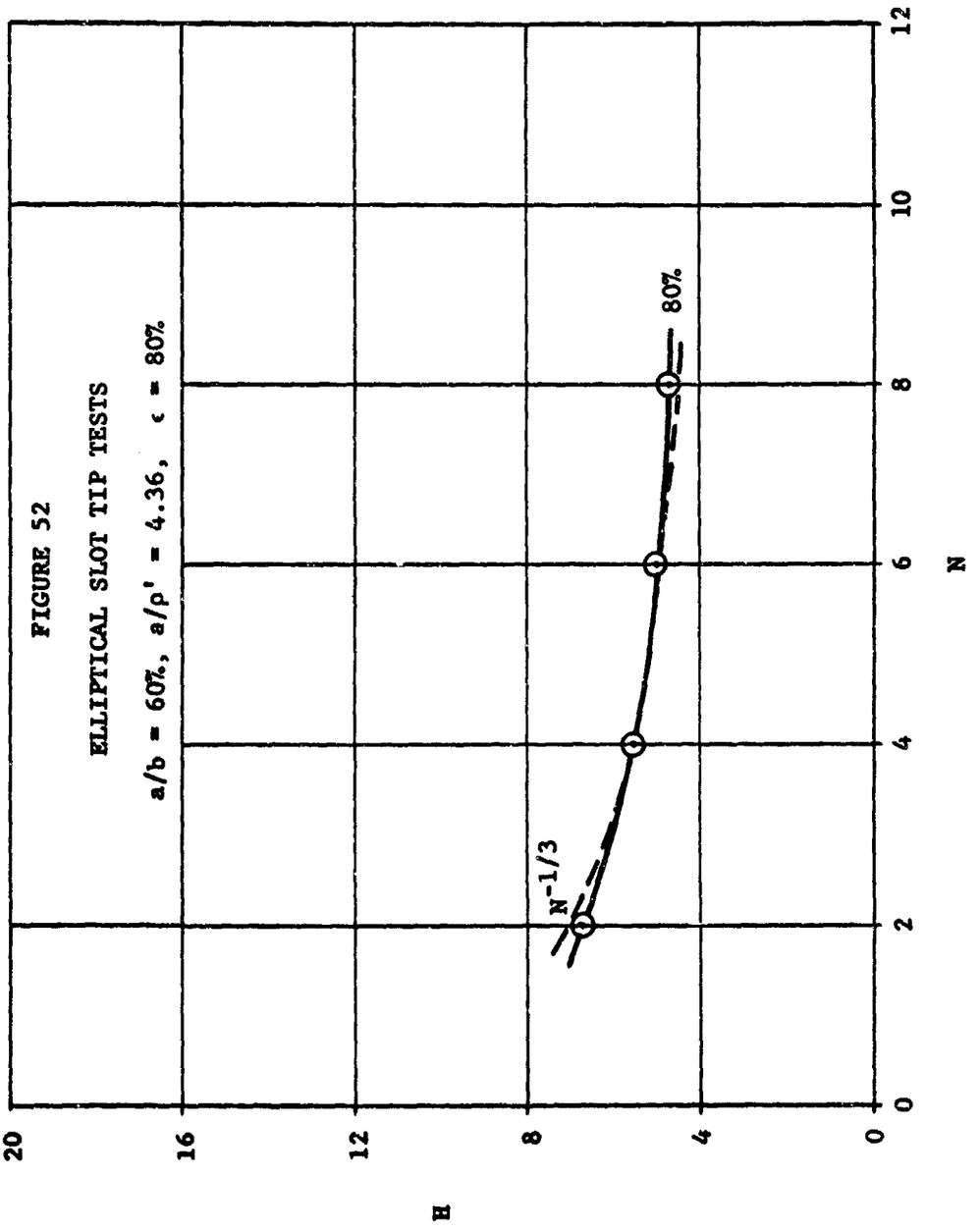
FIGURE 52
ELLIPTICAL SLOT TIP TESTS
a/b = 60%, a/ρ' = 4.36, ε = 80%
80%
N^-1/3
H
N
0
4
8
12
16
20
0
2
4
6
8
10
12

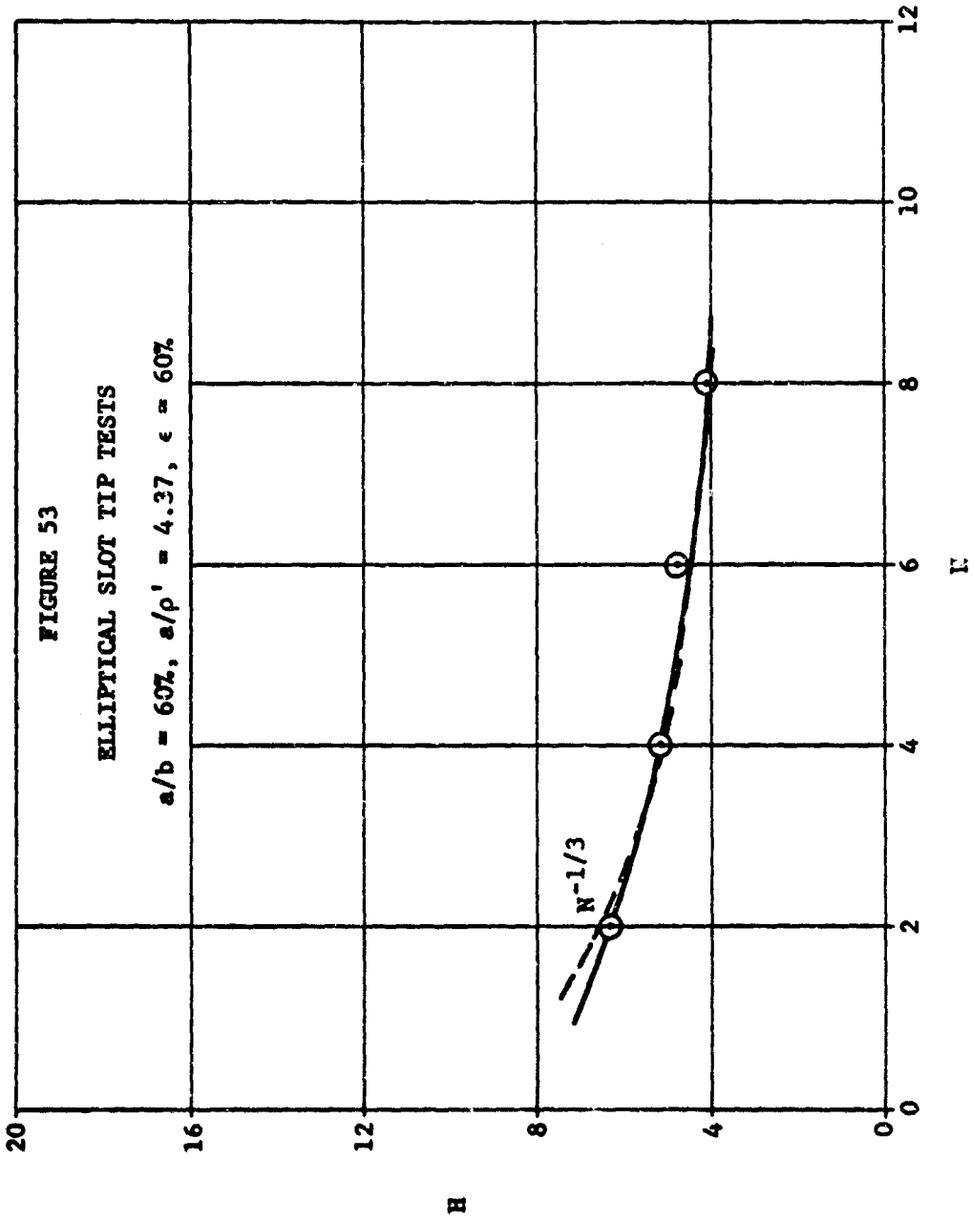
FIGURE 53
ELLIPTICAL SLOT TIP TESTS
a/b = 60%, a/ρ' = 4.37, ε = 60%
N^-1/3
H
T
0
4
8
12
16
20
0
2
4
6
8
10
12

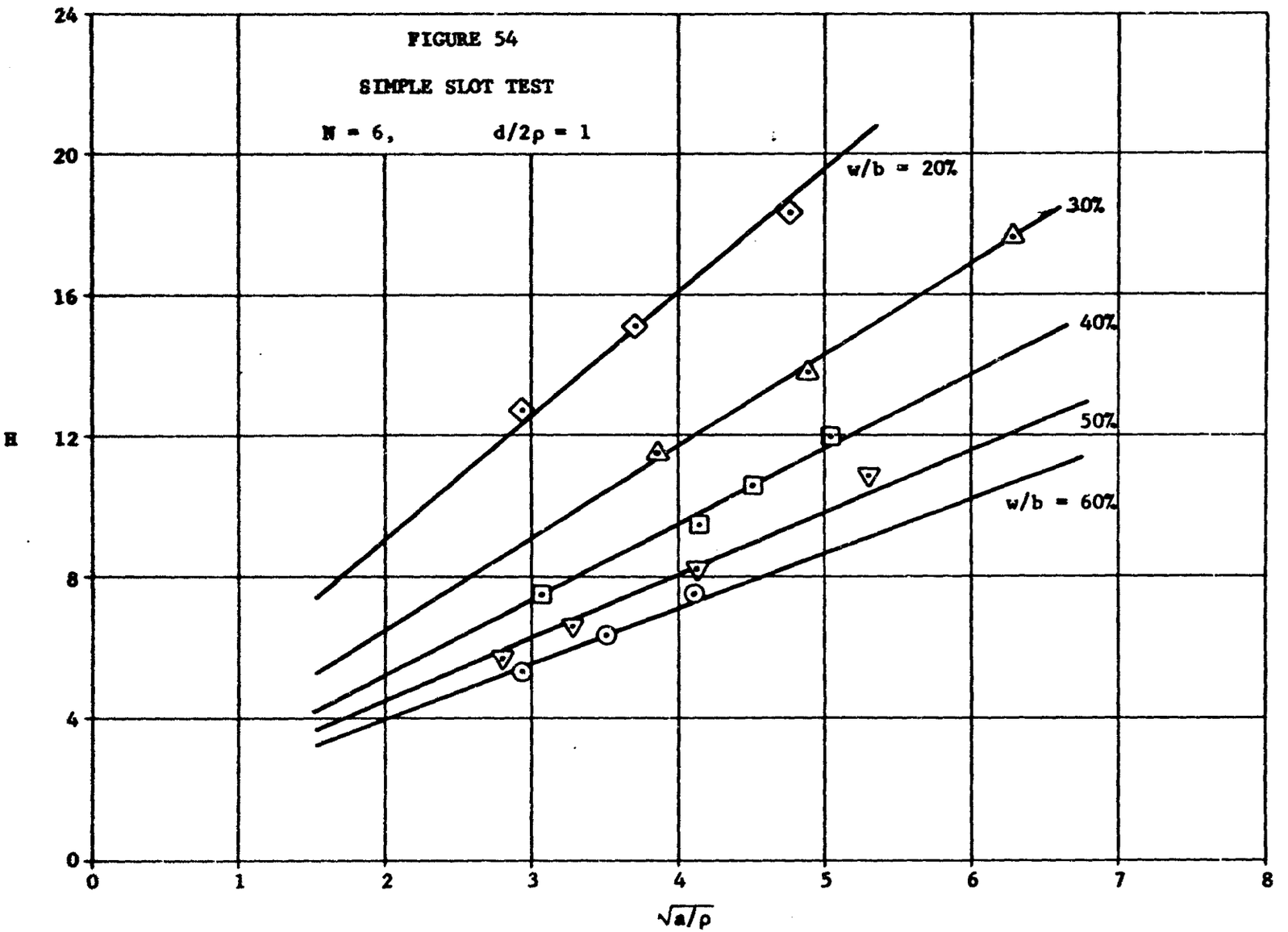
FIGURE 54
SIMPLE SLOT TEST
N = 6, d/2ρ = 1
w/b = 20%
30%
40%
50%
w/b = 60%
H
√a/ρ
0
4
8
12
16
20
24
0
1
2
3
4
5
6
7
8

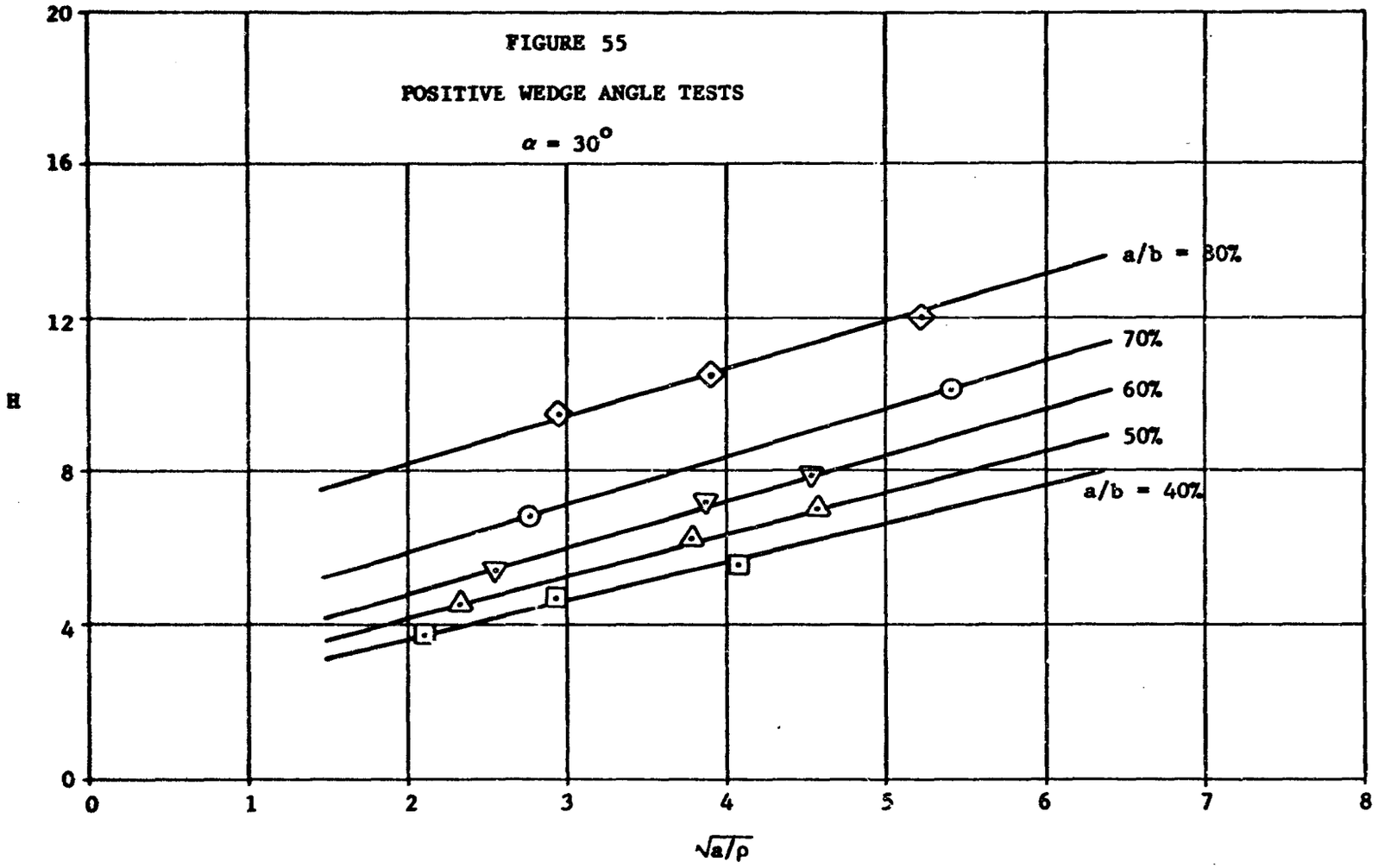
FIGURE 55
POSITIVE WEDGE ANGLE TESTS
α = 30°
H
√a/ρ
a/b = 80%
70%
60%
50%
a/b = 40%
0
4
8
12
16
20
0
1
2
3
4
5
6
7
8

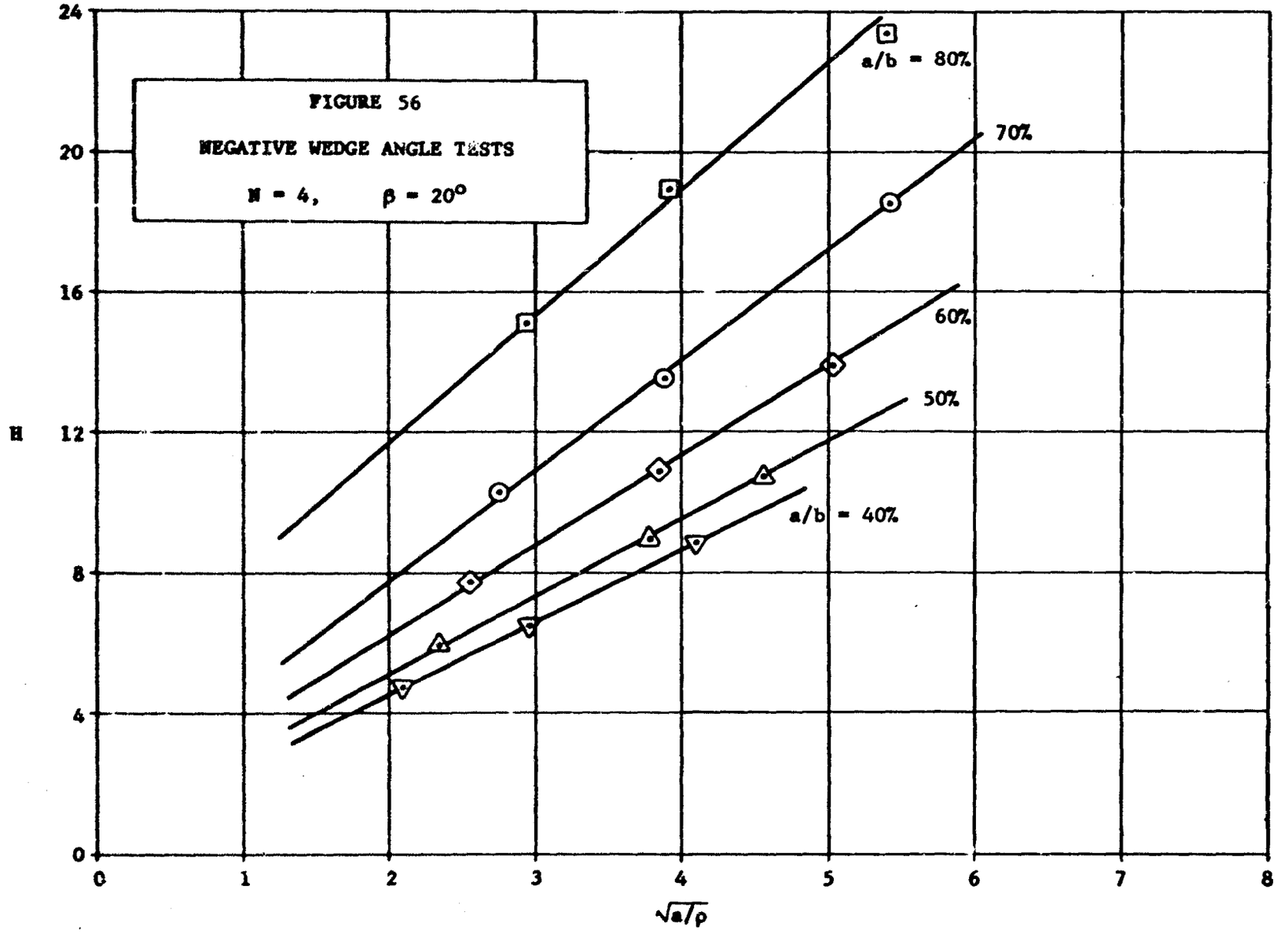
FIGURE 56
NEGATIVE WEDGE ANGLE TESTS
N = 4, β = 20°
a/b = 80%
70%
60%
50%
a/b = 40%
H
√a/ρ
0
4
8
12
16
20
24
0
1
2
3
4
5
6
7
8

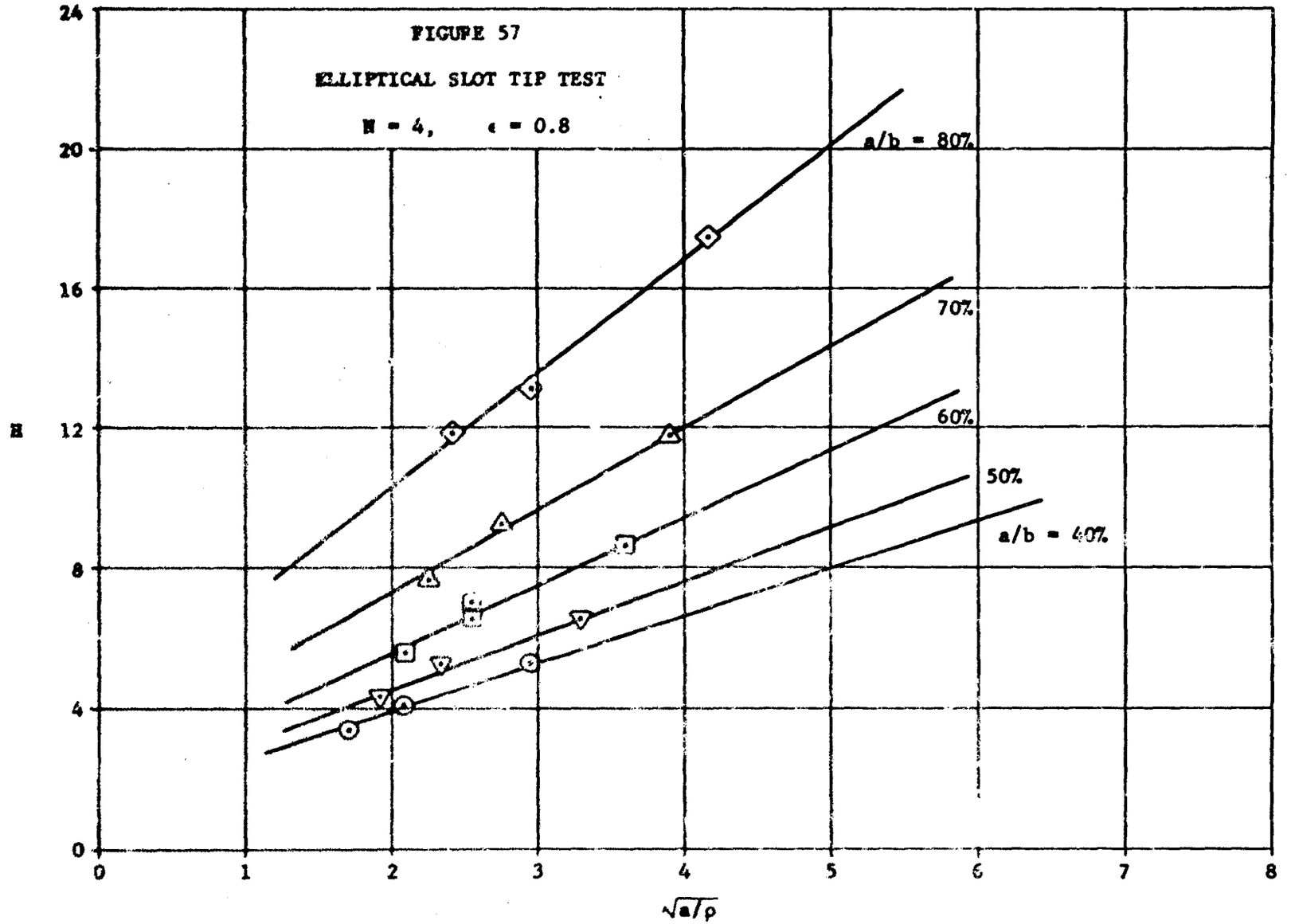
FIGURE 57
ELLIPTICAL SLOT TIP TEST
H = 4, ε = 0.8
a/b = 80%
70%
60%
50%
a/b = 40%
H
√a/ρ
0
4
8
12
16
20
24
0
1
2
3
4
5
6
7
8

UNCLASSIFIED
Security Classification

DOCUMENT CONTROL DATA - R&D
(Security classification of title, body of abstract and indexing annotation must be entered when the overall report is classified)

1. ORIGINATING ACTIVITY (Corporate author)	2a. REPORT SECURITY CLASSIFICATION
Mathematical Sciences Corporation 1107 Northeast 45th Street Seattle, Washington 98105	Unclassified 2b. GROUP

3. REPORT TITLE

Parametric Study of Rocket Grain Configurations by Photoelastic Analysis

4. DESCRIPTIVE NOTES (Type of report and inclusive dates)

Final Report

5. AUTHOR(S) (Last name, first name, initial)

Fourney, M. E.
Parmerter, R. R.

6. REPORT DATE	7a. TOTAL NO. OF PAGES	7b. NO. OF REFS
March 1966	120	9

8a. CONTRACT OR GRANT NO.	9a. ORIGINATOR'S REPORT NUMBER(S)
AF 04(611)-10529 b. PROJECT NO.	MSC Report No. 65-29-12
c. d.	9b. OTHER REPORT NO(S) (Any other numbers that may be assigned this report) AFSC Report No. AFRPL-TR-66-52

10. AVAILABILITY/LIMITATION NOTICES

This document is subject to special export controls and each transmittal to foreign governments or foreign nationals may be made only with prior approval of AFRPL (RPPR-STINFO), Edwards, California 93523.

11. SUPPLEMENTARY NOTES	12. SPONSORING MILITARY ACTIVITY
	Air Force Rocket Propulsion Laboratory Edwards, California

13. ABSTRACT

This report presents the results of parametric studies on several families of rocket grain configurations obtained by photoelastic analysis. In an earlier paper the authors described a parametric investigation of a family of grains which were defined by three parameters: N the number of star points, a/b the port fraction, and a/ρ the fillet radius factor. The results of that study led to the following empirical formula for the stress concentration factor,

$$K = \sqrt{\frac{1 + a/b}{1 - a/b}} \; N^{-1/3} \left\{ 1 + 2\sqrt{a/\rho} \right\}$$

In the present investigation the study has been extended to include families requiring four parameters to complete their description. Four additional families have been investigated to determine the effect of a) slot width, b) positive wedge angles of the star slot, c) negative wedge angles of the star slot, and d) eccentricity of elliptically shaped star tips. In each of the studies it is shown that the $N^{-1/3}$ rule holds approximately, and empirical formulas similar to the one given above have been derived in some cases.

A section on the application of the test results to more general engineering problems is presented. In this section a comparison is made between a recommended method of application and a limited number of numerical solutions obtained via computer analysis. Under the worst set of conditions available, the stress calculations agreed within 10% and the strain within 15%.

DD FORM 1 JAN 64 1473

UNCLASSIFIED
Security Classification

UNCLASSIFIED
Security Classification

14. KEY WORDS	LINK A		LINK B		LINK C	
	ROLE	WT	ROLE	WT	ROLE	WT
Solid Propellant Stress Analysis Stress Analysis Experimental Stress Analysis Photoelasticity Stress Concentrations Parametric Studies						

INSTRUCTIONS

1. ORIGINATING ACTIVITY: Enter the name and address of the contractor, subcontractor, grantee, Department of Defense activity or other organization *(corporate author)* issuing the report.

2a. REPORT SECURITY CLASSIFICATION: Enter the overall security classification of the report. Indicate whether "Restricted Data" is included. Marking is to be in accordance with appropriate security regulations.

2b. GROUP: Automatic downgrading is specified in DoD Directive 5200.10 and Armed Forces Industrial Manual. Enter the group number. Also, when applicable, show that optional markings have been used for Group 3 and Group 4 as authorized.

3. REPORT TITLE: Enter the complete report title in all capital letters. Titles in all cases should be unclassified. If a meaningful title cannot be selected without classification, show title classification in all capitals in parenthesis immediately following the title.

4. DESCRIPTIVE NOTES: If appropriate, enter the type of report, e.g., interim, progress, summary, annual, or final. Give the inclusive dates when a specific reporting period is covered.

5. AUTHOR(S): Enter the name(s) of author(s) as shown on or in the report. Enter last name, first name, middle initial. If military, show rank and branch of service. The name of the principal author is an absolute minimum requirement.

6. REPORT DATE: Enter the date of the report as day, month, year; or month, year. If more than one date appears on the report, use date of publication.

7a. TOTAL NUMBER OF PAGES: The total page count should follow normal pagination procedures, i.e., enter the number of pages containing information.

7b. NUMBER OF REFERENCES: Enter the total number of references cited in the report.

8a. CONTRACT OR GRANT NUMBER: If appropriate, enter the applicable number of the contract or grant under which the report was written.

8b, 8c, & 8d. PROJECT NUMBER: Enter the appropriate military department identification, such as project number, subproject number, system numbers, task number, etc.

9a. ORIGINATOR'S REPORT NUMBER(S): Enter the official report number by which the document will be identified and controlled by the originating activity. This number must be unique to this report.

9b. OTHER REPORT NUMBER(S): If the report has been assigned any other report numbers *(either by the originator or by the sponsor)*, also enter this number(s).

10. AVAILABILITY/LIMITATION NOTICES: Enter any limitations on further dissemination of the report, other than those imposed by security classification, using standard statements such as:

(1) "Qualified requesters may obtain copies of this report from DDC."

(2) "Foreign announcement and dissemination of this report by DDC is not authorized."

(3) "U. S. Government agencies may obtain copies of this report directly from DDC. Other qualified DDC users shall request through

_____."

(4) "U. S. military agencies may obtain copies of this report directly from DDC. Other qualified users shall request through

_____."

(5) "All distribution of this report is controlled. Qualified DDC users shall request through

_____."

If the report has been furnished to the Office of Technical Services, Department of Commerce, for sale to the public, indicate this fact and enter the price, if known.

11. SUPPLEMENTARY NOTES: Use for additional explanatory notes.

12. SPONSORING MILITARY ACTIVITY: Enter the name of the departmental project office or laboratory sponsoring *(paying for)* the research and development. Include address.

13. ABSTRACT: Enter an abstract giving a brief and factual summary of the document indicative of the report, even though it may also appear elsewhere in the body of the technical report. If additional space is required, a continuation sheet shall be attached.

It is highly desirable that the abstract of classified reports be unclassified. Each paragraph of the abstract shall end with an indication of the military security classification of the information in the paragraph, represented as *(TS), (S), (C), or (U)*.

There is no limitation on the length of the abstract. However, the suggested length is from 150 to 225 words.

14. KEY WORDS: Key words are technically meaningful terms or short phrases that characterize a report and may be used as index entries for cataloging the report. Key words must be selected so that no security classification is required. Identifiers, such as equipment model designation, trade name, military project code name, geographic location, may be used as key words but will be followed by an indication of technical context. The assignment of links, rules, and weights is optional.